

# A 3D culture system to study gene regulation in breast cancer cells

**Angélica Julieta Ramírez Cuéllar**

---

*DOCTORAL THESIS UPF /2021*

Thesis director: Dr. Miguel Beato

Codirector: Dr. Guillermo P. Vicent

Department of Experimental and Health Sciences  
Universitat Pompeu Fabra

Chromatin and Gene Expression || Gene Regulation, Stem Cells  
and Cancer || Center for Genomic Regulation (CRG)



Universitat  
Pompeu Fabra  
*Barcelona*



A mi familia.

A ti René.





## Abstract

The cellular processes required for the development and behavior of cancer cells are not only defined by their genome but also by their epigenome, which is largely influenced by the cell microenvironment. Routinely, cancer cells are studied in isolation, grown in 2D as monolayers on plastic surfaces. However recent studies highlight the impact of the 3D environment on multiple cellular functions. Therefore, cancer cells should be studied in contact with other cells and with the extracellular matrix (ECM).

In this thesis, we report the successful growth of hormone responsive T47D cells as 3D spheroids in Matrigel mimicking the ECM. By using a *genome-wide* approach we performed a detailed characterization of the main physical and biochemical differences between cells cultured in conventional 2D and as 3D spheroids, focusing on the particular pathways regulated through mechano-transductional signaling.

Compared to cells cultured in 2D, 3D grown cells have a rounder nucleus with less accessible and more compacted chromatin, impacting the regulation of over 2000 genes. We assessed how growing the cells in 3D affects the genome topology through Hi-C. Our results indicate that 3D cells exhibit a subtle trend towards enrichment in regions belonging to the B compartment (inactive chromatin), a decrease on chromatin bound architectural protein CTCF and increased fusion of Topologically Associating Domains (TADs).

Interestingly, the Hippo pathway kinase LATS involved in mechanosensing, is activated in 3D grown cells. In line with the observed p-LATS mediated phosphorylation of CTCF promoting its displacement from chromatin.

Regarding hormone regulation, 3D grown cells respond more efficiently and exhibit an increase in PR binding sites leading to chromatin remodeling and to a higher number of regulated genes. The increased activation of p-LATS promotes a cytoplasmic retention of YAP allowing binding of PR to new sites and thus regulating new genes. In conclusion, the Hippo pathway through p-LATS acts at least at two levels in 3D cells: i) through phosphorylation of CTCF and ii) through phosphorylation of YAP. Whether these two events are connected remains to be investigated.

Our results suggest that ECM exerts important effects on the structure and function of the breast cancer cell nucleus.



## Resumen

Los procesos celulares necesarios para el desarrollo y comportamiento de las células de cáncer están definidos por su genoma y por su epigenoma, influenciado por el su entorno extracelular. Usualmente, la célula se estudia de manera aislada, cultivada en monocapas sobre superficies de plástico. Sin embargo, estudios recientes destacan el impacto del entorno 3D en múltiples funciones celulares. Por lo que, la célula debe ser estudiada en contacto con otras células y una matriz extracelular (MEC).

En esta tesis informamos el crecimiento exitoso de células T47D que responden a hormonas como esferoides 3D en Matrigel imitando la MEC. Mediante un análisis global, realizamos una caracterización detallada de las principales diferencias físicas y bioquímicas entre las células cultivadas en 2D y como esferoides 3D, centrándonos en las vías particulares reguladas a través de la señalización mecanotransduccional. Observamos que las células 3D tienen un núcleo más redondo con cromatina menos accesible y más compactada que impacta sobre la regulación de más de 2000 genes. Al evaluar si el crecimiento de las células en 3D afecta la estructura 3D del genoma, resultados de Hi-C indican que los cambios son sutiles, pero con una tendencia consistente hacia el enriquecimiento en los compartimentos B (cromatina inactiva), así como hacia la fusión de Dominios de Asociación Topológica (TADs). Además, la presencia en cromatina de la proteína estructural CTCF se redujo considerablemente en 3D.

Por otro lado, la quinasa LATS de la vía Hippo, involucrada en la detección mecanosensorial, se encuentra más activada en 3D, en línea también con la fosforilación de CTCF mediada por p-LATS promoviendo su desplazamiento.

En cuanto a la regulación hormonal, las células 3D responden de manera más eficiente con un aumento de los sitios de unión a PR que promueve la remodelación de la cromatina regulando así más genes. El aumento de la activación de p-LATS promueve la retención citoplásmica de YAP permitiendo la unión de PR a nuevos sitios disponibles y así regular nuevos genes. En conclusión, la vía de Hippo a través de p-LATS actúa al menos a dos niveles en las células 3D: i) a través de la fosforilación de CTCF y ii) a través de la fosforilación de YAP, queda por investigar si éstos dos eventos están funcionalmente conectados.

Nuestros resultados sugieren que la MEC ejerce efectos importantes sobre la estructura y función del núcleo de las células del cáncer de mama.



## Table of Contents

Abstract .....	i
Resumen .....	iii
List of figures .....	viii
1. Introduction.....	1
1.1. Chromatin structure and organization .....	1
1.2. Chromatin dynamics in gene expression .....	4
1.2.1. Histone modifying enzymes .....	4
1.2.1.1. Histone acetylation/deacetylation .....	5
1.2.1.2. Histone methylation/demethylation .....	6
1.2.1.3. Histone phosphorylation/dephosphorylation.....	6
1.2.1.4. Other PTMS.....	7
1.2.2. ATP-dependent nucleosome remodelers.....	8
1.2.3. Histone variants .....	9
1.3. Hormone regulation in breast cancer .....	10
1.3.1. Nuclear receptors .....	11
1.3.1.1. Steroid hormone receptors .....	11
1.3.1.2. Progesterone receptor .....	12
1.3.2. MMTV promoter as a model system for PR studies.....	13
1.3.3. Chromatin remodeling and gene regulation in response to hormone.....	13
1.4. Role of the genome architecture .....	16
1.4.1. Chromosome territories .....	16
1.4.2. Genome compartments.....	19
1.4.3. Topologically Associating Domains (TADs).....	19
1.5. Towards a more physiological model to study breast cancer cell dynamics <i>Three-dimensional cell culture as a tool to overcome lack of microenvironment</i> .....	21
1.5.1. What is 3D cell culture? .....	22
1.5.2. Mammary gland 3D culture.....	24

1.5.3. 2D vs 3D .....	25
1.6. Mechanotransduction.....	27
1.6.1. Mechanoregulation of gene expression .....	31
1.7. Current approach: hydrogels .....	32
1.7.1. The stiffness in the environment of tumor cells.....	33
1.7.2. Organoids or spheroids? Depends on the context .....	35
1.8. Objective of the PhD project .....	37
2. Materials and methods.....	39
2.1. Materials .....	39
2.2. Methods.....	44
2.3. Bioinformatic methods .....	56
3. Results.....	61
Chapter I: Characterization 3D spheroids grown in the extracellular matrix.....	61
3.1. Implementation of 3D cell culture on breast cancer cell lines .....	61
3.2. Characterization of the T47D spheroids.....	63
3.3. Signaling pathways differentially regulated in 3D cells .....	66
Chapter II. Impact of the 3D growth on nuclear structure and function .....	70
3.4. Chromatin distribution 2D vs. 3D .....	70
3.5. Gene expression regulation .....	73
3.6. Possible molecular mechanism underlying the changes in gene expression.....	77
Chapter III. Impact of the ECM on genomic organization and signaling cascades .....	80
3.7. Genome architecture .....	80
3.8. How the Hippo pathway impacts the genome architecture in 3D cells.....	82

Chapter IV. Comparison of the hormonal response of breast cancer cells grown as monolayer (2D) and spheroids (3D) .....	89
3.9. PR signaling upon hormonal stimulation .....	89
3.10. Progesterone receptor binding upon hormone stimulation .....	95
3.11. Accessibility of the chromatin upon hormone exposure	100
4. Discussion.....	105
4.1. General characterization of 3D breast cancer spheroid development .....	105
4.2. Impact of the 3D growth on nuclear structure and function .....	107
4.3. Caudal Type Homeobox 2 (CDX2).....	109
4.4. Increased heterochromatin clusters near the nuclear lamina .....	109
4.5. Impact of the ECM on genomic organization and signaling cascades .....	110
4.6. Comparison of the hormonal response of breast cancer cells grown as monolayer (2D) and spheroids (3D) .....	111
5. Conclusions .....	117
6. Literature .....	119
Abbreviations .....	140

## List of figures

Figure I1 Conformation of the nucleosome	1
Figure I2 Hierarchy of the organization of DNA within the chromatin structure	2
Figure I3 The histone code	5
Figure I4 Histone variant hallmarks in tumorigenesis	10
Figure I5 General structure of steroid hormone receptors	12
Figure I6 Model for initial steps of MMTV promoter activation	15
Figure I7 3C and its derivatives	18
Figure I8 Hierarchical organization of the chromatin at different levels of resolution	20
Figure I9 A recent literature search in PubMed with the 3D culture related terms in combination with 'cancer' or 'tumor' in titles or abstracts	22
Figure I10 Timeline of techniques and experiments leading to the current organoid field	23
Figure I11 Physical links between ECM and nucleus	29
Figure I12 The cell microenvironment and mechanosensing	30
Figure I13 Regulation of genome structure and gene expression by mechanotransduction	32
Figure I14 Different types of cancer spheroid growth on Matrigel	34
Figure R1. Growth of breast cell lines on different hydrogels	62
Figure R2 Breast cell lines grown in 3D culture embedded in Matrigel	62
Figure R3. Cell proliferation rate in T47D spheroids	63
Figure R4 Cell proliferation in T47D representative spheroids	64
Figure R5 Physical properties of 3D cells	65
Figure R6 Expression of progesterone and estrogen receptors in T47D cells grown under 2D and 3D conditions	66
Figure R7 The Hippo pathway effector between cell models is controlled by the rigidity of the growing surface	67
Figure R8 Cells regulate focal adhesion dynamics in response to matrices with different biophysical properties	68



Figure R9 Chromatin in 3D nuclei is differentially distributed in the nucleus	70
Figure R 10 MNase digestion of nuclei obtained from T47D cells grown in 2D and in 3D conditions	71
Figure R11 ATAC-seq analysis performed in breast cancer cells grown in 2D and in 3D conditions	73
Figure R12 Heatmap and PCA of RNA-seq replicates obtained from 2D and 3D T47D cells	74
Figure R 13 Differential Expression Analysis 3D/2D	75
Figure R14 Gene Ontology of Biological Process (BP) and Cellular Component (CC) differentially regulated in 3D cells	75
Figure R15 KEGG enriched pathways	76
Figure R 16 Homer motif analysis of 3D up- and down-regulated genes.	78
Figure R17 Characterization of shAP2A, shYY1 and shCDX2 cells	79
Figure R18 Hi-C analyses of T47D cells grown in 2D vs 3D conditions	81
Figure R19 shLATS control over CTCF	83
Figure R20 HOMER motif analysis of the ATAC-seq peaks	85
Figure R 21 Loss of CTCF binding detected in 3D is not directly linked to TAD fusions	87
Figure R22 Activation of Progesterone Receptor in T47D cells in response to 10 nM R5020 in 2D vs 3D cells	91
Figure R23 Differential Expression Analysis performed in 2D and 3D T47D cells	92
Figure R 24 Significant GO terms in 3D T47D cells treated with R5020	94
Figure R 25 ChIP-seq of PR performed in 2D and 3D cells upon hormone exposure	97
Figure R 26 HOMER de novo motif enrichment analysis for 2D and 3D PR exclusive peaks	99
Figure R 27 ATAC-seq analysis reveals a more pronounced chromatin remodeling in 3D cells treated with hormone	102
Figure D 1 Comparison between the features of different models	106

Figure D 2 Overlap of heterochromatin H3K9me3 signal with Lamin A/C	110
Figure D 3 Venn diagram depicting the overlap between PR peaks detected in YAP KD cells grown in 2D and 3D- exclusive PR peaks	115

## List of tables

Table 1. Reagents	39
Table 2. Culture media	40
Table 3. Cell lines	41
Table 4. Primers used for qPCR analysis	41
Table 5a. Antibodies	42
Table 5b. Secondary antibodies	43
Table 6. Commercial kits	43
Table 7. shRNA vectors	43



## 1. Introduction

### 1.1. Chromatin structure and organization

In eukaryotic cells the genetic material is organized in the nucleus into nucleoprotein complexes called chromosomes, from the Greek "*khroma*" (colored) and "*soma*" (body). Nuclear DNA does not appear in free linear strands; rather it is wrapped around nuclear proteins and highly condensed as chromatin in order to fit inside the nucleus.

Early studies revealed that the basic repeating structural unit of chromatin is the nucleosome, composed of 147 base pairs (bp) of DNA wrapped as a left-handed 1.7 turns superhelix around an octamer of histones made of two copies of each histone H2A, H2B, H3 and H4 (Richmond et al., 1984) (Figure I1).

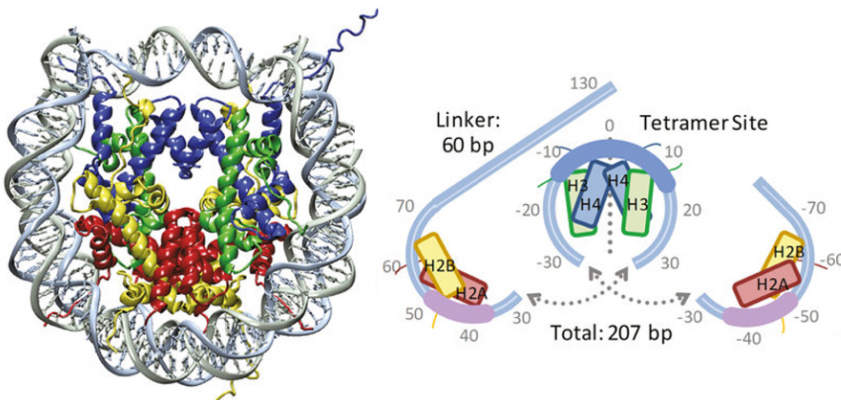


**Figure I1 Conformation of the nucleosome**

DNA wraps  $\sim 1.7$  left-handed turns around the histone octamer. Nucleosome arrays consist of repeats of this 11-nm diameter core particle (147 bp) and adjacent 60 bp linkers. The bases are numbered from the dyad axis (dotted line). Individual histones are represented by boxes aligned with each strand. At the dyad axis, the (H3-H4) tetramer binds up to 80 base pairs as the central region of DNA bound most strongly (shown in cyan). Off-dyad bases are bound to the H2A-H2B dimers over the whole length of the outer turn DNA where the bases binding is stronger (purple). Adapted from (McCauley et al., 2019).

The nucleosome cores are connected by linker DNA, which typically ranges from 10 to 90 bp in length, to form the “beads-on-a-string” nucleosomal array with a diameter of 11 nm. The nucleosomal array represents the first level of DNA compaction in chromatin (Felsenfeld & Groudine, 2003). This fiber can then adopt further levels of compaction, which ultimately result in highly condensed chromosomes (Figure 12). Linker histones (H1 and H5) bind to the DNA linker regions in close proximity to the entry and exit sites of DNA in the nucleosome core particle, and also contacts the dyad axis of the nucleosomal DNA. Linker histone H1 organizes the nucleosomal arrays into a more condensed chromatin fiber, regarded as the second level of DNA compaction (Felsenfeld & Groudine, 2003).

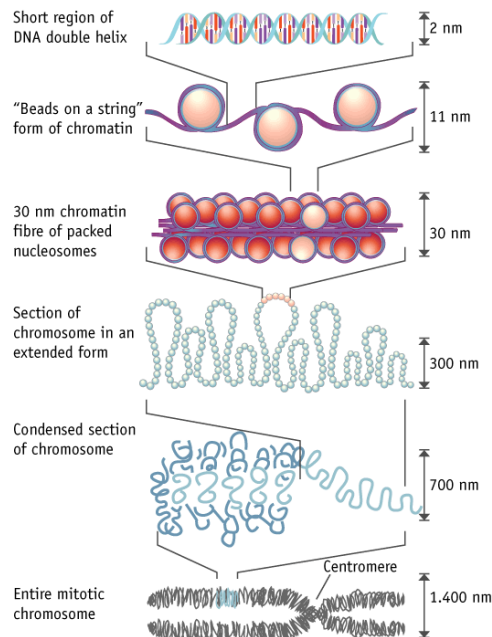


**Figure 12 Hierarchy of the organization of DNA within the chromatin structure**

The basic level of organization is the nucleosome, in which 1.7 super helical turns of DNA are wrapped around a histone octamer. Nucleosomes are connected by short stretches of linker DNA. At the next level, the string of nucleosomes is folded into a fiber of 30 nm in diameter, these fibers are then further folded into higher-order structures. Adapted from (Felsenfeld & Groudine, 2003).

Despite this high degree of compaction, DNA must be rapidly accessible to permit its interaction with protein machineries that act on chromatin during replication, transcription, repair and recombination.

The core histones have a classical histone fold composed of crossed  $\alpha$ -helices with basic amino acids that interact with the minor groove of the DNA helix. The terminal portions of the nucleosomal histones are unstructured disordered tails that extend from the core particle and are the substrate of a plethora of post-translational modifications (PTM) that have an impact on nucleosome interactions, chromatin accessibility and gene expression. As a consequence of DNA and histone modification, chromatin is organized into two functional compartments: **euchromatin** and **heterochromatin**, characteristic of different cell types.

**Euchromatin** is the more accessible fraction of chromatin enriched in expressed genes, distributed throughout the cell nucleus and replicates throughout the S phase, while **heterochromatin** is more condensed chromatin poor in highly expressed genes and enriched around the nucleolus, the centromeres and near the nuclear periphery, and it replicates toward the end of the S phase. There are two types of heterochromatin: facultative and constitutive. Facultative heterochromatin can be expressed whenever necessary (e.g., X chromosome inactivation in female mammals), while constitutive heterochromatin is never expressed (e.g., regions of Y chromosome) (Grewal & Elgin, 2002; Oberdoerffer & Sinclair, 2007). The two forms of **heterochromatin** are distinguished by their combination of PTMs, which influence the recruitment of regulatory proteins into chromatin. The best-studied types of heterochromatin are marked by the addition of one, two or three methyl groups to histone H3 lysine 9 (H3K9me1/2/3) or lysine 27 (H3K27me1/2/3) (Grant, 2001). Sequences embedded in heterochromatin often contain repetitive elements, such as satellite repeats and transposable elements. A crucial function of heterochromatin is to prevent such selfish sequences from producing genetic instability. Additional heterochromatin roles

include asserting cell-type-specific transcription and centromere function.

## 1.2. Chromatin dynamics in gene expression

Gene transcription is strictly regulated at different levels to ensure appropriate cell function. Activation or repression of gene transcription is typically accomplished by the recruitment of transcription factors (TF) that interact with several protein complexes to modulate the interaction between histones and DNA. There are two classes of chromatin modulating enzymes: histone modifying enzymes and ATP-dependent nucleosome remodelers.

### 1.2.1. Histone modifying enzymes

Post-translational modifications of histones are catalyzed by various enzymes and occur mostly on the terminal tails of the histones. The most common enzymes are methyltransferases and demethylases acting on lysines (K) and arginines (R); acetyltransferases and deacetylases acting on lysines and kinases; and phosphatases acting on serines (S) and Threonines (T) (Alaskhar et al., 2018). But there are many more modifications, briefly discussed below. These modifications conform a collection of combinatorial or sequential signals constituting the “histone code” (Figure I3), and their effects on gene transcription can be broadly categorized into active and repressive marks.

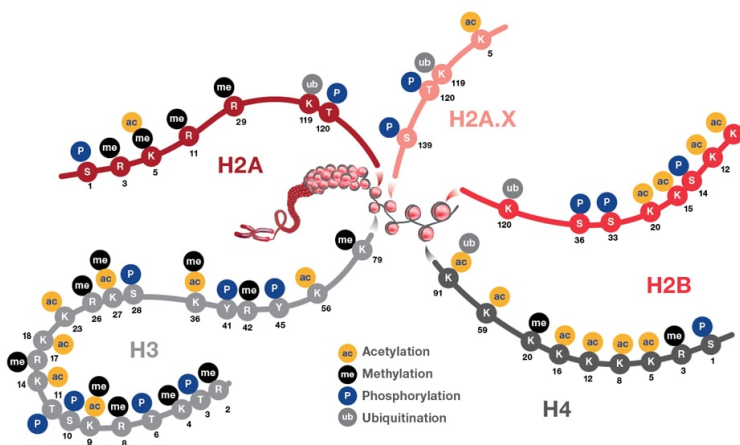




**Figure 13 The histone code**

The code is primarily divided into active and repressive marks. Histone tails are susceptible to post-transcriptional modifications. The nomenclature of the modifications is composed by the name of the histone followed by the position of the amino acid in the protein sequence continuing with the type and extent (mono-di-tri) of the modification. Example: '*H3K9me3*' H3 stands for the protein '*histone 3*', the letter '*K*' specifies the amino acid lysine and '*9*' its position within the protein sequence. Furthermore, '*me3*' explain that the lysine carries three methyl groups as chemical modification. Adapted from thermofisher.com.

**1.2.1.1. Histone acetylation/deacetylation**

Histone tails normally carry a positive charge due to amine groups present on their lysines and arginines. This positive charge is the means by which histone tails interact with and bind to the negatively-charged phosphate groups on the DNA backbone. Addition of acetyl groups neutralizes the positive charges on the histone by changing amines into amides, thus decreasing the ability of the histones to bind to DNA. This decreased binding allows chromatin expansion, permitting gene transcription to take place.

Histone acetylation occurs by the enzymatic addition of an acetyl group from acetyl coenzyme A. The process is tightly involved in the regulation of cellular processes including chromatin dynamics and transcription, gene silencing, cell cycle progression, apoptosis, differentiation, DNA replication and repair, and neuronal repression. The modifying enzymes involved in histone acetylation are called histone acetyltransferases (HATs) and they play a critical role in controlling histone H3 and H4 acetylation. More than 20 HATs have been identified and classified into five families: GNAT1, MYST, TAFII250, P300/CBP, and nuclear receptor coactivators (Kuo & Allis, 1998).

Histone acetylation may be increased by inhibition of histone deacetylases (HDACs) and decreased by HAT inhibition. HDACs catalyze the removal of acetyl groups from histone lysine residues. Like HATs, HDACs play a critical role in various cellular processes involving histone H3 and H4. At least 4 classes of HDACs have been identified. HDAC inhibition displays significant effects on

apoptosis, cell cycle arrest, and differentiation in cancer cells (Dokmanovic et al., 2007).

### **1.2.1.2. Histone methylation/demethylation**

Histone methylation is given by the transfer of one, two, or three methyl groups from S-adenosyl-L-methionine to lysine or arginine residues of histone proteins by histone methyltransferases (HMTs). HMTs regulate methylation through chromatin-dependent transcriptional repression or activation. In the nucleus, when histone methylation occurs, specific genes organized in chromatin may be activated or silenced (Greer & Shi, 2012). Several HMTs have been discovered and are specific for lysines or arginines. On histone H3 for example, SET1, SET7/9, ALL-1, MLL, ALR, Trx and SMYD3 catalyze methylation of H3K4. G9a, SUV39-h1, SUV39-h2, SETDB1, Dim-5, and Eu-HMTase catalyze methylation of H3K9. Polycomb group enzymes such as EZH2 catalyze methylation of H3K27 (Wood & Shilatifard, 2004). Both H3K9me3 and H3K27me3 mediates heterochromatin formation and participates in silencing gene expression at euchromatic sites.

### **1.2.1.3. Histone phosphorylation/dephosphorylation**

Activation of signaling cascades in response to stress, growth factors or immune stimulation ultimately results in the phosphorylation of many cellular targets including histone proteins. Histone phosphorylation was first described in rats in 1967 (Gutierrez, 1967). Like acetylation, phosphorylation of histone tails adds a negative charge to the histone tails, changing the conformation of chromatin structure and interactions with transcription factors. All core histones can be phosphorylated by a plethora of protein kinases and dephosphorylated by phosphatases. Phosphorylation occurs on serine, threonine and tyrosine, and is associated with DNA damage response (H2A.X S139 and H4S1), transcription regulation (H3S10, H3S28, H2BS32, H3T6, H3T11, H3Y41, H2BS36, H2BY37, H4S1 and H4S47), mitosis (H3S10 and H3S28), meiosis (H4S1 and H2BS10) and apoptosis (H2BS10, H2AXS139, and H3T45). Phosphorylation on Serine 139 of H2AX

( $\gamma$ H2AX) is induced by DNA damage and is an early response in DNA double-strand break signaling. Multiple kinases can mediate the phosphorylation on this particular site including ATM (ataxia-telangiectasia mutated), ATR (ATM and Rad3-related), and DNA-PK (reviewed in Rossetto et al., 2012).

While the role of protein kinases in chromatin dynamics has been well studied, the nature and regulation of the counteracting phosphatases represent an emerging field still in early stages.

Phosphorylation of Ser5 is important to recruit enzymes that cap the 5' end of the transcript, whereas phosphorylation of Ser2 activates elongation and splicing. Subsequent dephosphorylation of these sites is needed to finish transcription and enable detachment of RNAPII from the gene. Fcp1 phosphatase specifically dephosphorylates Ser2, while Ssu72 and Rtr1 in yeast, and SCP1 and RPAP2 in mammals are responsible for Ser5 dephosphorylation. PNUTs/PP1 was also shown to target Ser5ph, as PNUTs/PP1 co-localize with RNAPII at transcriptionally active sites and *Drosophila* PNUTs mutants increased the levels of RNAPII Ser5ph levels but not of Ser2ph (reviewed in Gil et al., 2019).

Many lines of evidence support a crosstalk between histone phosphorylation and other PTMs. A preexisting histone phosphorylation can recruit another histone-modifying enzyme, promoting the related modification (i.e., phosphorylation of H3S10 enhances acetylation of neighboring H3K14 by Gcn5 to promote transcription (Lo et al., 2000) or a preexisting histone phosphorylation disrupts binding of a chromatin factor from an adjacent modification (i.e., phosphorylation of H3S10 affects HP1 binding to methylated H3K9) (Fischle et al., 2005).

#### **1.2.1.4. Other PTMS**

A plethora of other modifications have also been reported for histones including lysine crotonylation, ubiquitination, butyrylation, propionylation, tyrosine hydroxylation, biotinylation, neddylation, sumoylation, O-GlcNAc, ADP ribosylation, N-formylation, proline

isomerization, and citrullination (which are detailed further in Zhao & Shilatifard, 2019). Each of these modifications affect in a different way, diverse functions in which chromatin is involved. Thus, some modifications act directly on chromatin, others act through scaffold proteins, some activate, and others inhibit the same pathway. Therefore, the variability and the combination of these modifications are the basis of the histone code. For example:

*Ubiquitination.* The ubiquitination of histones most commonly occurs on H2A and H2B (Yi Zhang, 2003). H2AK119 ubiquitination by RING1A/B in the PRC1 complex is linked with chromatin compaction and transcriptional silencing (Wang et al., 2004). H2BK120ub1 by the UBE2A/B E2 ubiquitin conjugating enzyme and RNF20/40 E3 ligase at actively transcribed genes (Kim et al., 2009). The crosstalk between histone modifiers themselves can also control states of cell proliferation.

*Neddylation.* The covalent conjugation of NEDD8, is deposited on histone H2A by the E3 ligase RNF168. Neddylation of H2A on K119 prevents ubiquitination at this site and results in decreased response to DNA damage (Li et al., 2014).

Finally, *hypercitrullination* can promote chromatin decondensation (Wang et al., 2009), to name a few.

Overall, some of the more recently identified histone modifications could affect the conventional modifications (methylation, acetylation, and phosphorylation) via competing for the same sites on histones for modification or through a crosstalk that could induce a conformational change in the target region, altering the downstream signaling and gene regulation.

### **1.2.2. ATP-dependent nucleosome remodelers**

In contrast to histone modifying enzymes, chromatin remodeling complexes utilize the energy of ATP to disrupt nucleosome DNA contacts, move nucleosomes along DNA, and remove or exchange nucleosomes. Thus, they make DNA/chromatin accessible during

cellular processes. These enzymes are essentially required for diverse but specific aspects of embryonic development including pluripotency, cardiac development, dendritic morphogenesis and self-renewal of neural stem cells (Vignali et al., 2000).

Most ATP-dependent chromatin remodeling factors are multi subunit complexes with an ATPase as the catalytic center. ATPase subunits can be classified into three families; the SWI2/SNF2-, the Mi-2/CHD-1, and the ISWI-ATPases (Eisen et al., 1995). ATPases contain a highly conserved core domain, surrounded by N- and C-terminal domains, which differ considerably between families. The complexes differ in the number of subunits, ranging from two in some ISWI complexes to 11 or more in the SWI/SNF complexes (reviewed in Kingston & Narlikar, 1999; Vignali et al., 2000).

### **1.2.3. Histone variants**

Histone variants share protein sequence homology with canonical histones. They also harbor a similar repertoire of PTMs at key residues to regulate chromatin accessibility or gene expression. They have unique biophysical properties, genomic localization patterns and binding partners, conferred by differences in primary amino acid sequence and structure. Histone variants can replace existing canonical histones and their associated PTMs, thus remodeling the epigenome throughout the cell cycle and during development (Filipescu et al., 2014). The described variants consist of: H2A.Z, macroH2A, H3.3, HJURP and centromeric protein A (CENP-A).

Histone variants contribute to various processes associated to the so-called 'hallmarks of cancer' (Hanahan & Weinberg, 2011). Since the stages of tumorigenesis from initiation to growth, metastasis, dormancy, and treatment resistance are driven by distinct cellular pathways, deregulation of histone variant functions is co-opted by transformed cells with distinct consequences along the evolutionary trajectory of a tumor. In breast cancer, CENP-A, H2A.Z, HJURP and macroH2A are up-regulated resulting in increased cancer cell proliferation, EMT, invasion and migration (reviewed in (Ghiraldini et al., 2021) (Fig. I4).

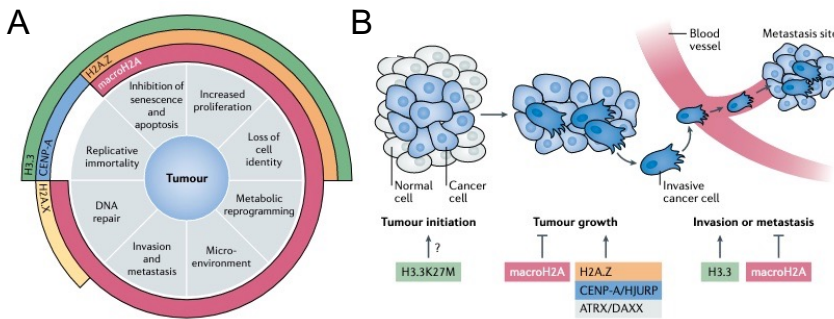


**Figure 14 Histone variant hallmarks in tumorigenesis**

A) The role of altered histone variants in tumorigenesis is categorized into eight major hallmarks. MacroH2A is associated with the highest number of hallmarks, underlying its highly versatile role in tumor development. H3.3 alteration affects pathways involving replicative immortality due to its role in telomere maintenance, senescence, increased proliferation and loss of cell identity. H2A.Z alterations affect mainly proliferation-associated pathways. B) contribution of altered histone variants and their chaperones to the stages of tumour development. Adapted from (Ghiraldini et al., 2021).

### 1.3. Hormone regulation in breast cancer

Breast Cancer (BC) is a heterogeneous disease and differs greatly among patients. Even within an individual tumor, distinct cell types such as cancer stem cells (CSCs) can be distinguished from endothelial cells, infiltrating immune cells and stromal cells as well as a complex network of extracellular matrix (ECM), which defines spatiotemporal differences in the tumor microenvironment.

Classically, immunohistochemistry markers, together with clinicopathologic variables, are used for BC prognosis, prediction and selection of therapeutic treatment (Dunnwald et al., 2007; Walker, 2008). About 85 % of the tumors express any/or combinations of the commonly used markers: estrogen receptor alpha (ER $\alpha$ ), progesterone receptor (PR) and human epidermal growth factor receptor 2 (HER2). In fact, ER $\alpha$ -positive (ER+) tumors account for >70 % of BC cases (Masood, 1992).

Although epidemiological studies confirmed that estrogens are breast carcinogens, the exact contribution of steroid hormones to BC etiology is only partially understood. Estrogens play a major role in promoting the proliferation of both the normal and the neoplastic breast epithelium. ER $\alpha$  is the main nuclear receptor

involved in mammary gland morphogenesis. Accordingly, ER $\alpha$ + tumors require estrogen for their growth and respond to anti-estrogen treatment (e.g., tamoxifen) or aromatase inhibitors (Dunnwald et al., 2007). In contrast, the role of progesterone for growth regulation of BC is still controversial (Carroll et al., 2017). Progesterone treatment has been shown to be antiproliferative in ER $\alpha$ + PR+ BC cell lines (Musgrove et al., 1998; Rochfort et al., 1984). However, there is compelling evidence that inclusion of synthetic progestins as part of hormone replacement therapy increases the risk of BC, implying that PR signaling can contribute to tumor formation (Patten et al., 2018; Chlebowski, 2010).

### **1.3.1. Nuclear receptors**

To modulate gene expression, nuclear receptors act as ligand inducible transcription factors (TFs) by interacting as mono-, homo- or heterodimers with the DNA responsive elements localized in the proximity of target genes, or through a crosstalk with other cell signaling pathways. The final effects on transcription are mediated through receptor binding, interactions with other TFs and recruitment of coregulators, coactivators or corepressors.

#### **1.3.1.1. Steroid hormone receptors**

Hormones are molecules produced by the endocrine glands of vertebrates and other organisms. Depending on the tissue of secretion and the receptor involved, the physiological functions can be different. Several hormones and their receptors have been shown to play an important role in cellular events, including metabolic regulation, immune system responses, cell growth and development.

Steroid hormones (SH) are small cholesterol-derived hydrophobic molecules that can cross the cell membrane and activate their corresponding receptors. In mammals, SHs are grouped into progestogens, estrogens, androgens, glucocorticoids and mineralocorticoids. Once the SHs find their specific receptor they exert their regulatory effects in reproduction, differentiation, development, cell proliferation, apoptosis, inflammation,

metabolism, homeostasis and brain function (Mangelsdorf et al., 1995).

All SHR share a similar structure: a central short DNA-binding domain (DBD) composed of two zinc fingers; a C-terminal ligand binding domain (LBD) responsible for hormone binding and interaction with co-regulators (AF-2); and a N-terminal domain, that can be post-translationally modified to tune the receptors' functional activity (AF-1) (Figure I5) (Gronemeyer, 1992).

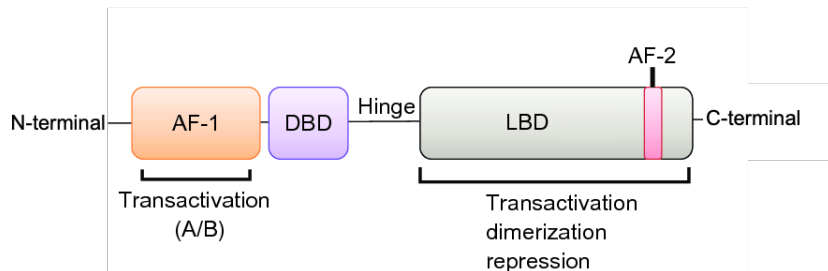


**Figure I5 General structure of steroid hormone receptors**

The N-terminal domain A/B contains the ligand-independent activation function (AF-1); the highly conserved DNA binding domain (DBD) recognizes specific DNA sequences (hormone responsive elements) and is located in the C domain, which also contains a dimerization and nuclear localization signal (NLS). Domain E (LBD and AF-2) is connected by the hinge region (D) and is responsible for ligand binding, dimerization, and also contains a ligand-dependent NLS.

### **1.3.1.2. Progesterone receptor**

The progesterone receptor (PR) is a nuclear SHR that mediates the physiological effects of progesterone (Pg). It is encoded by a single gene, but it produces two isoforms that differ in molecular weight: PR-A and PR-B by differential promoter usage (Kastner et al., 1990). In the absence of a proper ligand, unliganded SHR remain bound to molecular chaperones that will prevent its degradation and prepare them for an expected ligand (Pratt & Toft, 1997).



### **1.3.2. MMTV promoter as a model system for PR studies**

For many years, PR action studies were based on the Mouse Mammary Tumor Virus (MMTV) model. MMTV expression was shown to be regulated by progestins via the PR (Von der Ahe et al., 1985). Receptors like PR and GR bind cooperatively to DNA sequences of the MMTV long terminal repeat (LTR), upstream of the TATA box of the MMTV promoter (Scheidereit et al., 1983). Similar sequences are found in many other Pg-regulated genes, although at different locations relative to the gene promoter. The regions where the PR homodimer can bind to the DNA was identified as Hormone Response Elements (HRE) and contains the consensus sequence GGTAAnnTGTCT (Beato, et al., 1989). Downstream of the receptor-binding sequences is a palindromic binding site for nuclear factor 1 (NF1), important for efficient hormonal regulation. PR and NF1 synergize in an ATP-dependent process upon exposure to hormone. Thus, efficient MMTV induction depends on the proper nucleosome organization of its promoter (Chávez & Beato, 1997; Di Croce et al., 1999).

### **1.3.3. Chromatin remodeling and gene regulation in response to hormone**

The arrival of whole genome sequencing made it possible to explore the global landscape of PR occupancy over the entire genome and to correlate this with the changes in the transcriptome detected upon hormone exposure. In the breast cancer cell line T47D, thousands of PR-binding sites were identified through ChIP-seq upon 30 min of exposure to 10 nM R5020, and significant changes in expression of approximately 2000 genes using RNA-seq was observed (Ballaré et al., 2013). By using MNase-seq, it was found that most PR binding sites were located over regions of chromatin enriched in nucleosomes prior to hormone exposure. However, upon hormone there was a significant decrease in the number of MNase reads over the PR binding sites, suggesting nucleosome remodeling and gained sensitivity to MNase digestion (Ballaré et al., 2013).

Chromatin remodeling and gene expression induced by progestins are dependent on the activation of PR attached to the cell membrane that forms a complex with ER $\alpha$  and Src (Migliaccio et al., 1998). Five minutes after hormone treatment, Erk activation leads to phosphorylation of the PR, activation of Msk1, and recruitment of a complex of the three proteins to a nucleosome on the MMTV promoter. Msk1 phosphorylates histone H3 at S10, leading to displacement of HP1 $\gamma$  and recruitment of Brg1 and RNA polymerase II (Vicent et al., 2006).

In our model, the hormone-dependent gene activation process consists of two consecutive cycles, both involving the collaboration between activated kinases, histone modifying enzymes and ATP-dependent chromatin remodelers (Vicent et al., 2009; Wright et al., 2012). The first cycle occurs within 1–5 min after hormone exposure, involving CDK2/CyclinA-mediated phosphorylation and activation of PARP1, the MLL complex and the NURF complex. Ultimately leading to phosphorylation and PARylation of histone H1 and resulting in its displacement from chromatin. The second cycle takes place between 5-30 min after hormone exposure and requires the kinase MSK1, the acetyltransferase PCAF and the ATP-dependent chromatin remodeling complex BAF, leading to additional nucleosome remodeling and the displacement of histone H2A/H2B dimers (Figure I6) (Vicent et al., 2006). More recently, our lab discovered that hormone-activated chromatin remodeling also requires nuclear synthesis of ATP from ADP-Ribose and PPi by NUDIX5 (Wright et al., 2016).

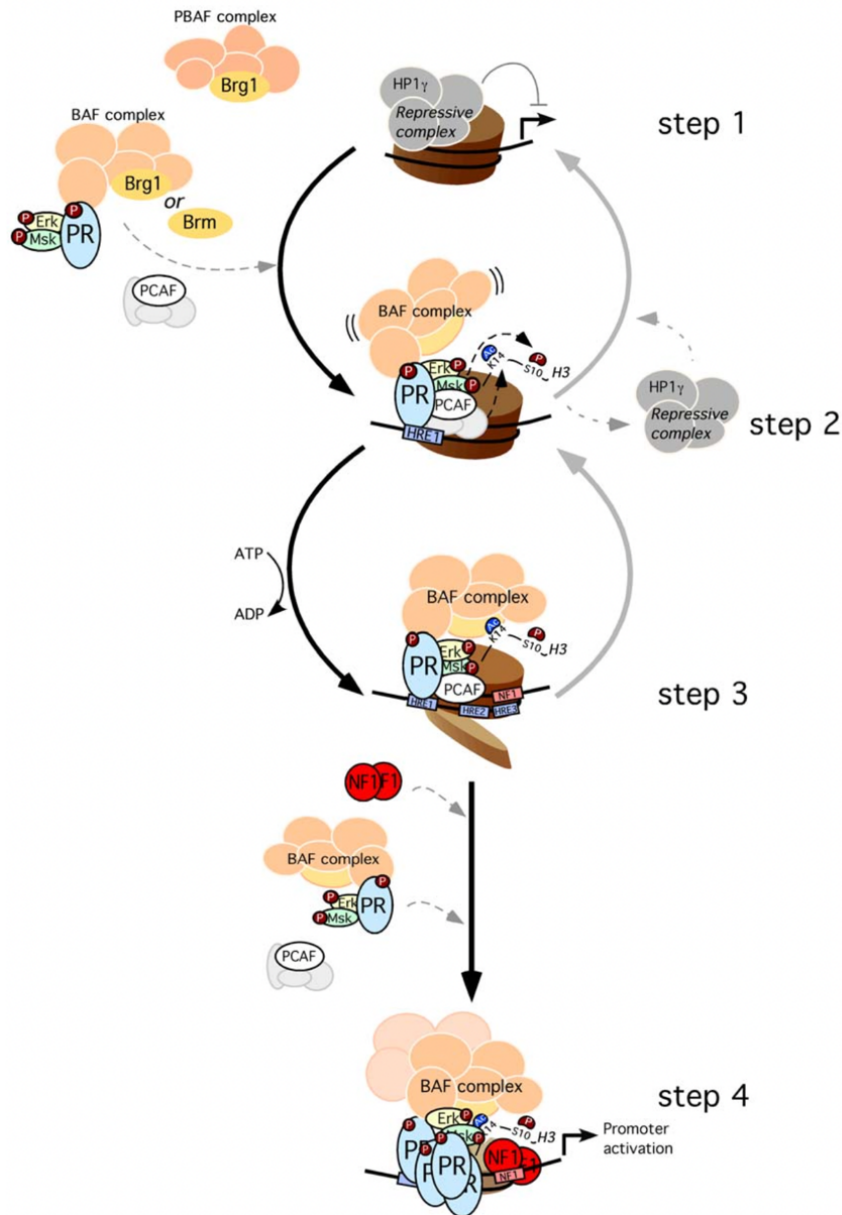


**Figure I6 Model for initial steps of MMTV promoter activation**

1) Before hormone addition the MMTV promoter is silent and associated with a repressive complex. 2) After hormone addition the activated complex pPR-pERK-pMsk1, and PCAF and BAF, are recruited to the MMTV promoter. Msk1 and PCAF phospho-acetylates H3 leading to H3S10phK14ac. 3) Displacement of the repressive complex and BAF complex anchoring, enables ATP-dependent H2A/H2B displacement. 4) The nucleosome opening facilitates NF1

binding to generate a stable platform of HREs for further recruitment of PR and BAF complexes, coactivator and eventually promoter activation. Consequent depletion of BAF prevents progression of the activation process to step 2: no histone displacement is observed, NF1 cannot bind and less PR/BAF complexes are bound to the promoter. Adapted from (Vicent et al., 2009).

It was found that in breast cancer cells, the unliganded PR binds genomic sites and targets a repressive complex containing HP1 $\gamma$ , LSD1, HDAC1/2, CoRest, KDM5B and the non-coding RNA, SRA (steroid receptor RNA activator). Upon hormone exposure and as a result of H3S10 phosphorylation by MSK1, the HP1 $\gamma$ -LSD1 repressive complex is displaced, allowing the recruitment of co-regulators needed for full de-repression (Vicent et al., 2013). On the other hand, in a subset of genes, hormone exposure leads to the recruitment of HP1 $\gamma$  and the ATPase BRG1 resulting in hormone-induced gene repression (Vicent et al., 2013). In this case, the active repression is mediated by BRG1-dependent deposition of linker histone H1.2 (Nacht et al., 2016).

#### **1.4. Role of the genome architecture**

At a higher level, chromatin is organized within the 3D nuclear space, efficiently packaging the genome allowing proper expression and replication of genes. Global molecular approaches like Hi-C are used to trace and measure all interactions between distant loci of the genome (Lieberman-Aiden et al., 2009).

Genome structure studies indicate the existence of two main principles involved in the formation and maintenance of the 3D genome organization: small compartmental domains that form as a consequence of the transcription/chromatin state and CTCF/cohesin loops.

##### **1.4.1. Chromosome territories**

It was suggested that DNA is organized in a defined volume, forming discrete entities inside the nucleus termed: chromosome territories (CTs) (Cremer & Cremer, 2001). Chromosomes conserved their individuality during interphase but with a certain possibility to overlap with its neighbors' regions. The chromosome

conformation capture (3C) technologies disentangled the genome topology at high resolution by detecting the physical interaction of DNA segments in the nuclear space.

The 3C methods are depicted in Figure 17. Basically, 3C consists of the following steps: (I) crosslinking of a cell population with formaldehyde promoting the covalent bonds between DNA fragments, (II) isolation and digestion of chromatin using restriction enzymes, (III) proximity ligation of restricted fragments, (IV) reverse crosslinking and DNA purification, and finally (V) assessment of the proximity ligation fragments by PCR or sequencing technologies which reflect the interaction frequency between pairs of genomic loci close in the 3D space (Dekker et al., 2002).

The original 3C method allows the deduction of interactions between one specific pair of loci (“one-to-one”), this then evolved into multiple techniques all with the same principle: 4C (“one-to-all”) (Simonis et al., 2006), chromosome conformation capture carbon copy 5C (“many-to-many”) (Dostie et al., 2006), and high-throughput 3C (Hi-C, “all-to-all”) (Lieberman-Aiden et al., 2009) among others not discussed here.

Hi-C, being the most popular, requires special steps: after DNA digestion, the overhangs are filled with biotinylated-nucleotides. Next, DNA is sheared and purified by biotin pull-down with streptavidin beads to ensure the exclusive capture of the biotinylated DNA junctions, which are then submitted to high-throughput sequencing and subsequent computational analysis.

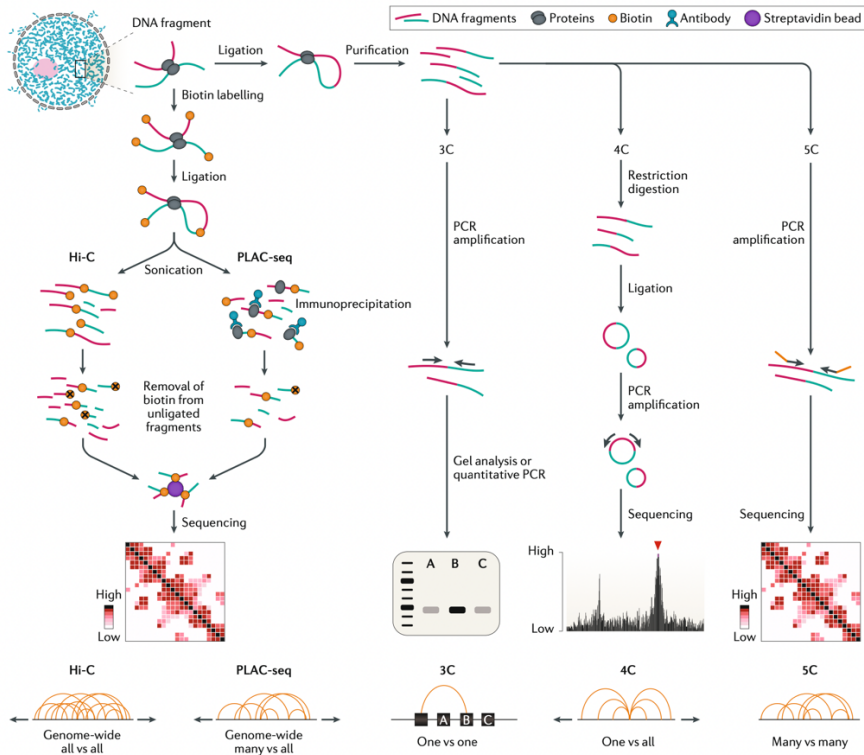


**Figure I7 3C and its derivatives**

Chromosome conformation capture (3C)-based assays measure the contact frequencies of DNA loci by proximity ligation of crosslinked chromatin. 3C-based assays involve fixation of the chromatin, isolation of nuclei and DNA fragmentation with restriction enzymes. In 3C, 4C and 5C, the crosslinked chromatin fragments are ligated, and the DNA is purified. In 3C, the interactions between two regions are detected through PCR with primers specific to the two regions of interest. In Hi-C and PLAC-seq, digested DNA fragments are labelled with biotin, ligated and fragmented by sonication. In PLAC-seq and Hi-C, DNA is purified, biotinylated nucleotides are removed from unligated fragment ends and all ligated DNA fragments are pulled-down. DNA fragments are sequenced and analyzed for interaction frequencies of all pairs of loci in the genome. Adapted from (Kempfer & Pombo, 2020).

The localization of CT in the nucleus, is determined by the position of a target chromosome relative to the center of the nucleus and appears to be evolutionarily conserved (Tanabe et al., 2002). The largest chromosomes are preferably located in the periphery of the nucleus while the shortest tend to be more internal. CTs near the

nuclear envelope are mainly associated with a decrease in gene expression and often repressed genes in chromosomes 2, 3, 8, 12, 13 are found attached to the nuclear lamina (Schneider & Grosschedl, 2007). On the other hand, gene-rich chromosomes (16, 17, 19 and 22) are localized in a central position in the nucleus (Boyle et al., 2001). Chromosomal arrangements can change during states of differentiation (Rozwadowska et al., 2013), DNA damage response (Mehta et al., 2013) and in response to changes in cellular homeostasis (i.e., in response to serum starvation or in the presence of a soft extracellular matrix) (Pradhan et al., 2018).

#### **1.4.2. Genome compartments**

With 3C technologies, it is possible to evaluate the *compartments* in individual chromosomes. The compartments are distinct sets of chromosomal regions that tend to interact preferentially with each other. Compartments are depicted as a checkerboard pattern that reflects the preference to keep close those loci that present the same interaction profile, epigenomic status and genomic content while separating them from those that have opposite features; establishing a functional segregation of the genome into, at least, two compartments.

Regions that present a similar pattern of active chromatin marks, DNaseI hypersensitivity, transcription activity, enrichment of RNA polymerase II, early replication domains, high GC content, and high gene density are categorized as **A compartments**. On the contrary, regions enriched in H3K9me2, H3K9me3 inactive chromatin marks, lamina-associated domains, late replication domains, and presenting low gene density are annotated as **B compartments**. By definition then, the A and B compartments are associated with the euchromatin (active) and heterochromatin (repressed), respectively (Lieberman-Aiden et al., 2009).

#### **1.4.3. Topologically Associating Domains (TADs)**

Metazoan genomes share a compatible organization of their chromatin in structures called “Topologically Associating Domains” (TADs). These are defined as linear units of chromatin that serve to spatially arrange enhancer–promoter interactions and control gene



expression levels, folding into discrete three-dimensional structures and favouring internal highly self-interacting chromatin regions (Dixon et al., 2012). According to the authors, TADs are delimited by sharp abrupt boundaries, enriched for housekeeping genes, transfer RNAs, short interspersed element (SINE), retrotransposons and the insulator binding protein CTCF; all factors that may have a role in establishing the TAD structure of the genome given its precise locations (Figure I8). TADs are defined by an elevated frequency of contacts within them and reduced contacts to loci found in adjacent TADs.

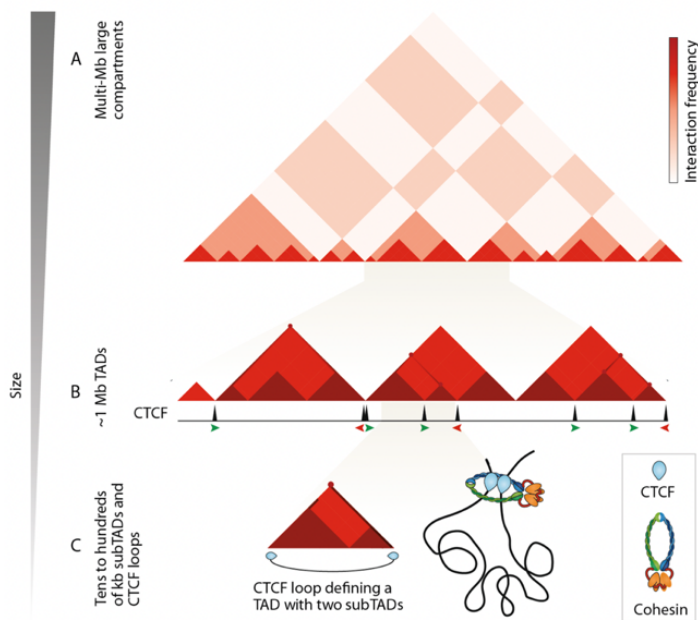


**Figure I8 Hierarchical organization of the chromatin at different levels of resolution**

A) Depiction of a Hi-C map, checkerboard pattern segmenting the genome into A/B mega-sized compartments. B) TADs contain smaller sub-TADs characterized by an increase of interaction frequencies. TADs are confined by a specific architectural protein called CTCF. C) CTCF loop, characterized by a strong dark peak on the Hi-C map. Its formation is a result of a looping structure established between DNA sequences that recruit two convergent CTCF motifs and the cohesin complex. Adapted from (Rowley & Corces, 2018).



Structurally, TADs appear as globular units formed by looping structures, isolated from the rest in the 3D space even if they are adjacent in the genome (Fraser et al., 2015). Functionally, they are considered “genomic regulons” that allow spatial proximity of the genes that work in a coordinated fashion (Le Dily et al., 2014). TADs have been described across species and in multiple cell types suggesting evolutionary conserved domains and an inherent principle of chromatin folding (Dixon et al., 2012).

In our lab we have used Hi-C to explore the role of genome topology in gene regulation by progestins. TADs 1 Mb in size, are not affected by exposure of breast cancer cells to progestins, but many of the hormone regulated genes are clustered in a subset of hormone responsive TADs. All coding and non-coding genes within a regulated TAD tend to respond in the same direction, suggesting that these TADs represent units of hormonal response (Le Dily et al., 2014). Hormone activated TADs expand in size and lose histones when exposed to hormone, while hormone repressed TADs become more compacted and enriched in histones (Le Dily et al., 2014). All the gene promoters within a TAD interact with a hormone control region (HCR) encompassing several PR- and ER $\alpha$ -binding sites. Around 200 HCRs in T47D cells were identified to interact with each other at long distances at higher frequency in the absence of hormone (Le Dily et al., 2019).

This view of the 3D genome organization suggests that transcription and architecture are closely interdependent and influence each other.

### **1.5. Towards a more physiological model to study breast cancer cell dynamics**

#### *Three-dimensional cell culture as a tool to overcome lack of microenvironment*

Over the years, 2D cultures have provided a rich amount of information on biology and disease. Yet, in recent years an increasing number of publications have shown that 2D cultures do not fully reflect the complexity of the microenvironment that cells

find in a tissue and provide supporting evidence of the need for a more complex 3D culture based on the presence of extracellular space (Figure I9).

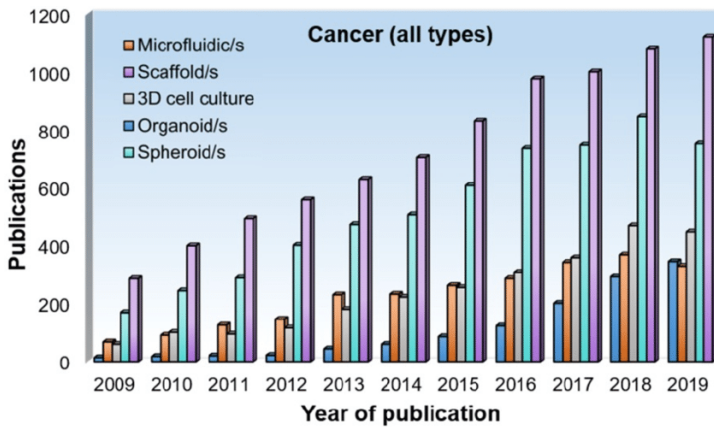


**Figure I9** A recent literature search in PubMed with the 3D culture related terms in combination with 'cancer' or 'tumor' in titles or abstracts

Adapted from (Bort et al., 2020).

3D culture systems are nothing new, they have been experimented on for decades (Figure I10). Yet, pioneered in the 1980s performing studies on the importance of the ECM in cell behavior and gene expression, it is now well-accepted that culturing cells in three-dimensional systems that mimic tissue is a better representation of an *in vivo* environment than simple two-dimensional monolayers (Pampaloni et al., 2007).

### **1.5.1. What is 3D cell culture?**

The function of a tissue is determined by both its *cellular* and *non-cellular* composition. In fact, as the cell culture system takes more into account these two conditions, the closer those cells will mimic the behaviors and responses of cells in the body. This makes 3D cell cultures appealing.

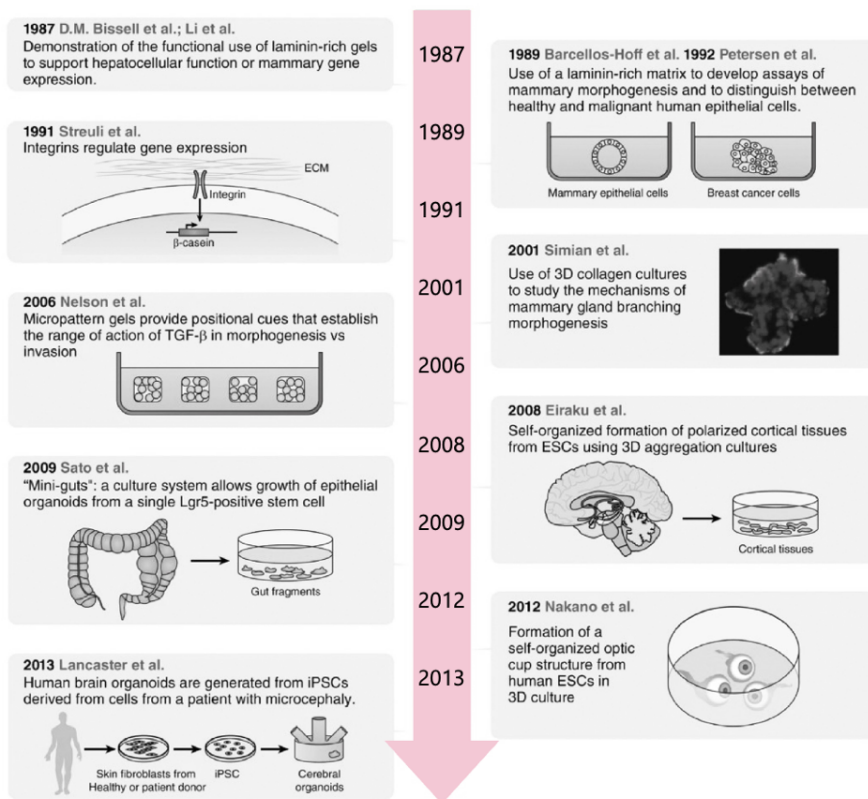


**Figure I10 Timeline of techniques and experiments leading to the current organoid field**

3D culture experiments using different gels have been experimented for over 30 years on different types of cells to study cell morphology, disease, molecular mechanisms, signal transduction and more recently for patient therapy. Adapted from (Simian & Bissell, 2016).

Cells *in vivo* are exposed to several external factors, a three-dimensional environment that exposes them to circulating molecules, neighboring cells, and the ECM. With these environmental cues in mind, biologists developed more physiologically accurate methods for culturing cells and tissues, including new media formulations and co-culture techniques. Back in the early days of cell culture, the most critical part of the method was to keep the cells alive and growing. Now, we have more ambitious goals: we want to pursue to keep the cells alive, growing and behaving as they would in the body tissue. By focusing on mimicking cell-matrix and cell-cell interactions, the 3D cell culture is

simply one step towards this goal. Thus, 3D cell culture offers an unparalleled ability to recreate physiological compositions and spatial arrangements of cells *in vitro*.

### **1.5.2. Mammary gland 3D culture**

The mammary acinus exists in the context of a rich stromal and ECM milieu that is constantly changing and is subject to different signaling cues. Breast cells in monolayers lose functional differentiation even in the presence of lactogenic hormones but when transplanted into the gland-free fat pads of mice they form tubular structures and are able to respond to the correct hormonal stimuli (Daniel & Deome, 1965).

The microenvironment surrounding mammary epithelial cells (MECs) exerts an essential role in driving their functional differentiation. In contrast to cells cultured on attached Col-I gels, MECs grown on floated collagen gels reorganized and formed secretory structures capable of *de novo* expression of milk proteins (Emerman et al., 1977; Lee et al., 1984). When cultured in laminin-rich matrices (lrECM), these cells clustered with apico-basal polarity and junctions, expressed the milk protein  $\beta$ -casein and expressed whey acidic protein (WAP) (Barcellos-Hoff et al., 1989). Laminin-111 (LN1) was shown to be the main component of the ECM that drives milk protein expression (Streuli et al., 1991) and promotes proper acinar polarity (Gudjonsson et al., 2002). Interestingly, the prolactin receptor required for milk proteins to be expressed, needs to be present in the appropriate mechanical and structural form in order to transmit the signal (Xu et al., 2009).

In addition to ECM and hormone signaling, the role of neighboring cells and intercellular interactions within the breast tissue are important for functional differentiation (Nguyen & Neville, 1998). Currently, mammary culture systems range from monotypic cell culture models grown in different 3D microenvironments to co-cultures of epithelial, endothelial and stromal fibroblasts, but also culturing them in different gels. These models are in constant evolution, trying to reach the full spectrum of cell-cell interactions found in the mammary gland and mimicking the breast tissue for biomedical research.

### 1.5.3. 2D vs 3D

Some of the main advantages for the increasing acceptance and use of 3D cell cultures include:

- *More relevant cell models:* 3D cell cultures are physiologically more relevant and predictive than 2D cultures. 3D cultures show a higher structural complexity and present a more accurate gene and protein expression pattern.
- *Interaction between different cells and with the extracellular matrix:* this allows the creation of complex system that can better model how cells interact *in vivo*.
- *Establishment of barrier tissues:* epithelia separate organ compartments and protect the organism from the environment. Representation of barrier tissues is greatly enhanced in 3D culture with the use of a matrix.
- *Better simulation of conditions in a living organism:* nutrients are present in a more heterogeneous manner than in 2D, meaning cells and organs grow in a more realistic manner.
- *Reduces use of animal models:* due to their own nature, animal systems are not always fully suitable to recapitulate the environment nor the biology of a human cell. Screening drugs using human organoids turns out to be a more reliable method.

As mentioned above, the study of cell behavior in general and in our case of breast cancer cells and their regulation by hormone in particular, is much more appropriate in 3D systems. Three components play a relevant and exclusive role in 3D: **i) the ECM, ii) cell-cell contacts and iii) the integration and transduction of given signals.**

#### **i) The extracellular matrix (ECM)**

The membrane of a cell is constantly interacting with a wide range of physical and chemical signals (Discher et al., 2005). Molecules that form the extracellular space include collagens, elastin, glycoproteins, glycosaminoglycans, proteoglycans, growth factors and other secreted proteins. Dynamic changes synchronized along these components are able to regulate cellular events like cell

cycle, differentiation, migration, survival, adhesion, cytoskeletal organization and cell signaling. This dynamic system is easily influenced by physiological effectors (i.e., growth factors, cytokines and hormones) and mechanical properties of the microenvironment (stiffness, tension and compression), making it a continuously changing system throughout development.

## **ii) Cell to cell contacts**

In 3D culture, cell–cell contacts are formed spontaneously and become stable. Cells interact with each other forming spheroids, and the anoikis-induced cell death signal is blocked (Lagies et al., 2020).

Cell adhesion molecules allow cells to communicate with one another or to the extracellular environment (Freemont & Hoyland, 1996). Cell–cell junctions regulate homeostasis in critical cell processes like tissue barrier function, proliferation and migration.

Apart from participating in the development and maintenance of tissue architecture, cell adhesion molecules serve as cell surface receptors critical for capturing, integrating and transmitting signals from the extracellular space into the cell (reviewed in Freemont & Hoyland, 1996). Disruption of cell-cell or cell-ECM adhesion significantly contributes to uncontrolled cell proliferation and distortion of normal tissue. More importantly, loss of cell adhesion contacts allows malignant cells to detach and escape from the primary tumor.

## **iii) Integration and transduction of signals from the environment**

Focal adhesions have very dynamic function. For migration to occur, a cell must extend a protrusion to make an initial contact with the ECM. Membrane protrusion is stabilized by small adhesive foci that contain paxillin followed by  $\alpha$ -actinin (Edlund et al., 2001). Initial foci of adhesion grow into focal complexes abundant in tyrosine phosphorylation, and containing integrin, talin, paxillin, vinculin and FAK. Subsequently, zyxin and tensin are recruited to these complexes as they remodel into focal adhesions, which stabilize the protrusion (Zaidel-Bar et al., 2003).

FAK is the key signaling component of focal adhesions. It is a tyrosine kinase that can be phosphorylated in response to Src transformation (Schaller et al., 1992). It is activated via autophosphorylation at tyrosine 397 (Y397) initiated by integrin engagement with its ligand (Schaller et al., 1994). When phosphorylated, FAK Y397 becomes a binding site for the tyrosine kinase Src, which then phosphorylates FAK at Y576 and Y577 to further activate FAK kinase activity (Calalb et al., 1995).

An elegant study by Choquet et al. (Choquet et al., 1997) used optical tweezers to physically hold fibronectin-coated beads attached to the cell through integrins to demonstrate that the strength and rigidity of the link between the integrin and the cytoskeleton increases proportionally to the amount of restraining force placed on the bead. These findings demonstrated that the physical rigidity of the ECM can regulate focal adhesion formation. Relative to cancer, an increase in cell stiffness was found to enhance integrin/FAK signaling pathways leading to tumor hyperproliferation and increased motility (Paszek et al., 2005).

Even though focal adhesions are well-characterized structures, most studies have investigated tissue culture cells plated on a two-dimensional surface. However, epithelial cells maintain contact with basement membrane, which includes several different ECM proteins. As a consequence, different integrins are activated, resulting in the integration of multiple signaling pathways. Plating cells on a Petri dish, imposes a physical environment that differs from physiological conditions and the existing focal adhesions of the cell. Studies using 3D matrices show that cells form 3D matrix adhesions different from their 2D counterparts, suggesting that these different focal adhesions will alter signaling events in 3D to regulate cell behavior and phenotype (Cukierman et al., 2002).

## **1.6. Mechanotransduction**

Mechanotransduction is the ability of a cell to sense mechanical cues from its microenvironment and convert them into biochemical signals to promote adaptive transcription, cell responses and homeostasis. In this way, cells are then able to adapt to their

microenvironment by fine-tuning their mechanical properties (Vogel & Sheetz, 2006).

As stated before, living cells can *sense* mechanical forces or deformation, and convert them into biological responses.

The mechanosensing machinery can be broadly classified into two groups: (i) **proximal mechanosensing** apparatus: which is composed of cell surface receptors, focal adhesion (FA) complexes including integrins, cell–cell junctions, and the actomyosin cytoskeleton, and (ii) **proteins of the nuclear envelope**.

The process of mechanosensing has been described in adherent cells. The integrins connect the cell to the ECM through maturation of focal adhesion (FA) complexes, which can sense the rigidity and geometry of the ECM (Stutchbury et al., 2017). Stretch-activated receptors receive the signal and adapt their permeability for extracellular ions (Coste, et al., 2012). Cell–cell junction complexes, adherens junctions (AJs) and tight junctions (TJs) serve as mechanosensors of adhesive contacts between cells (Figure I11), and finally through adaptor proteins such as  $\alpha$ -actinin, talin, and vinculin FAs are physically connected to the actin cytoskeleton.

External cues are transduced through secondary messengers to activate transcription factors. These TF are then transduced to their DNA target sites inside the nucleus.

The transmission of biochemical signals is facilitated by cytoskeletal remodeling. Such is the case of the actomyosin cytoskeleton remodeling in the transduction of YAP/TAZ - Hippo pathway (Panciera et al., 2017). The cytoskeleton networks connect the cell membrane and the nucleus through the linker of nucleoskeleton and cytoskeleton (LINC) complex, allowing the direct transmission of mechanical signals. These networks are attached to the nuclear membrane on one side and link to the adhesive complexes of the ECM and cell–cell junctions on the other side (Starr & Fridolfsson, 2010). Thus, the actin cytoskeleton is itself a highly dynamic and polymorphic structure that rapidly reorganizes itself in response to mechanical stimuli (Blanchoin et al., 2014).



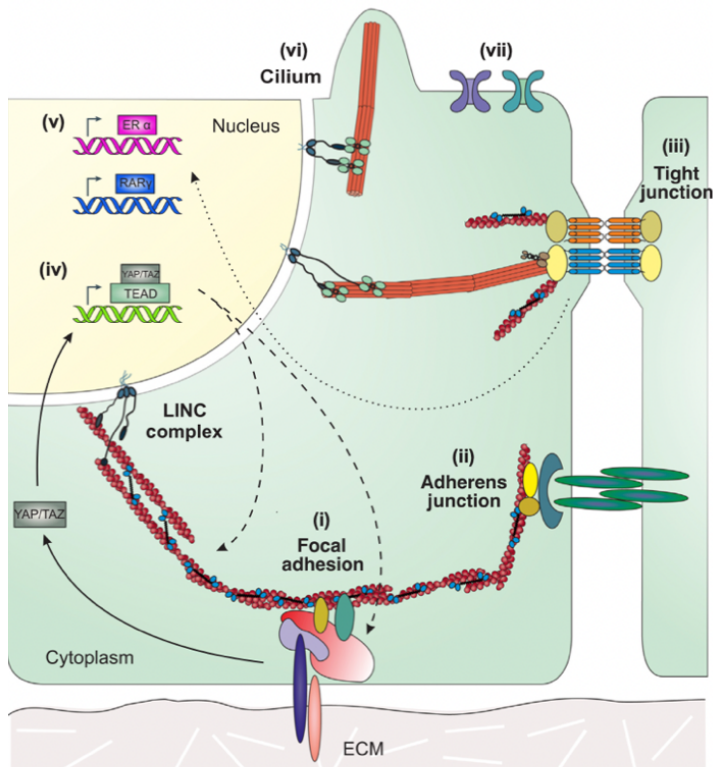


**Figure I11 Physical links between ECM and nucleus**

The cell responds to external mechanical stress through mechanosensitive transmembrane junctions. From the ECM: (i) Integrins connect the cytoskeleton to the ECM through vinculin, talin, paxillin, and adaptor proteins within FA. (ii,iii) Mechanical forces between neighboring cells are transmitted to the cytoskeleton through cell-cell junctions. (iv) Cell-matrix and cell-cell junctions transmit external forces via the cell cytoskeleton to the nucleus through LINC complex. An example of integrin control: YAP/TAZ phosphorylation, regulating its nuclear translocation and subsequent transcriptional regulation of the Hippo pathway through TEAD TF. (v) Cell-cell junctions activate Src family kinases, followed by regulation of nuclear receptors like RAR $\gamma$  and ER $\alpha$ . (vi) Microtubules sense and transmit physical forces through the LINC complex. Adapted from (Wagh et al., 2021).

Nesprins are a family of proteins found primarily in the outer nuclear membrane (ONM) and are connected to LINC proteins at the inner nuclear membrane (INM) forming a physical bridge between both layers (Figure I12) (Rajgor & Shanahan, 2013). The SUN-domain proteins in the INM, are in turn connected to the nuclear lamina and chromatin, providing a direct physical signal

transmission from the cell membrane into the nucleus (Sosa et al., 2011).

Nuclear lamins are filaments that provide structural integrity to the cell nucleus. In fact, there are two types of nuclear lamina, A/C and B and the levels of expression of each type can alter nuclear stiffness and cell geometry (Makhija et al., 2016) (Swift et al., 2013).

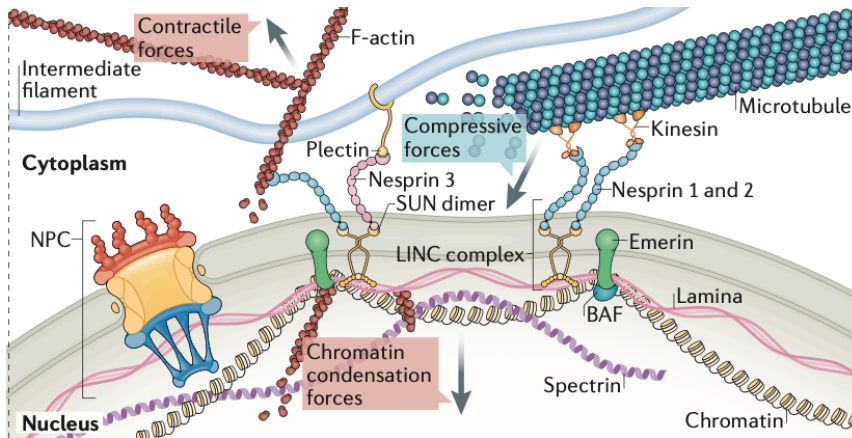


**Figure I12 The cell microenvironment and mechanosensing**

Link of cytoskeleton and nucleus through the LINC complex. Nesprins on the ONM physically link with actin, microtubules and intermediate filaments. On the inner side of the nuclear membrane, nesprins find dimers of SUN proteins, which then link to the nuclear lamina and chromatin. Adapted from (Uhler & Shivashankar, 2017).

The actin cytoskeleton and nucleus act together to sense mechanical forces and allow cells to adapt to these forces. The nucleus physically adapts to applied stress in order to protect the genome (Guilluy et al., 2014).

Interestingly, studies have revealed that lamin A/C phosphorylation and turnover are determined by the topography and rigidity of the extracellular matrix. Cells grown on rigid substrates have higher levels of lamin A/C than their counterparts grown on soft substrates (Buxboim et al., 2014). These cells also present stronger actin mediated links to the nucleus than those growing on soft substrates determining the size and shape of the cells (Kim & Wirtz, 2015).

Importantly, the delicate balance between the contractile and compressive forces by actin and microtubules, determines the nuclear morphology and affects gene expression.

Mechanical forces modulate nuclear and chromatin dynamics through physical links as well as biochemical pathways, which tune histone PTM and chromatin structure and lead to differential accessibility of transcription factors to gene-regulatory regions on DNA.

### **1.6.1. Mechanoregulation of gene expression**

In addition to serving as physical links between the cell and ECM, FAs also regulate expression of mechanosensitive genes (Kechagia et al., 2019). The Hippo signaling proteins YAP and TAZ, often used as reporters of mechanotransduction (Figure I11), are key mechanosensitive transcriptional coregulators that alter their subcellular localization in response to extracellular cues (Dupont et al., 2011). For instance, cells that experience increased stiffness of the environment, tend to present nuclear YAP/TAZ, regulating hereafter cell proliferation, organ growth, and tumorigenesis (Pancieria et al., 2017). Upon integrin binding to fibronectin in the ECM, focal adhesion kinase (FAK) regulates YAP localization via the FAK/Src/PI3K pathway (Kim & Gumbiner, 2015).

Cells have been found to activate different genes, change their nuclear shape, proliferation, differentiation and apoptosis when they are subjected to shear, compression or stretch (Humphrey et al., 2014; Kutys & Chen, 2016), to different surface topographies (Jain et al., 2013) or to different substrate rigidity (Engler et al., 2006). This suggests three possible, non-exclusive mechanisms by which the microenvironment can regulate gene expression: control of the nuclear import of different TF, alteration of 3D nuclear organization and chromosome intermingling, and spatiotemporal mechanoregulation of gene clustering (Figure I13).

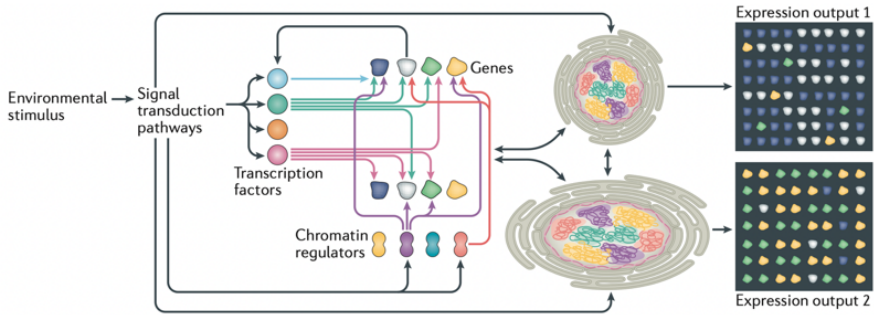


**Figure I13 Regulation of genome structure and gene expression by mechanotransduction**

Environmental signals can affect changes at all levels of the cell. In the nucleus, extracellular activated signaling pathways, shuttling of TF and physical state of the cell will produce a different expression output. Adapted from (Uhler & Shivashankar, 2017).

Naturally, these changes in gene expression profiles in return modulate the microenvironment by changing cellular contractility and adhesion, secreting structural proteins, and regulating surrounding cells to create a feedback loop between the transcriptome and the mechanical properties of the environment. These reciprocal interactions are finely tuned to maintain homeostasis. Disruption of this balance can cause tissue deformation and the onset of several pathologies including cancer (Friedl & Alexander, 2011).

### 1.7. Current approach: hydrogels

An ideal 3D culture model should recapitulate a tissue-specific physiological microenvironment (healthy or diseased) where cells are able to proliferate, interact and differentiate as they do in the original tissue. This model has to include cell-to-cell and cell-to-ECM interactions, specific stiffness, oxygen, nutrient and metabolic waste gradients (Griffith & Swartz, 2006).

Scaffold-based culture technologies provide physical support, ranging from simple mechanical structures to ECM-like matrices, on which cells aggregate, proliferate and migrate. Hydrogels can be obtained from natural sources or they can be synthetic, with the possibility of mixing them to obtain hybrid hydrogels possessing

new physical and biological properties according to the needs of the proposed study.

### **1.7.1. The stiffness in the environment of tumor cells**

Changes in ECM composition is accompanied by physical changes in rigidity, leading to bidirectional changes in cells and the ECM. The elastic modulus of normal mammary gland tissue is 100–200 Pascals (Pa), while malignant mammary tumors have been measured to be as stiff as 1000 to 4000 Pa (Levental et al., 2009; Paszek et al., 2005). Tumor stiffness increases over time as a tumor develops and it correlates well with disease progression due mainly to extracellular matrix remodeling.

Both healthy and malignant mammary epithelia, can be modeled *in vitro* by culturing them in different available hydrogels that recapitulate essential composition and mechanic features of an *in vivo* microenvironment. Non-malignant mammary epithelial cells, grown in reconstituted basement membrane extract (Matrigel), form acini, spheres that are multicellular, polarized with lumen, which represent the basic functional unit of the mammary gland. On the contrary, malignant cells cultured in these gels create a range of morphologies from multicellular clusters to invasive-like masses (Kenny et al., 2007) (Figure I14).

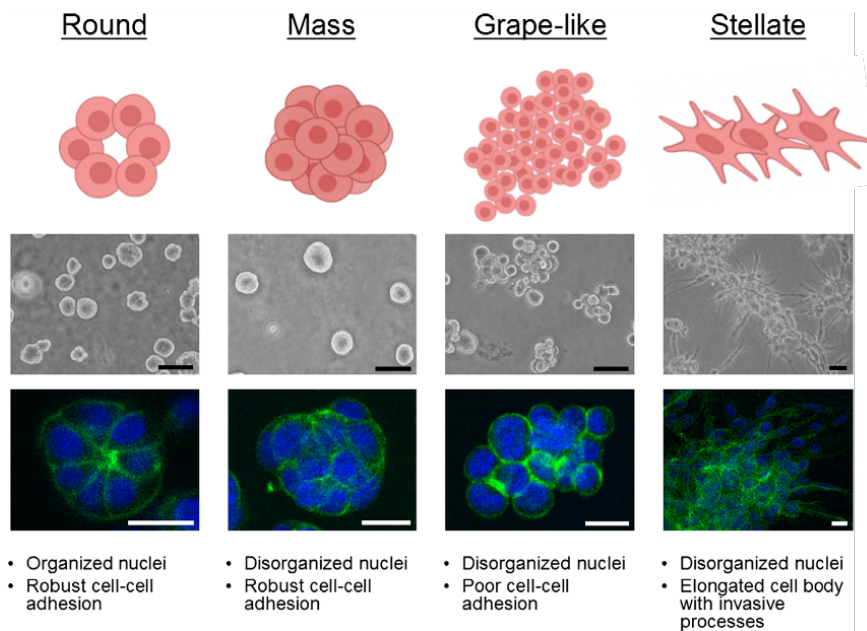


**Figure I14 Different types of cancer spheroid growth on Matrigel**

Description of the different morphologies spheroids adopt when cultured in the Matrigel. Commonly used cell lines are able to form round or mass-like spheres, while others are incapable of growing in this orderly manner and only aggregate as grape-like clumps or in stellate unorganized shape. Adapted from (Kenny, 2007).

Matrigel has an elastic modulus of 175 Pa. Similarly, other commonly used gels in 3D culture are also able to form acini from MCF10A cells in soft gels (90 Pa) and adopt malignant and invasive phenotypes in stiffer gels (945 Pa). Therefore, modulating the elasticity of the gel will promote differences in cell behavior.

In 2017, Stowers et al. studied the effects of matrix stiffening on MCF10A cells. Acini in control gels formed a basement membrane, that became disorganized upon stiffening-induced invasion. Besides invasion, stiffening also increased the size of their MCF10A acini, suggesting a loss of growth-arrest signals and induction of cell proliferation; features that can be observed in cancer cells grown in 3D gels and in *in vivo* tumors (Stowers et al., 2017).

### **1.7.2. Organoids or spheroids? Depends on the context**

Even though the use of 3D cell culture is relatively new, the different methods in which these can be studied present a wide range of options. The term organoid in its origin referred to primary cultures of tissue fragments separated from the stroma within 3D gels to form organ-like structures (Simian & Bissell, 2017). Over the past decade, the term has broadened and now encompasses a variety of tissue culture techniques that result in self-organizing, self-renewing 3D cultures derived from primary tissue, embryonic stem cells, cell lines or induced pluripotent stem cells that have a similar functionality as the tissue from which the cells originate.

Organoid cultures have been described for a variety of organs, including normal tissue and disease models of the digestive tract, breast, prostate, lung, kidney and the brain (reviewed in Clevers et al., 2016; Dutta et al., 2017; Fatehullah et al., 2016).

Despite advances, further studies on chromatin topology, nuclear architecture, transcription factor kinetics, and gene regulation in response to mechanical forces in tissues are still missing. Thus, 3D models constitute a good approach to recreate more physiological conditions and to perform global analysis.

Complementary to microscopy, ChIP-seq and Hi-C provide insight into the organization of chromatin. Moreover, ATAC-seq which allows the mapping of accessible genomic regions, is especially suitable for mechanobiology assays to examine how 3D chromatin architecture adapts to 3D context. These studies can be used in parallel with mechanobiology assays (i.e., measuring the effects of cell geometry and substrate rigidity) to uncover the spatiotemporal context of gene expression patterns (Asp et al., 2019).

Studies beginning with Mina Bissell's pioneering work on dynamic reciprocity (Bissell et al., 1982) have delineated differences between 2D plastic cultures and *in vivo* conditions. However, a need for application of such *state-of-the-art* techniques to cells grown in clusters, tissues, organs, or even *in vivo* is required. Elucidating how mechanical forces regulate transcription is the first step to obtaining a broader understanding of how cells integrate and respond to physical cues.





## 1.8. Objective of the PhD project

Our group is interested in studying steroid hormone action in breast cancer cells; specifically, how signals are transduced to the nucleus and modulate chromatin structure and gene expression.

In order to understand how the extracellular matrix, cell-cell contacts, the stiffness of the microenvironment and the mechanical forces affect nuclear function, we will carry out an extensive characterization of breast cancer cells grown as 3D spheres in Matrigel. This objective will be achieved by using techniques that allow us to evaluate global changes in gene expression, genome structure, chromatin accessibility and binding of key transcription factors. The results obtained will be contrasted with similar studies performed on cells grown as a monolayer.

Thus,

- We will provide a characterization of breast cancer spheroids grown in the matrix (Matrigel).
  
- We will study the impact of the 3D growth on nuclear structure and function; with an emphasis in chromatin remodeling, nuclear factors affected by the presence of the extracellular matrix (ECM) and the enriched pathways controlled by the mechano-regulation provided by the ECM.
  
- Once the 3D system is characterized, I will investigate the hormonal response of breast cancer spheroids compared to the conventional 2D cell culture.



## 2. Materials and methods

### 2.1. Materials

#### Chemicals and reagents

Table 1. Chemicals and reagents

Name	Supplier
$\beta$ -Mercaptoethanol 50mM	GIBCO by Life Technologies
Agarose, ultra-pure	Sigma-Aldrich Life Sciences
BSA	Sigma-Aldrich Life Sciences
DAPI	Sigma-Aldrich Life Sciences
DMSO	Sigma-Aldrich Life Sciences
EDTA	-
Ethanol absolute	Chemsolute
Fetal Bovine Serum (FBS)	BioScience LifeSciences
Formaldehyde 37 %	Sigma-Aldrich
Glycine	Sigma-Aldrich Life Sciences
IGEPAL NP40	Sigma-Aldrich Life Sciences
L-Glutamine	GIBCO by Life Technologies
Matrigel® Growth Factor Reduced (GFR) Basement Membrane Matrix - 356230	Corning Life Sciences
Matrigel® Growth Factor Reduced (GFR) Basement Membrane Matrix, Phenol Red-free - 356231	Corning Life Sciences
Methanol	Chemsolute
MgCl <sub>2</sub>	-
Mowiol 4-88 mount medium	Sigma-Aldrich Life Sciences
NaCl	-
Pen/Strep (100x)	GIBCO by Life Technologies
PBS	-
PFA 16 %	Alfa Aesar, Thermo Fisher Scientific

SDS 10 %	Calbiochem
Tris-HCl	-
Triton X-100	Sigma-Aldrich Life Sciences
TRULI (LATS inhibitor)	CSNpharm
Trypsin-EDTA 0.05 % (1x)	GIBCO by Life Technologies
Trypsin-EDTA 0.25 % (1x)	GIBCO by Life Technologies
Water RNase-, DNase- free	Sigma-Aldrich Life Sciences

### Buffers and solutions

All buffers and solutions described below were prepared using MQ (Millipore) water.

- RIPA Buffer (protein lysis): 25 mM Tris HCl pH 7.6, 1 % SDS, 1 mM EDTA, 1 mM EGTA, protease inhibitors, PIC (Protein Inhibitor Cocktail, ROCHE).
- Lysis Buffer I (LBI): 5 mM PIPES pH 8, 85 mM KCl, 0.5 % NP40, 1x protease inhibitors.
- Lysis Buffer II (LBII): 1 % SDS, 10 mM EDTA pH 8, 50 mM Tris-HCl pH 8, 1x protease inhibitors, PIC.
- Elution Buffer (ChIP) (EB): 1 % SDS, 0.1 M NaHCO<sub>3</sub>.
- Hi-C lysis buffer (Hi-C LB): 10 mM Tris-HCl pH 8; 10 mM NaCl; 0.2 % NP40; 1x protease inhibitors.
- RBS buffer (ATAC-seq): 10 mM Tris-HCl pH 7.4, 10 mM NaCl, 3 mM MgCl<sub>2</sub>.
- IF solution: PBS 5 % BSA, 0.5 % Triton.
- RBS buffer (MNase): 10 mM Tris-HCl pH 7.4, 10 mM NaCl, 3 mM CaCl<sub>2</sub>.

Table 2. Culture media

DMEM for MCF7 cells	DMEM red (1x), 10 % Fetal Bovine Serum, Penicillin (100 U/ ml)/Streptomycin (100 mg/ ml), Sodium Pyruvate [2 mM].
F-12 for MCF10A cells	DMEM/F12, Horse Serum 5 %, EGF (20 ng/ ml), hydrocortisone (0.5 µg/ ml), cholera toxin (100 ng/ ml), Penicillin (100 U/ ml)/Streptomycin (100 mg/ ml), Insulin (10 µg/ ml).

Basic RPMI red	RPMI 1640 red medium (1x), L-Glutamine [2 mM], (100x) Penicillin (100 U/ ml) /Streptomycin (100 mg/ ml), 10 % Fetal Bovine Serum.
RPMI for ZR75 cells	RPMI 1640 red medium (1x), (100x) Penicillin (100 U/ ml) /Streptomycin (100 mg/ ml), 10 % Fetal Bovine Serum.
RPMI white	RPMI 1640 white (phenol-red free) medium (1x); L-Glutamine [2 mM], Penicillin (100 U/ ml)/Streptomycin (100 mg/ ml), 10 % dextran-coated charcoal treated FBS (DCC/FBS).
RPMI white 0 % FBS	RPMI 1640 white (phenol-red free) medium (1x); L-Glutamine [2 mM], Penicillin (100 U/ ml) /Streptomycin (100 mg/ ml).

### Cell lines

Table 3. Cell lines

Name	Origin
BT474	ATCC Manassas, Virginia, USA
HEK293 (for infection)	ATCC Manassas, Virginia, USA
MCF-7	ATCC Manassas, Virginia, USA
MCF10A	ATCC Manassas, Virginia, USA
T47D cell clone 3.17 containing a single copy of the MMTV promoter	ATCC Manassas, Virginia, USA
ZR-75	ATCC Manassas, Virginia, USA

### Primers

Table 4. Primers used for ChIP qPCR analysis.

Gene	Forward primer Sequence (5'-3')	Reverse primer Sequence (5'-3')
<i>DUSP1</i>	GAGGTTAGGCAATCTG TCCAAAG	ATAAGGAAGAAAATGA GAGGAAC

<i>EGF</i>	GAATCTCTGGACTCTGT TCTCAGGTA	CTAGGACTATGTCATT AGCAGATCAG
<i>EGFR</i>	GCGTGAGACACAAACA TTCCAAACTGTA	GTTCAAGCAATGGGAT CGAGTTGTT
<i>FSIP1</i> (Site #1)	GGCTAACCGAATTCAC CACCT	TTTGGGAAGGCCATAG TGGAG
<i>GREB1</i>	CAGCTGACTGTCTTCC ACCA	CCACCGTTTCGTGTCT TCTT
<i>KRT23</i>	GGAAAGCCAGCTCAGA ACCAG	TGGAAGGTTTCGGTCAT TCCAT
<i>MMTV</i>	GGTTACAAACTGTTCTT AAAACGAGGATG	GGTTTACATAAGCATT TACATAAGATTTGG
<i>NEMF</i> (Site #2)	GCAGGTAGGCCAGTCA GATG	TTACTAGCCAAAGTGC TGCCA
<i>BLC2L1</i> (Peak A)	GCCTGAATTTATCCACC TGTACG	CTGTGTCTCCCCTAG AATGTCAGC
<i>SAT_1</i> (Site #3)	CCAGAGCTCCTGAGTT TGCT	AACCCGGAGGACAAA AGTG

## Antibodies

Table 5a. Antibodies

Detects	Name	Company	Used for
$\beta$ -catenin	138400	Thermo-Fisher	IF
BRG1	ab110641	Abcam	WB
Cdx2	A300-691A	Bethyl laboratory	WB
CTCF	07-729	Millipore	WB, ChIP
E-cadherin	13-1700	Thermo Fisher	IF
ER $\alpha$	H20	Santa Cruz	WB, IF
FAK (PTK2)	3285	Cell signaling	WB
H3	ab1791	Abcam	WB
H3K27ac	ab4729	Abcam	ChIP
H3K9me2	ab1220	Abcam	IF
H3K9me3	ab8898	Abcam	IF
Ki67	550609	Becton Dickinson	IF
LATS	3477	Cell signaling	WB
LATS-S909	9157	Cell signaling	WB
LSD1	ab17721	Abcam	WB

pFAKT397	ab81298	Abcam	WB
pPRs294	Ab61785	Abcam	WB, IF
PR	H190	Santa Cruz	WB, IF, ChIP
pYAP127	4911	Cell signaling	WB
Tubulin	T9026	Sigma-Aldrich	WB, IF
YAP1	sc-101199	Santa Cruz	WB, IF

Table 5b. Secondary antibodies

<b>Name</b>	<b>Origin</b>
Alexa Fluor® 488 donkey anti-rabbit IgG (H+L)	Invitrogen by Life Technologies
AlexaFluor® 594 goat anti-mouse IgG (H+L)	Invitrogen by Life Technologies
NA931V ECL Anti-mouse horseradish peroxidase linked whole antibody	Amersham
NA934V ECL Anti-rabbit horseradish peroxidase linked whole antibody	Amersham

### Kits

Table 6. Commercial kits

CellTiter-Glo® Luminescent Cell Viability Assay Promega-G7571
Live/dead cell imaging kit Cat. R37601
Nextera Tn5 Transposase, Illumina Cat. FC-121-1030
Ovation® Ultralow System V2 – NuGEN Cat. 0344
Qiagen MiniElute Kit Cat. 28004
Qiagen RNeasy mini-Kit Cat. 74134
Quantas cDNA Cat. 95047-100

Table 7. shRNA Vectors obtained from MISSION™ shRNA Library (Merck)

<b>Vector reference</b>	<b>Protein to KD</b>
TRCN00000358357	CDX2
TRCN00000013687	CDX2
TRCN0000001777	LATS
TRCN0000001779	LATS
TRCN0000019898	YY1

TRCN0000019894	YY1
TRCN0000020207	ZBTB7B
TRCN0000020208	ZBTB7B
TRCN0000004926	TFAP2A
TRCN0000004922	TFAP2A

## 2.2. Methods

### Cell culture and hormone exposure

#### Thawing of cell stocks

Frozen cryostocks of T47D cells ( $1.5 \times 10^6$  cells/ml) were removed from  $-80$  °C and thawed in ice. Next, the cells were transferred to 6 ml of pre-warmed medium containing 10 % FBS and pelleted by centrifugation (5 min, 112 xg). The entire volume of the supernatant (containing cytotoxic DMSO) was discarded, the resulting pellet was resuspended in 5 ml of medium and seeded in a p100 plate. The cells were maintained in culture with medium change and split every three days for at least a week at 37 °C and under a humidified atmosphere at 5 % CO<sub>2</sub> before being used for subsequent experimental work.

#### Splitting of cells

Monolayered cells were split every 3-4 days upon reaching 75-80 % confluency by washing with PBS and trypsinizing with 3 ml of 0.05 % Trypsin/EDTA for 5 min at 37 °C. Digestion was stopped by adding 7 ml of medium containing FBS and cells were separated to a single cell stage by carefully pipetting up and down. Subsequently, cells were seeded in p150 plates for 2D culture or p60 plates coated with Matrigel for 3D culture.

#### 2D cell culture

For 2D monolayer culture, 4 million cells were plated on p150 plates containing RPMI 1640 red medium and harvested after 3 days for each assay.

When measuring effects of the hormonal exposure, cells were deprived of phenol red by changing the medium to RPMI white medium supplemented with dextran-coated charcoal treated Fetal Bovine Serum (FBS) for 48 h prior to an overnight starvation RPMI



without FBS. Then, cells were exposed to 10 nM R5020 for x time depending on the assay.

### **3D cell culture on Matrigel**

The Matrigel was thawed overnight at 4 °C on ice. The seeding procedure took place on ice. Prechilled p60 plates were coated with a thin layer of Matrigel slowly pipetting the appropriate volume onto the surface and spread evenly and carefully on the plate area not touching the walls of the dish. Plates were then incubated for 20–30 min at 37 °C to allow the Matrigel to polymerize without over drying. Trypsinized cells were resuspended to obtain a single cell suspension. 200,00 cells were diluted in 4 mL of medium and plated on-top of the Matrigel without disrupting the capsule. Culture was maintained for 10 days changing medium every 2-3 days.

For hormonal induction on the 3D spheroids, T47D cells were plated on top of phenol red-free Matrigel and after 7 days of culture the cells were deprived of phenol-red by changing the medium to RPMI white medium supplemented with dextran-coated charcoal treated FBS for 48 h prior to an overnight starvation of FBS in fresh white medium. As mentioned before cells would then be exposed to 10 nM R5020 for x time depending on the assay.

### **3D spheroids harvest**

Colonies were fully extracted from the 3D matrix for further analyses. All following steps were performed on ice. Dishes were rinsed twice with PBS followed by addition of 3 mL ice-cold PBS-EDTA. Matrigel including the 3D colonies was carefully detached with a plastic scraper and left on ice for 30 min to allow complete depolymerization of the gel. Liquid solution was transferred to a conical tube, centrifuged for 5 min at 112 xg and rinsed twice with 0.5 volume of PBS-EDTA. Pellet was then ready to be processed for the following assay.

### **RNA extraction for RT qPCR and sequencing**

RNA extraction was performed using the RNeasy Mini Kit (Qiagen cat. no. 74134) following provided protocol instructions. Briefly, T47D cells were placed on ice for 30 min to allow Matrigel to dissolve in PBS-EDTA solution. Cells were then harvested as a cell pellet, lysed with Buffer RLT and immediately centrifuged for 2

min at maximum speed. The resuspension was then washed once with 1 volume of 70 % ethanol and placed in a RNeasy Mini spin column in a collection tube for a brief centrifuge. The column was then washed once with Buffer RW1 and twice with RPE Buffer. The RNA was collected by adding 30  $\mu$ l RNase-free water followed by a brief centrifugation. The RNA obtained was quantified with a NanoDrop and was ready for subsequent assays as cDNA synthesis and RNA sequencing.

### **cDNA synthesis**

The synthesis of DNA from an RNA template, via reverse transcription, produced complementary DNA (cDNA). Reverse transcriptases (RTs) used an RNA template and a short primer complementary to the 3' end of the RNA to direct the synthesis of the first strand cDNA, which could be used directly as a template for the Polymerase Chain Reaction (PCR) in gene transcription studies. A kit from Qantas was used for cDNA synthesis. Briefly, 500 ng of RNA were incubated with qScript reaction mix and qScript RT enzyme. The reaction was subjected to PCR amplification using the following conditions: 22 °C for 5 min, 42 °C for 30 min and 85 °C for 5 min. The synthesized cDNA was then diluted 1:2 and used for the consecutive quantitative PCR analysis.

### **Verification through qPCR**

Quantitative polymerase chain reaction, qPCR, allows the monitoring of PCR product during every PCR cycle, that is evaluated in “real-time”, by the use of fluorescent dyes. In quantitative PCR, the fluorescence signal is directly proportional to the amount of target mRNA in the sample at the threshold value. The threshold value is defined at the point where the target mRNA doubles for every cycle. The number of cycles at which the fluorescence exceeds the threshold is called the threshold cycle (Ct). A low Ct value reflects a high concentration of target mRNA present in the sample.

Gene expression qPCR and ChIP-qPCR reactions were done with the ROCHE™ Lightcycler FastStart DNA MasterPlus SYBR Green I Kit (according to the manufacturer's protocol) in a Roche real-time PCR system. The analyses were made using the following

conditions: 95 °C, 5 min; 40 cycles of: 95 °C, 10s; 60 °C, 8s; 72 °C, 10s; 70 °C, 20s. Each value calculated using the standard curve method was corrected by the human Glyceraldehyde 3-phosphate dehydrogenase (GAPDH) or actin, in the case of experiments involving the effect of hormone, the value was expressed as the relative RNA abundance over time zero.

### **Protein extraction**

Matrigel-free cell pellets were collected and washed twice with PBS-EDTA and lysed with RIPA buffer followed by incubation at 95 °C for 10 min. For western blotting, pellets were centrifuged and quantified with Bradford or BCA before being loaded and analyzed in acrylamide gels.

### **Western blotting**

To compare protein levels between samples through western blotting 30 µg of protein extracts were used. Briefly, electrophoresis in 12 % polyacrylamide gels was performed for 1.5 h at 110 V. The gel was then transferred to a membrane trans-blot Pure nitrocellulose (Bio-rad) for 90 min at 90 V at 4 °C; blocked with 5 % BSA during 1 h at RT and incubated overnight at 4 °C with the selected primary antibody in 2.5 % BSA. On the second day, the membrane was washed three times with T-TBS and incubated with the secondary antibody for 1 h at RT. Protein bands were revealed using LG-ECL solution and autoradiography films.

### **ChIP-seq**

Chromatin immunoprecipitation (ChIP) assays were performed as follows. Treated and untreated monolayered and 3D cells still in culture were crosslinked with 1 % formaldehyde at RT, quenched with 125 mM Glycine for 5 min at RT followed by 10 min on ice. Then cells were collected in a 5 mL Eppendorf tube, washed twice with PBS-EDTA-PIC and lysed in freshly prepared Lysis Buffer I (LBI) to break the cell membrane for 10 min on ice. After the first lysis, the pellet was resuspended in Lysis Buffer II (LBII) to break the nucleus membrane on ice for 10 min and immediately sonicated for 7 cycles 30" on / 30" off using a Bioruptor Pico from Diagenode.

The size of the sonicated chromatin was checked by taking an aliquot 10  $\mu$ l of the material and submitted to an overnight de-crosslinking in LB1 containing proteinase K (20 mg/ ml) at 65 °C. DNA was purified using the phenol/chloroform method and further resolved in a 1.2 % agarose gel.

#### Immunoprecipitation (IP)

25  $\mu$ g of chromatin were used for every IP diluted in 1x IP buffer (Diagenode), every input sample was taken before addition of the antibody of interest (5  $\mu$ g/ IP) and then the mix was incubated o/n at 4 °C on a rotation wheel. On the following day, protein A agarose beads (Diagenode) were washed and blocked with 5 % BSA during 15 min at 4 °C. IP samples were then incubated with the appropriate amount of beads for 3 h at 4 °C in a rotation wheel. After incubation, beads and input samples were washed with IP buffer and eluted in 400  $\mu$ l of elution buffer (EB). For crosslinking reversion, the material was incubated with 200 mM NaCl o/n at 65 °C. On the final day of the protocol, samples were treated with RNase A (10 mg/ ml) during 1.5 h at 37 °C immediately followed by a Proteinase K digestion (20 mg/ ml) for 2 h at 45 °C before obtaining DNA through a phenol/chloroform/isoamyl alcohol purification.

#### Phenol/chloroform DNA purification

Phenol/chloroform/isoamyl alcohol (25:24:1, v/v/v) was used to remove proteins from DNA. After crosslinking reversion of the material 1 volume of equilibrated phenol:chloroform:isoamyl alcohol mix was added to the sample. Followed by mixing by inversion and centrifugation for 5 min at 18,928 xg. The aqueous phase was transferred into a fresh tube containing 20  $\mu$ g of glycoblue, 300 mM NaAc pH 5.2 and 2.5 volumes of 100 % ethanol. After mixing by inversion DNA precipitation was done at -80 °C for 30 min and maximum centrifugation for 30 min at 4 °C. The pellet was washed with 1 mL of 70 % ethanol and centrifuged at RT for 5 min at maximum speed. The pellet was shortly air-dried and resuspended in 20  $\mu$ L of 10 mM Tris-HCl pH 8 and quantified with a Qubit system. ChIP DNA was analyzed by qPCR in Roche Lightcycler PCR system using specific primers. Percentage of input was used

for the quantification of the immunoprecipitated material with respect to the total starting chromatin.

#### ChIP-seq library preparation

From the final eluted DNA, 1 ng was required to prepare the library with the Ovation Ultralow V2 DNA-Seq Library Preparation Kit (Nugen). Libraries were purified as indicated in the protocol and 50 million reads per sample were sequenced in a HiSeq 2500 sequencer (Illumina) at the Genomics facility of the CRG.

#### ***In nuclei Hi-C***

Hi-C is a technique based on high-throughput sequencing used to analyze the spatial organization of nuclear chromatin and identify contacts between different regions of the genome.

#### Cell preparation and crosslinking

To perform Hi-C, 2-5 million cells were grown under their respective conditions (3D or 2D, +/- hormone). Cells were then washed once with PBS and incubated with a solution of 1 % formaldehyde in PBS and incubated for 10 min at RT, reaction was then quenched and stopped with glycine to a final concentration of 0.125 M for 5 min at RT and followed by 15 min on ice. The crosslinking solution was removed, cells were washed once with PBS+EDTA to completely remove debris. Cells were harvested with a scraper and collected in an Eppendorf tube. To achieve a better suspension of nuclei, cells were treated with trypsin 0.05 % for 5 min at RT.

#### Cell lysis, nuclei preparation and restriction enzyme digestion

The pellet of cells was then resuspended in 500  $\mu$ L of freshly prepared ice-cold lysis buffer (Hi-C LB) supplemented with protease and incubated on ice during 30 min. Each pellet was then centrifuged for 5 min at 1,008  $xg$  at 4 °C and quickly washed twice with cold 2X NEBuffer2 before being resuspended in 1X NEBuffer2 0.5 % SDS and incubated at 65 °C during 10 min. SDS was then quenched by adding Triton X-100 and incubating at 37 °C for 15 min. Finally, each sample was digested o/n with 400 U of the restriction enzyme Mbol at 37 °C.

End-repair and labeling

*Non-ligated control: 5  $\mu$ L aliquot.* To generate blunt-ends and label with biotin the created overhangs, Hi-C samples were incubated with the following mix: 1.5  $\mu$ L of 10 mM dCTP; 1.5  $\mu$ L of 10 mM dGTP; 1.5  $\mu$ L of 10 mM dTTP; 37.5  $\mu$ L of 0.4 mM Biotin-11-dATP; 1  $\mu$ L of 50 U/  $\mu$ L DNA Polymerase I Large (Klenow) fragment for 45 minutes at 37 °C followed by a 15 min incubation at 65 °C to inactivate the enzymes.

In nuclei ligation and reversion of the crosslink

For ligation to take place, nuclei were then centrifuged at 1,008 xg during 5 minutes, and resuspended in 1.2 mL of Ligation Mix (120  $\mu$ L of 10X T4 DNA Ligase Buffer; 100  $\mu$ L of 10 % Triton X-100; 12  $\mu$ L of 10 mg/ mL BSA; 963  $\mu$ L of H<sub>2</sub>O) and finally adding 2000 U/  $\mu$ L T4 DNA Ligase for incubation at 16 °C o/n. Prior to DNA purification, samples were treated with 10 mg/ mL RNase A and incubated for 15 min at 37 °C followed by 10 mg/ mL Proteinase K o/n at 65 °C to reverse the crosslink.

DNA purification

DNA samples were then purified following the phenol/ chloroform/ isoamyl alcohol protocol previously described and resuspended in 100  $\mu$ L of nuclease-free water and quantified with Qubit.

Hi-C library preparation

2  $\mu$ g of Hi-C sample were sonicated on the Diagenode Bioruptor-Pico using the following settings: 10 cycles of 20" on / 60" off. Efficiency of shearing was checked by 1.2 % agarose gel electrophoresis and/or with a bioanalyzer.

Biotin Pull-Down and preparation of sequencing libraries

- Binding Buffer (BB) 2X: 10 mM Tris-HCl pH7.5; 1 mM EDTA; 2M NaCl
- BB 1X: 5 mL 2X BB +5 mL Nuclease-free H<sub>2</sub>O
- BB1X + Tween 20: add 5  $\mu$ L of 10 % Tween 20

Magnetic Streptavidin T1 beads were washed and resuspended in BB 1X + 0.05 % Tween. The beads were separated on a magnet and reclaimed in 150  $\mu$ L of BB 2X before adding the sonicated

DNA and incubated at RT under rotation during 30 min. Beads attached to DNA fragments were then recovered by using the magnet and washed twice with BB and once with T4 DNA Ligase Buffer. Afterwards, beads were resuspended in the library end-repair mix (1x T4 DNA Ligase Buffer; 25 mM dNTP mix; 50 U T4 PNK; 12 U of T4 DNA Polymerase; 5 U of DNA Polymerase I large (Klenow) fragment) and incubated at RT for 30 min.

Beads were separated on a magnet and washed twice with BB 1X and once with 1X NEBuffer2 before resuspending them in A-tailing mix (10X NEBuffer2; 10 mM dATP; 25 U of Klenow 3'-> 5' exo- and H<sub>2</sub>O) to be incubated for 30 min at 37 °C. Finally, beads were washed and ligated in 1X Quick Ligation Buffer containing the Illumina Adaptors and 4,000 U of T4 DNA Ligase (cohesive ends) for 15 min at RT. Beads were reclaimed in 50 µL of 10 mM Tris-Cl, pH 8.

#### Library amplification and purification

PCR reactions for library amplification were set up as follows: 5 µL of beads; 2.5 µL of Illumina library amplification primer mix; 12.5 µL of 2X NEBNext High Fidelity PCR Master Mix and 5 µL of H<sub>2</sub>O. Amplification PCR conditions: 30 min at 98 °C; 8 cycles of: 10 s at 98 °C, 30 s at 65 °C, 30 s at 72 °C; 5 min at 72 °C. At the end of the PCR reaction, the beads were separated on a magnet and the PCR product was transferred to new tube for size selection.

#### Size selection

To purify the library and remove primer dimers we used pre-warmed AMPure XP beads. To achieve this, the PCR product of the previous step was added to an equal volume of AMPure XP beads, then each sample was mixed by pipetting and incubated for 5 min at RT. Beads were separated by magnet and washed 2x with EtOH 70 % without removing the tubes from the magnet. Final product was eluted in 30 µL of 10 mM Tris-Cl, pH 8.5 and quantified using the Qubit fluorometer before being submitted to sequencing.

## ATAC-seq

**Assay for Transposase-Accessible Chromatin sequencing (ATAC-seq)** relies on the hyperactive transposase Tn5. Adapters are loaded onto the transposase allowing simultaneous fragmentation of chromatin and integration of those adapters into open chromatin regions. The library generated is then sequenced and the regions of the genome with open chromatin can be analyzed. We took advantage of this method to compare the changes reflected on the chromatin of a 3D breast cancer cell nucleus to its 2D counterpart. The method taken from (Buenrostro, 2016) requires very low input material and consists of the following steps:

### Nuclei preparation

Treated cells were harvested as previously mentioned and collected in a 5 mL Eppendorf tube and washed twice with 1X cold PBS + PIC. Pellet of cells was incubated with 0.25 % Trypsin and incubated for 10 min at 37 °C to obtain a homogeneous single cell suspension. Cells were then centrifuged and gently resuspended in RBS buffer + PIC, followed by incubation of RBS buffer + NP40 for 10 min to break the cell membrane and obtain single nuclei. Nuclei suspension was resuspended in RBS buffer and counted in a hemocytometer.

### Transposition reaction

To make the Transposition reaction, 50,000 nuclei were mixed with 25 µl 2X TD Buffer, 2.5 µl Tn5 Transposases in a final volume of 50 µl for 30 min at 37 °C. Immediately following transposition, transposed DNA was purified using Qiagen MiniElute Kit and eluted in 10 µL of 10mM Tris, pH8.0.

### PCR Amplification

To amplify transposed DNA fragments, all 10 µL of DNA were combined in a PCR tube with: 2.5 µL 25 µM Custom Nextera PCR Primer 1, 2.5 µL 25 µM Custom Nextera PCR Primer 2 (Barcoded), 25 µL NEBNext High-Fidelity 2X PCR Master Mix to a final volume of 50 µL. PCR conditions were as follows: 72 °C for 5 min, 98 °C for 30 s, 5x (98 °C for 10 s, 63 °C for 30 s, 72 °C for 1 min). To reduce GC and size bias in PCR, the appropriate number of PCR cycles was determined using qPCR allowing to stop amplification



prior to saturation. To run a qPCR side reaction, the following were combined: 5  $\mu$ L of PCR amplified DNA, 0.25  $\mu$ L 25  $\mu$ M Customized Nextera PCR Primer 1, 0.25  $\mu$ L 25  $\mu$ M Customized Nextera PCR Primer 2, 0.09  $\mu$ L 100x SYBR Green I and 5  $\mu$ L NEBNext High-Fidelity 2X PCR Master Mix. Using a qPCR instrument with the cycle as follows: 1 cycle of 98 °C for 30 s; 20 cycles of 98 °C for 10 s, 63 °C for 30 s; 72 °C for 1 min.

Additional number of cycles required were determined according to the original protocol and remaining sample amplified accordingly with the initially described conditions. Amplified DNA libraries were purified using Qiagen MinElute PCR Purification Kit and eluted in 20  $\mu$ L of 10 mM Tris Buffer, pH 8.

### Size Selection

Prior to sequencing, libraries must be size selected, briefly: prior to their use Ampure beads were equilibrated for 30 min at RT. The volume of DNA was adjusted to 50  $\mu$ L and incubated for 10 min at RT with 25  $\mu$ L Ampure XP beads (0.5x), placed on a magnetic rack and the supernatant was transferred to a new tube. 75  $\mu$ L of Ampure XP beads were then added and again incubated for 10 min at RT. Beads placed on the magnetic rack were washed twice with freshly prepared EtOH 80 %. Beads were left to air-dry and resuspended in 20  $\mu$ L of 10 mM Tris Buffer, pH 8. 75 million reads per sample were sequenced in a HiSeq 2500 sequencer (Illumina).

### **Seeding 3D cells for immunostaining**

For immunostaining, the cell number after trypsinization was determined by counting in a Neubauer hemacytometer. Subsequently,  $1 \times 10^3$  cells per well were seeded on Matrigel precoated 8-well LabTek (10 mm). The cells were grown for 10 days before paraformaldehyde (PFA) fixing for immunostaining.

### **Immunofluorescence**

2D and 3D cells ( $1 \times 10^3$  cells) grown for 3 and 10 days respectively were washed twice with PBS and fixed for 10 min with 4 % fresh PFA, before being permeabilized during 30 min with 0.5 % Triton X-100 in PBS. Samples were then blocked during 1.5 h with 5 % BSA solution. Then, the cells were put in the corresponding antibody in the IF solution and left incubating o/n at 4 °C.

The following day, cells were washed three consecutive times with IF solution and left washing during 10 min each wash. The samples were then incubated with the correspondent secondary antibody during 1 h at 4 °C, in a humid dark chamber.

Secondary antibodies used: AlexaFluor 488 anti-rabbit IgG (1:1000; raised in donkey) and AlexaFluor 546 anti-mouse (1:1000; raised in goat). After incubation with the secondary antibody, cells were washed once with IF solution, incubated during 10 min with 0.1 mg/ ml DAPI in PBS and washed with PBS three times, before mounting in Mowiol 4-88 Mounting Medium for imaging. Images were collected sequentially on a Leica SP8-STED confocal laser-scanning microscope using the software Leica Application Suite X. All collected images conserved an optical thickness of 0.25 µm. Image analysis for marker distribution, quantification and colocalization were performed using ImageJ (Schindelin et al., 2012).

### **MNase digestion**

Micrococcal nuclease is an endonuclease that preferentially digests single-stranded nucleic acids, especially at AT- or AU-rich regions. The enzyme will also digest double-stranded DNA or RNA, making it an essential component of chromatin studies. Micrococcal Nuclease digests 5'-phosphodiester bonds of DNA and RNA, yielding 3'-phosphate mononucleotides and oligonucleotides. This enzyme requires  $\text{Ca}^{2+}$  as a cofactor for its activity and is completely inactivated by EDTA.

Our samples were treated with different concentrations of the nuclease to obtain differential digestion patterns of mono-, di- and tri- nucleosomes in both models.

2D and 3D plated cells were washed once with PBS, collected in 2 mL cold PBS + PIC and centrifuged 5 min at 900  $xg$  at 4 °C. The cell pellet was then gently resuspended in 50 µL RBS buffer + PIC followed by addition of 1.3 mL RBS buffer + 0.1 % NP40. Cells were centrifuged again for 10 min at 500  $xg$  at 4 °C and the nuclei were resuspended in RBS buffer to be counted.

An amount of 600,000 nuclei were used for each reaction. The MNaseI titration was carried out as follows: 0, 30, 45, 90 Units prepared in 500 µL final volume reaction. The nuclei were then incubated for 2 min at 37 °C. The reaction was stopped with 40 mM

EDTA 0.5 M and treated with RNaseA 10 mg/ mL for 30 min at 37 °C and Proteinase K (1.2 µg/ µL) for 1 h at 45 °C. Final DNA product was purified with Phenol/Chloroform and 600 ng of material was loaded in a 1.2 % agarose gel which ran for 45 min at 100 V.

### **Proliferation assay**

The amount of ATP in cells correlates with cell viability. Within minutes after a loss of membrane integrity, cells lose the ability to synthesize ATP, and endogenous ATPases destroy any remaining ATP, thus the levels of ATP fall precipitously and rapidly. The CellTiter-Glo® Cell Viability Assay is a method used to determine the number of viable cells in culture. Detection is based on a luciferase reaction to measure the amount of ATP in viable cells. The reagent lyses cell membranes to release ATP, it inhibits endogenous ATPases, and it provides luciferin and luciferase necessary to measure ATP using a bioluminescent reaction. The signal is then recorded with a luminometer.

Proliferation of both 2D and 3D T47D cells was measured. A total of 1,000 cells in 100 µL were maintained in quadruplicates per hormone concentration (R5020: 0, 0.025, 0.05, 0.1, 0.5 and 10 nM) or red condition in an opaque-walled 96-well plates. For 3D cells seeded on Matrigel, the corresponding wells were previously coated on ice with 20 µl of Matrigel and incubated at 37 °C for 20-30 min to allow the matrix to polymerize. Half an hour before measurement, the plate was equilibrated at RT, washed and resuspended in 50 µl PBS-EDTA. The TiterGlo reagent (50 µL) was added to every well, the cells were then incubated for 2 min at RT with agitation, followed by 10 min incubation at RT. Bioluminescence was detected in a Barthold luminometer system allowing 0.25 second per well.

### **Live/dead assay**

To visualize the number of viable cells in a 3D spheroid the LIVE/DEAD™ Cell Imaging Kit was used following the included protocol, briefly: reagents A (Live, green) and B (Dead, red) were mixed to create a 2X working solution. This mix was then added to fresh culture of 3D spheroids grown for 10 days in a LabTek 8-well slides and incubated for 15 min at RT. Images were collected sequentially on a Leica SP8-STED confocal laser-scanning

microscope using the software Leica Application Suite X with filters 488 (green) and 546 (red).

### **shRNA transfection and infection**

To knockdown a given protein we followed a transfection protocol by plating 1.5 million HEK 293T cells in p100 (1 for each type of virus to be produced) in 8 mL DMEM (10 % FBS, antibiotics). On the following day reactions to transfect were made as follows: in an Eppendorf tube 500  $\mu$ l HBS2x buffer were thawed, while on a second tube a mixture of the following plasmids was prepared: 5  $\mu$ g VSVG, 8  $\mu$ g H8.91, 7  $\mu$ g plasmid of interest, 62.5  $\mu$ l of 2 M  $\text{CaCl}_2$  in a final volume of 500  $\mu$ l.

The mix containing the plasmid was added drop by drop to the first tube. The reaction was incubated for 35 min at RT and added to the cells seeded the previous day.

On the third day of protocol, cells were incubated with the same medium to be used to infect the cells of interest. After 24 h, the media was saved, filtered and added to monolayered T47D cells for 24 h. The same step was repeated one more time to increase the infection efficiency. Infected cells were selected through Puromycin antibiotic resistance.

### **Colony Formation Assay (CFA)**

To evaluate the clonal capacity of infected cells, 1,000 cells of each line were plated in 3 cm diameter wells. Medium was changed every three days for a period of 14 days. After this incubation period, cells were washed twice with PBS before being stained with crystal violet for 5 min. The plates were then washed to remove debris, imaged and quantified.

## **2.3. Bioinformatic methods**

*Preprocessing and mapping.* Quality of the raw data was checked with FastQC (Andrews, 2010).

### **RNA-seq**

Raw fastq reads were mapped to the reference genome (Homo sapiens assembly GRCh38/hg38, release 31, using STAR (Dobin

et al., 2013). Qualimap (Okonechnikov, et al., 2016) was used to check quality of the aligned reads.

*Differential expression analysis and related figures.* Pairwise gene-level differential expression analysis was performed in the R (version 3.6.0)/ Bioconductor environment, using the DESeq2 package version 1.26.0.

Genes were selected as significantly differentially expressed if the FDR-adjusted p value was less than 0.05, and the absolute log<sub>2</sub> fold change was more than 1.

*Functional analysis.* Gene Ontology enrichment was assessed using the GOstats R/Bioconductor package (Falcon & Gentleman, 2007).

### **ChIP-seq**

Reads were mapped with bowtie2 version 2.3.2 to the reference genome (Homo sapiens assembly GRCh38/hg38, release 31 of the Gencode annotation) using default parameters. *Peak calling + annotation.* Peak calling was performed on de-duplicated mapped reads with macs2 callpeak method (Zhang et al., 2008).

*Differential binding analysis* was done with the DiffBind R/Bioconductor package (Stark & Brown, 2011) version 3.2.1. Regions were considered as differentially bound if the obtained FDR was less than 0.05.

### **ATAC-seq**

The Illumina universal adapter sequence was trimmed off the raw reads with skewer (Jiang et al., 2014) version 0.2.2. Reads were mapped with bowtie2 as previously described.

*Peak calling (Genrich) + annotation.* Genrich version 0.6 was used for peak calling of the ATAC-seq deduplicated BAM files. Overlap of peaks between biological replicates of the ATAC-seq experiment was checked with ChIPpeakAnno package (Zhu et al., 2010).

*Differential binding / accessibility analysis* was done considering the biological duplicates of each experiment. Regions were considered as differentially bound if the obtained FDR was less than 0.05.

## Integration

*DEGs + PR peaks.* We retrieved genes in which promoter region (defined as -1500 bp/+100 bp around the transcription start site) there is a PR peak. This list was overlapped with the differentially expressed gene lists.

*Distance PR peaks with DEGs.* Distance was calculated between transcription start sites (TSS) of RNA-seq DEGs and PR peaks (3D unique, extracted from the DiffBind data) that fall in the promoter region of those genes. We checked if the overlap between the PR 3D exclusive peaks and the 3D-exclusively regulated genes is significantly higher than the overlap obtained when randomly selecting 1,000 genes instead of the differentially expressed one. Significance between the overlaps was tested with a Fisher's exact test.

*ATAC-seq differentially accessible regions + DEGs.* We retrieved the DEGs from the RNA-seq experiment (up- and down- regulated separately). We then retrieved the ATAC-seq peaks enriched/depleted (as selected in the differential accessibility analysis) that mapped either inside those genes, or in their promoter regions (-1500/+500 from TSS).

*Distance between 3D exclusive DEGs TSSs and PR peaks overlapping H3K27ac.* First, we retrieved the TSS coordinates of exclusive 3D DEGs on one hand, and of non-regulated genes on another hand (randomly selecting 5,000 TSSs from the latter selection 5 times, so as to obtain 5 random selections).

Then, we considered only the PR ChIP-seq peaks that overlapped with an H3K27ac peak.

Finally, we calculated the distance between those peaks and the TSS of the exclusive 3D DEGs and the distance between those peaks and the 5,000 randomly selected non-regulated TSSs. We visualized the distribution of these distances with boxplots.

Whether the distances distribution was different between the exclusive 3D data set and the randomly selected data sets was checked with a Wilcoxon test (Ahlmann-Eltze & Patil, 2021).

## Hi-C processing

The reads of each individual replica were mapped onto the GRCh38 reference genome and filtered using TAD bit (Serra et al., 2017) with the default settings. The two replicas of the T47D 2D

condition were compared at 100 kb resolution using the Stratum-adjusted Correlation Coefficient (SCC) (Yang et al., 2017) yielding a value of 0.96 and merged to a final set containing 560 million valid interactions. Similarly, the two replicas of the T47D 3D condition were compared (SCC = 0.9) and merged to a final set containing 502 million valid interactions. Topologically associating domains (TADs) were identified using TADbit internal algorithm in matrices binned at 50 kb. When needed, matrices were normalized using OneD (Vidal et al., 2018) as implemented in TADbit. The Hi-C analysis was carried on in collaboration with David Castillo from Marc Martí-Renom's lab in CNAG.





### **3. Results**

#### **Chapter I: Characterization 3D spheroids grown in the extracellular matrix**

##### **3.1. Implementation of 3D cell culture on breast cancer cell lines**

Cells embedded in an artificial environment require the proper signaling to proliferate and develop structures that resemble their physiological counterpart. Given the variety of 3D culture techniques and the different hydrogels used for each purpose, the first task was to test different matrices available for embedded cell growth. Below we describe the growth of MCF10A (non-tumoral) and T47D (breast cancer) cells, when exposed to different hydrogels. As shown in Figure R1, when MCF10A cells are exposed to synthetic gels such as gelatin or PuraMatrix, cells attach in a 2D structure or do not progress, while T47D cells do not survive, because of the low pH in the environment. When grown in absolute collagen I, MCF10A cells organize as spheres, but without an acinar inner structure. In the same conditions, T47D cells form complex flat structures. In a mixture of collagen and Matrigel, MCF10A cells start to form but are unable to reach the acinar structure, while T47D cells did not progress in this matrix. However, with the appropriate proportions of proteins in the Matrigel (51 % laminin, 10 % nidogen, 35 % collagen, 4 % varying proteins) MCF10A cells form round structures with a polarized acinar internal pattern, and T47D cells form spheroids of different sizes containing proliferating cells. We conclude that Matrigel has the correct combination of extracellular matrix components for the 3D culture of these breast tubular epithelial cells (Figure R1).

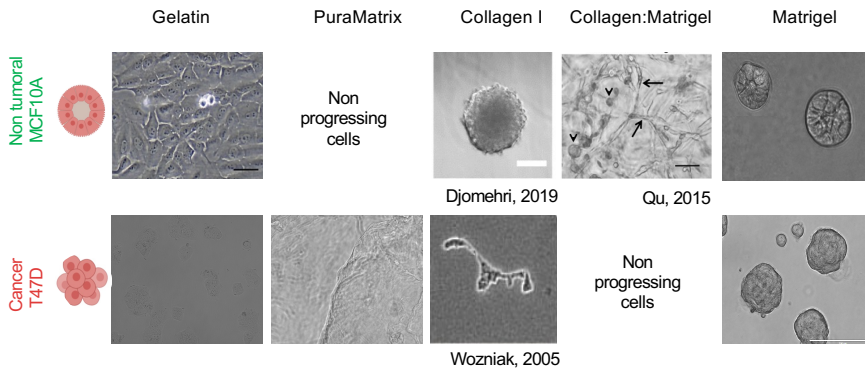


**Figure R1. Growth of breast cell lines on different hydrogels**

MCF10A and T47D cells were seeded on distinct hydrogels to evaluate the optimal condition to generate spheres. As depicted, the viability was compromised in most gels. However, both non-tumoral and tumoral cancer cells were able to develop and grow in the Matrigel. Scale bar 100  $\mu\text{m}$ , gelatin scale bar 20  $\mu\text{m}$ .

To ensure that other breast cancer cells could also be grown in 3D embedded in Matrigel (Lee et al., 2007), we tested MCF7, BT474 and ZR75 breast cancer cells and compared their morphologies to those previously described (Kenny et al., 2007). MCF7 and BT474 cells grow similarly as T47D cells, and ZR75 cells formed a grape-like structure as seen in (Kenny et al., 2007) (Figure R2).

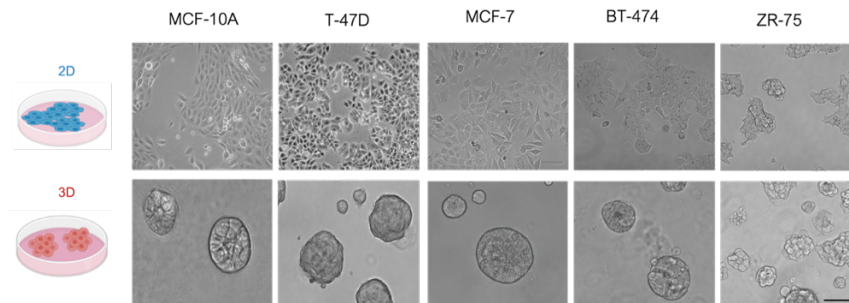


**Figure R2 Breast cell lines grown in 3D culture embedded in Matrigel**

Comparison of different breast cell lines grown as 2D on the plastic dish and 3D culture in the Matrigel. All cell lines in 3D can create a defined sphere except for ZR75 which forms grape-like structures. Scale bar: 50  $\mu\text{m}$ .

As one of the aims for this project was to explore the response of breast cells to progestins, we focused on the T47D cells, which

express high levels of progesterone receptor (PR) and whose behavior in 2D cell culture has been extensively studied in the laboratory (Beato et al., 2020).

### 3.2. Characterization of the T47D spheroids

Prior to exploring the changes in gene expression and general behavior of the cells grown in 3D, we performed a functional and phenotypic characterization. First, we evaluated for 10 days the proliferation capacity of 1,000 cells cultured in 3D immersed in Matrigel compared to cells grown in 2D. We found that 3D cells are able to proliferate at a rate 2.6 times faster than its 2D counterpart (Figure R3, lower panel). Within 10 days of culture the 3D cells formed spheroids with an average diameter of 100  $\mu\text{m}$ , and are composed of approximately 100 cells (Figure R3, upper panel).

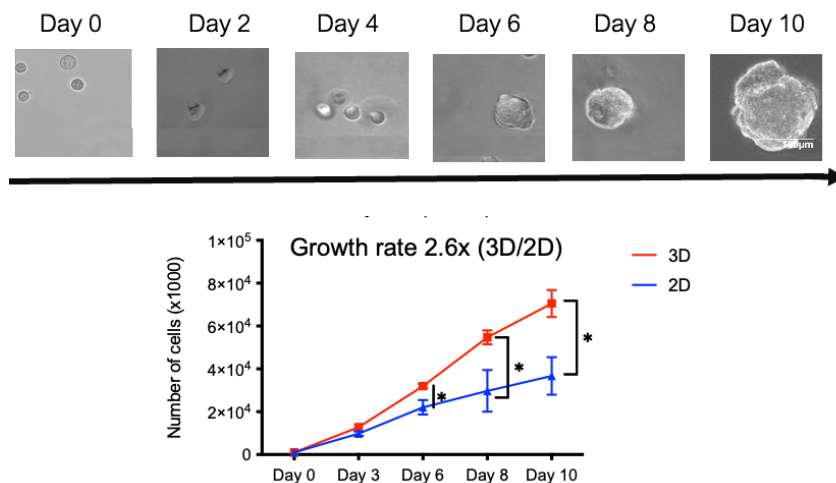


**Figure R3. Cell proliferation rate in T47D spheroids**

Cell growth of T47D cells over the course of 10 days embedded in the Matrigel hydrogel (3D) against 2D monolayered cells. The 3D cells proliferate faster than 2D cultured cells and form round spherical tumoroids without compromising adhesion. Scale bar: 100  $\mu\text{m}$ .

This increased cell proliferation detected in 3D cells is in accordance to the high levels of proliferative cells that conform the spheres, evident by using a live/dead cell imaging Kit where, as described in the methods section, reagent A stains green for living

cells, which are distinguished by the presence of ubiquitous intracellular esterase activity as determined by the enzymatic conversion of the virtually non-fluorescent cell-permeant calcein AM to the intensely fluorescent calcein, which is well-retained within live cells. Reagent B is cell-impermeant and therefore only enters cells with damaged membranes. In dying and dead cells, a bright red fluorescence is generated upon binding to DNA. Proliferating cells are also detected by Ki67 staining (Figure R4).

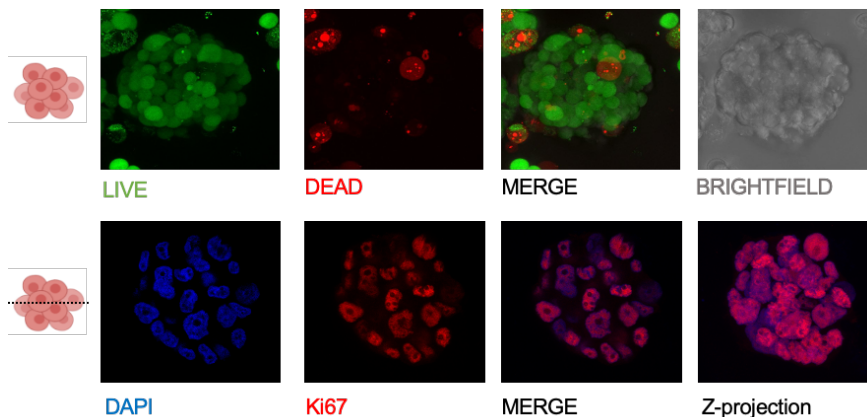


#### Figure R4 Cell proliferation in T47D representative spheroids

Top: 3D T47D spheroid stained for live/dead cells after 10 days in culture. Apoptotic cores are rather small, sporadic and not predominant in the core of the spheroid. Bottom: Slice of a 10-day spheroid that was stained for Ki-67 proliferative marker and overlapped with DAPI, accordingly most cells up to this stage of the sphere are proliferating. Images were acquired on a Leica SP8-STED confocal laser-scanning microscope using the software Leica Application Suite X with filters 488 (green) and 546 (red).

To further characterize the properties of the spheroids, we used the IMARIS software and ImageJ to measure the physical properties of the cell nuclei. The nuclear volume of 3D cells, detected by DAPI staining, is significantly enlarged ( $488.7 \mu\text{m}^3$ ), compared to the 2D cell nuclei ( $408.5 \mu\text{m}^3$ ) ( $p$  value $<0.001$ ) while the diameter of the 3D nuclei ( $9.173 \mu\text{m}$ ) was smaller compared to 2D nuclei ( $15.56 \mu\text{m}$ ) ( $p$  value $<0.001$ ). This translates into an increased sphericity coefficient of the 3D nuclei ( $0.74$  vs  $0.57$  in 2D) ( $p$  value $<0.001$ ).

and larger surface area ( $643.3 \mu\text{m}^2$  vs.  $381.6 \mu\text{m}^2$ ) ( $p$  value  $< 0.001$ ) (Figure R5).

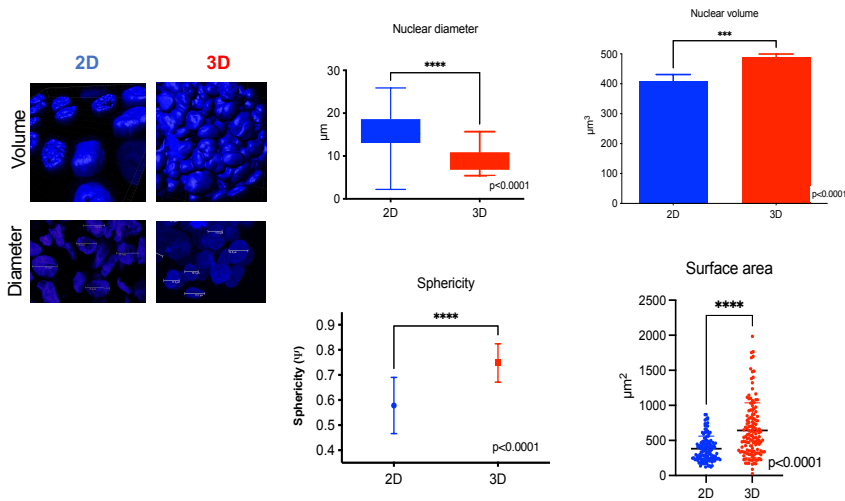


#### Figure R5 Physical properties of 3D cells

The nuclei of the 3D cells measured with Imaris/ImageJ show a larger volume accompanied by an increase of sphericity and larger surface area compared to 2D nuclei.

T47D cells are able to respond to hormonal stimulus as they express estrogen and progesterone receptors (ER+/PR+). To evaluate their response to hormone we first measured the levels of ER and PR in 3D and 2D cells. Immunofluorescence and Western blots with specific antibodies showed similar immunostaining and protein levels for ER and PR in both growing conditions (Figure R6). In the last chapter I will describe in more detail the differences in gene regulation between 2D and 3D cultured breast cancer cells (BCC).

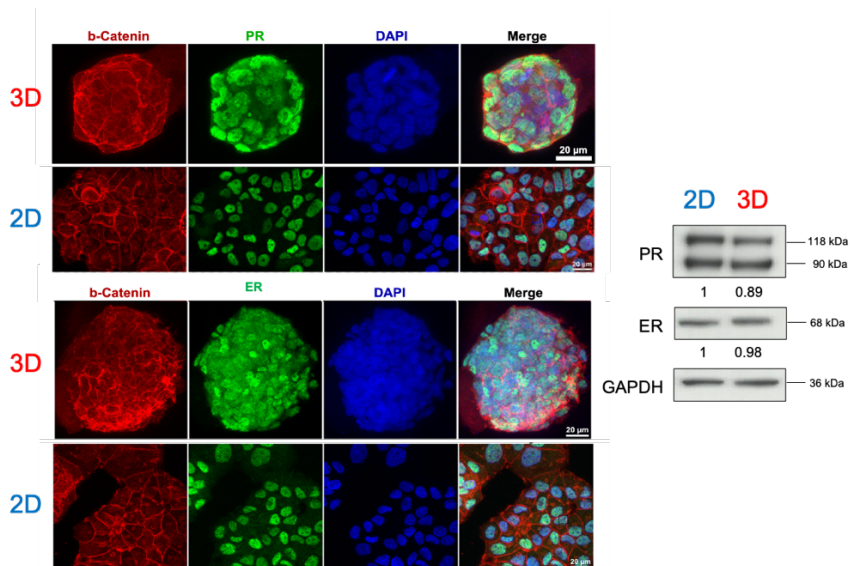


**Figure R6 Expression of progesterone and estrogen receptors in T47D cells grown under 2D and 3D conditions**

Distribution of total ER $\alpha$ , PR and b-catenin was assayed by immunofluorescence (IF) in 2D and 3D conditions. Western blot assay performed with extracts obtained in the same conditions as the IFs confirm comparable levels of PR and ER $\alpha$  between models. Scale bar: 20 $\mu$ m.

### 3.3. Signaling pathways differentially regulated in 3D cells

As mentioned in the introduction, the external microenvironment surrounding a cell is able to regulate signaling cascades by activating specific membrane kinases. Some of the main events regulated by the presence of the ECM are: i) the Hippo signaling pathway and ii) the activation of focal adhesion through Y397 phosphorylation of the Focal Adhesion Kinase (FAK/ PTK2) protein.

Regarding the Hippo pathway, the transcriptional co-activators Yes-associated protein (YAP) and the Transcriptional coactivator with PDZ-binding motif (TAZ) act as nuclear relays of mechanical signals exerted by ECM rigidity and cell shape (Dupont et al., 2011). It has been previously described that on soft substrates, YAP is inactivated by phosphorylation on Serine 127 and later tagged for degradation in the cytoplasm; while its activation

(unphosphorylated YAP) leads to translocation into the cell nucleus to promote regulation of gene transcription (Zanconato et al., 2019).

In 2D cultured breast cancer cells, which grow attached to the hard plastic, YAP is less phosphorylated in S127 compared to 3D, while total YAP levels remain unchanged (Figure R7, western blot). In addition, YAP is found largely in the nucleus of 2D cells to promote regulation of gene transcription (Figure R7, upper staining panel) confirming previous studies (Zanconato et al. 2019). In contrast, in 3D cells cultured in Matrigel, YAP is mainly found in the cytoplasm (R7 lower panel).

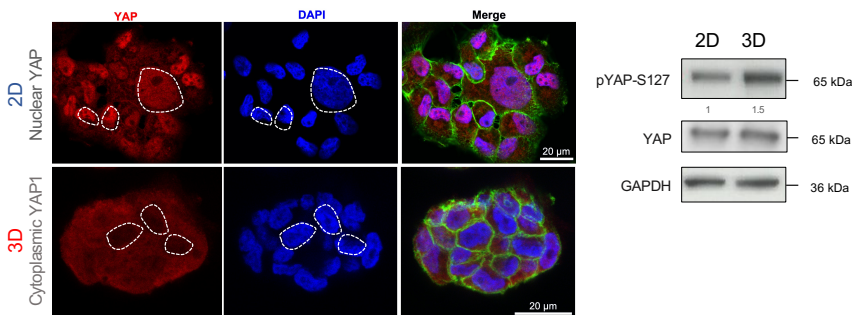


**Figure R7 The Hippo pathway effector between cell models is controlled by the rigidity of the growing surface**

Left: the distribution of total YAP (red), b-catenin (green) and DAPI (blue) was assayed by immunofluorescence in T47D cells grown under 2D and 3D conditions. Scale bar: 20 μm. Right: Western blot shows increased levels of YAP pS127 in 3D cells.

On the other hand, phosphorylation at Y397 of the FAK through integrin activation by a rigid matrix (Figure R8, left) links to several signaling pathways that regulate cell proliferation, survival, migration, and invasion. FAK has been implicated in mechanosensing as FAK-null cells do not detect differences in ECM rigidity (Wang et al., 2001). Moreover, the autophosphorylation site, Y397, is involved in the mechanosensing response, FAK is phosphorylated when mechanical strain is applied to endothelial cells (Tang et al., 1999; Wozniak et al., 2004).



Focal adhesions have been proposed to be mechanosensors because they provide a link between the ECM and the cytoskeleton, and they respond to external force. This is an important concept because cells in 3D matrices are not receiving the same physical signals and forces as those on more rigid 2D matrices or direct plastic.

Although the Hippo pathway and focal adhesions are only two of the several pathways that are considered hallmarks of 3D matrix-embedded cells (see Pickup et al., 2014 for more details and pathways), we decided to evaluate whether some of these pathways are altered depending on the growth condition in T47D cells. We found that p-FAK is deregulated in 3D cells, as indicated by the significant reduction of FAK-Y397 phosphorylation signals compared to the levels detected in 2D cells (Figure R8, left). This implies that in 2D cells the presence of a rigid surface is sensed, integrated and transduced leading to increased activation of focal adhesions. It is yet unclear how the mentioned events are modulated in different soft matrices.

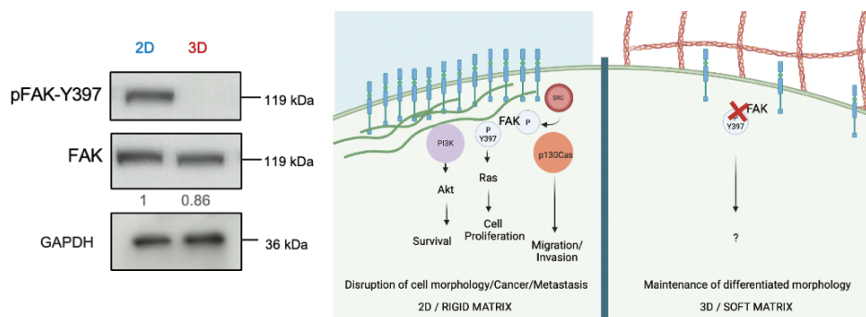


**Figure R8 Cells regulate focal adhesion dynamics in response to matrices with different biophysical properties**

Focal adhesions are key regulators of the response to ECM rigidity. The phosphorylation of FAK at Y397 is regulated by ECM rigidity and this modification may alter signaling events such as PI3K/Akt leading to disruption of cell morphology. Several of these behaviors, such as cell proliferation, survival, and migration, contribute to cancer and metastasis. Cells in a 3D soft matrix down-regulate phosphorylation of FAK and its downstream pathways. Adapted from (Wozniak et al., 2004).

As described in the introduction, once the signal crosses the cell membrane it is capable of impacting several cell compartments and



general structures in the cytoplasm before reaching the nuclear membrane. On this trajectory we do not find meaningful variation in total levels of cytoskeletal proteins, such as  $\beta$ -actin,  $\alpha$ -tubulin and cortactin (data not shown). However, we cannot exclude that the rearrangement of these proteins could be impacting the ECM-mechanosensored signaling pathway.

## Chapter II. Impact of the 3D growth on nuclear structure and function

### 3.4. Chromatin distribution 2D vs. 3D

To explore the changes in nuclear structure following BCC culture in 3D, we measured the distribution of the chromatin throughout the nucleus by determining the coefficient of variation on the distribution of DAPI immunostaining in 100 nuclei by using ImageJ tools (Figure R9A). We found a significant increase of the coefficient in 3D nuclei, which reflects a more heterogeneous distribution of chromatin compared to the gaussian distribution of its 2D counterpart (Figure R9B).

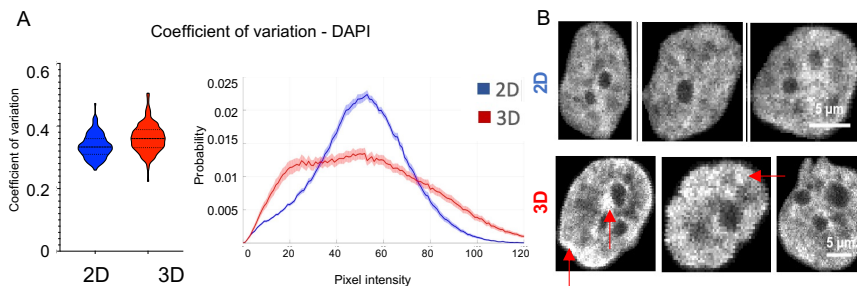


**Figure R9 Chromatin in 3D nuclei is differentially distributed in the nucleus**

Measure of the coefficient of variation of DAPI staining distribution between BCC grown in 2D and in 3D allows us to observe the degree of intensities at different loci. A, left: Violin plot. A, right: Probability of different pixel intensities. B) Images of BCC stained with DAPI exhibiting a clearer pattern of condensed heterochromatin clusters in 3D grown BCC. Scale bar: 5 μm.

To further characterize this observation, we performed a micrococcal nuclease (MNase) digestion assay. This assay is used to estimate the accessibility of the chromatin for DNA enzyme cleavage. A suspension of isolated nuclei was treated with increasing concentrations of MNase, which preferentially cleaves the linker region between nucleosomes, and then the products of MNase digestion were analyzed by gel electrophoresis (Figure R10A). As observed in Figure R10B-C, nuclei from 3D grown BCC were less efficiently cleaved by MNase compared to 2D cells at all

MNase concentrations tested (Figure R10B and R10C). Also, the amount of undigested DNA fragments was higher in 3D cells, even at the highest MNase concentration (marked with an asterisk in R10A). These results confirm that chromatin is less accessible in 3D nuclei compared to BCC grown in 2D.

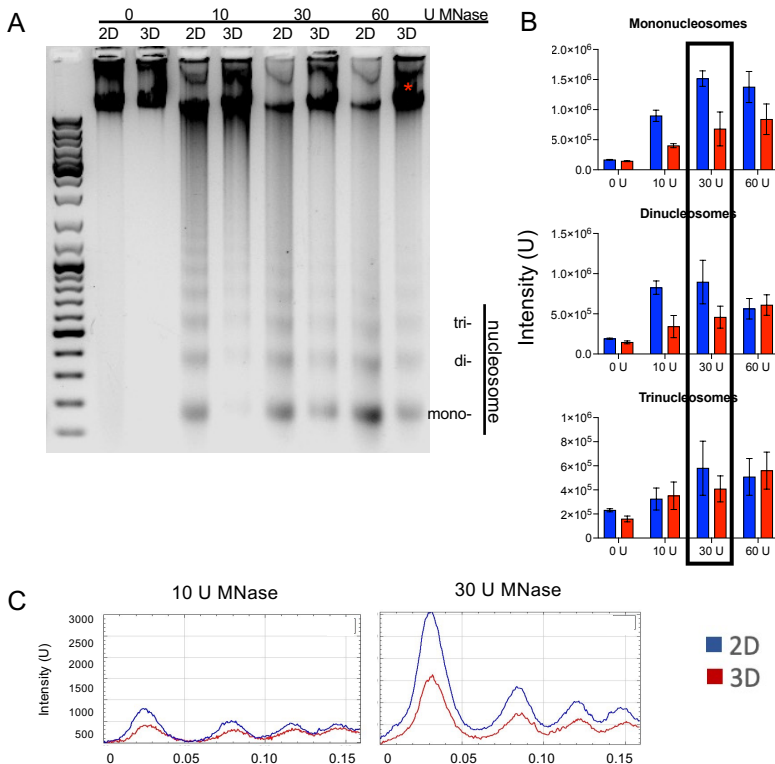


**Figure R 10 MNase digestion of nuclei obtained from T47D cells grown in 2D and in 3D conditions**

A) Analysis of the digestion products in 1.2 % agarose gel electrophoresis. The positions of the mono-, di- and tri-nucleosomes are indicated. B) Histogram of the amount of mono-, di- and tri- nucleosomes at the different concentrations of MNase used for digestions. The results obtained with 30 units of MNase are highlighted. C) A scan of the lanes in A for 10 and 30 units of MNase.

To confirm these results with a different enzyme, we performed an Assay for Transposase-accessible chromatin followed by sequencing (ATAC-seq), which is a technique used to assess genome-wide chromatin accessibility. Cells were grown in 2D and 3D as described in chapter 2.2 *Methods* and a suspension of

individual nuclei was incubated with 2.5 U of the tagmentase Tn5. For this experiment two replicates for each condition were performed. We noted that the replicates for the 3D showed high dispersion (Figure R11A); thus, to overcome this issue, only ATAC peaks present in both replicates were used for further analysis (Figure R11B).

The average number of ATAC peaks was significantly higher in 2D (93,850 peaks) than in 3D (38,542 peaks) (Figure R11B); pointing to a general decrease of accessibility in nuclei from 3D grown cells. When comparing the 1,000 most accessible ATAC regions detected in both 2D and 3D, we observed that they contained less reads/peak in 3D (Figure R11C). Most of the peaks detected in 3D grown cells also appeared in 2D grown cells (37,342, 96.88 %). Only 547 new ATAC peaks were detected in 3D, while 24,242 sites were lost when comparing all replicates (Figure R11C). Thus, the chromatin of BCC grown in 3D appeared to be in a less accessible conformation compared to chromatin of BCC grown in 2D, supporting the results obtained with MNase. It should be noted that in both experiments isolated nuclei from cells in 2D or 3D culture were used, ruling out the possibility that the differences in enzyme digestion accessibility were due to the 3D structure of the spheroids *per se*.

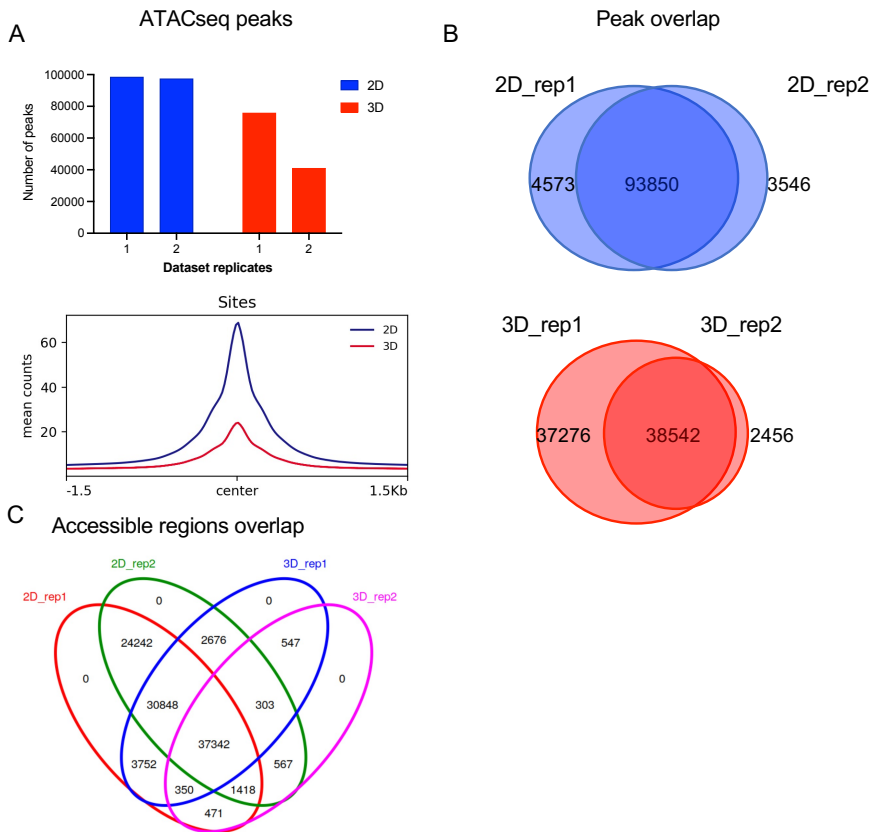


### Figure R11 ATAC-seq analysis performed in breast cancer cells grown in 2D and in 3D conditions

A) Number of peaks per sample of ATAC-seq experiments. We observed a significant decrease in accessibility in 3D cells. The 1,000 peaks with the highest score for 2D and 3D condition were plotted (bottom panel). B) Overlap between ATAC-seq replicates. C) Overlap between all the samples used for this analysis; more than 95 % of the peaks detected in 3D cells are also present in 2D.

### 3.5. Gene expression regulation

We envisage that the overall changes in morphology, chromatin reorganization and accessibility observed so far should be reflected in changes in gene expression. Thus, to acquire further knowledge into the biology of the 3D cells exposed to the ECM, we used whole genome RNA sequencing to analyze their transcriptional profile compared to 2D cultured cells.

We purified total RNA from four samples of 2D and 3D grown T47D cells and performed poly-A RNA sequencing. The 2D samples replicas were reproducible (Fig R12A) and clustered together in the Principal Component Analysis (PCA) (Fig R12A and R12B), while the 3D samples clustered into two groups in the PCA (Fig R12B), likely because these samples were processed at different timepoints.

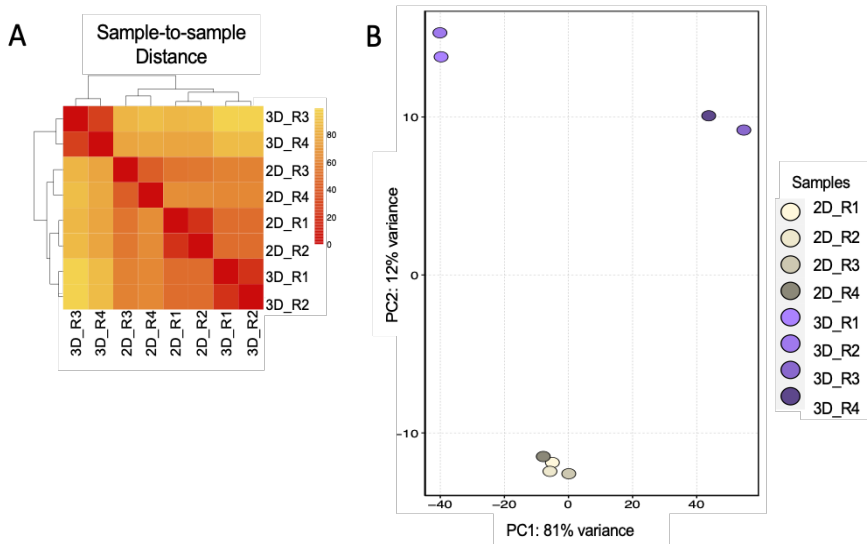


**Figure R12 Heatmap and PCA of RNA-seq replicates obtained from 2D and 3D T47D cells**

A) Clustered heatmap of sample-to-sample distance. B) PCA of RNA-seq samples, PC1: 81 % and PC2: 12 % variance, clusters the samples separately from both cell cultures.

The transcriptional profiles of four control 2D and four 3D samples, yielded statistically significant changes for 2,377 transcripts: 619 were up-regulated and 1,758 down-regulated in 3D cultured cells over the 2D cells [ $\log_2$  FC=2 and  $p$  value<0.05]. The higher proportion of genes down-regulated in 3D (Figure 13) are in line and supports the results obtained in the accessibility assays (Figures R10-11).

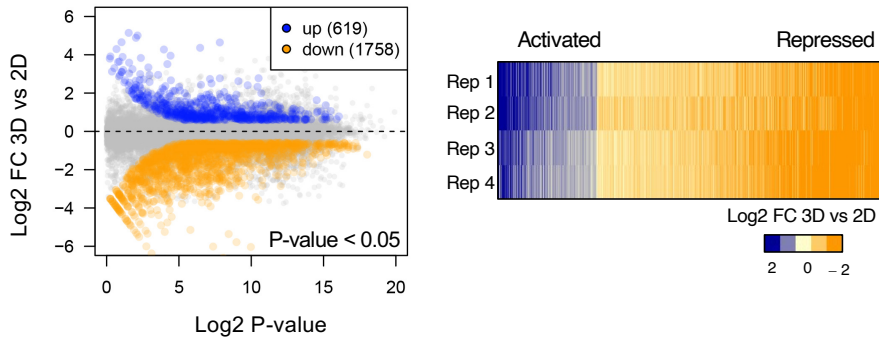


**Figure R 13 Differential Expression Analysis 3D/2D**

Using [ $\log_2FC=2$  and  $p$  value $<0.05$ ], the experiment reveals over 2,300 genes deregulated when cells were grown in 3D. More than 75 % of the DEG showed down-regulation in 3D.

To further understand the differences in gene regulation between 2D and 3D, we performed Gene Ontology analysis of biological processes and cellular compartments using the genes deregulated in each condition. A KEGG enrichment analysis of the regulated genes to identify those pathways most sensitive to this change of environment was also performed.

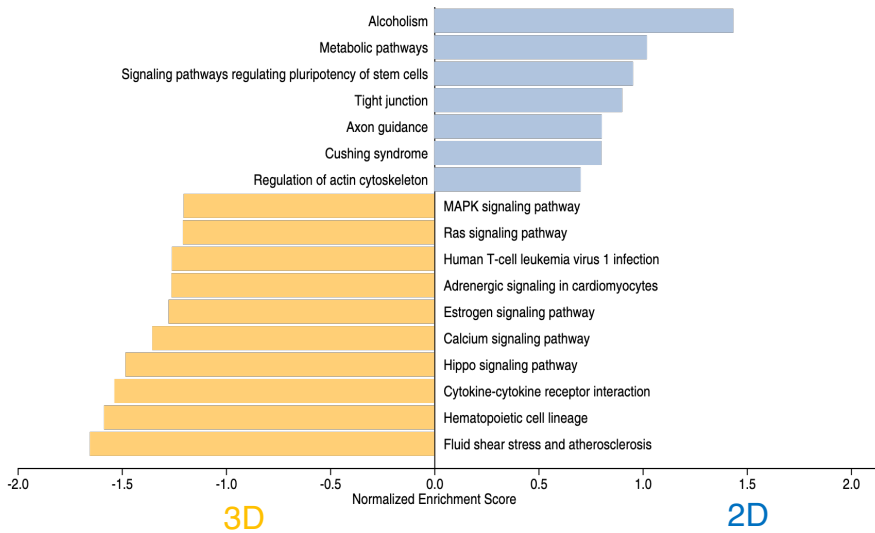
GO: Biological process	Activated	Repressed
Term Name	p_adj	p_adj
biological adhesion	$1.329 \times 10^{-2}$	$9.544 \times 10^{-16}$
cell adhesion	$1.105 \times 10^{-2}$	$1.433 \times 10^{-14}$
multicellular organism development	$2.632 \times 10^{-8}$	$2.732 \times 10^{-13}$
generation of neurons	$8.158 \times 10^{-11}$	1.000
neurogenesis	$9.481 \times 10^{-11}$	1.000
nervous system development	$7.917 \times 10^{-9}$	1.000
actin filament-based process	1.000	$4.081 \times 10^{-7}$
response to wounding	1.000	$5.117 \times 10^{-7}$
regulation of neurogenesis	$1.882 \times 10^{-6}$	1.000
regulation of cell development	$1.885 \times 10^{-6}$	1.000
axonogenesis	$3.274 \times 10^{-6}$	1.000
positive regulation of cell migration	1.000	$3.687 \times 10^{-6}$
positive regulation of cell adhesion	1.000	$4.530 \times 10^{-6}$
regulation of cell differentiation	$5.195 \times 10^{-6}$	$2.721 \times 10^{-4}$
neuron projection development	$6.385 \times 10^{-6}$	1.000
axon development	$6.450 \times 10^{-6}$	1.000

GO: Cellular Component	Activated	Repressed
Term Name	p_adj	p_adj
anchoring junction	1.000	$2.102 \times 10^{-13}$
focal adhesion	1.000	$2.120 \times 10^{-10}$
extracellular region	$8.600 \times 10^{-2}$	$2.810 \times 10^{-10}$
cell-substrate junction	1.000	$3.898 \times 10^{-10}$
cell junction	$4.029 \times 10^{-2}$	$4.072 \times 10^{-9}$
cell periphery	$1.477 \times 10^{-3}$	$1.112 \times 10^{-8}$
plasma membrane	$1.217 \times 10^{-3}$	$4.337 \times 10^{-8}$
contractile fiber	1.000	$5.826 \times 10^{-6}$
actin cytoskeleton	1.000	$8.362 \times 10^{-6}$

**Figure R14 Gene Ontology of Biological Process (BP) and Cellular Component (CC) differentially regulated in 3D cells**

Using the DEA results, GO was performed for Biological Process (left) and Cellular component (right). The main terms enriched are associated with cell adhesion processes, cell structure and regulation of neurogenesis.



### Figure R15 KEGG enriched pathways

Using the DEA results 3D/2D, enriched signaling pathways (KEGG) were obtained, FDR <0.05.

Interestingly, 3D up-regulated genes were significantly enriched in unexpected new terms associated to neurogenesis, nervous system development, axon genesis and neuronal projection. While 3D down-regulated genes were overrepresented in cell and focal adhesion, cell junction and periphery (Figure R14). These results suggest that cells cultured in 3D possess a unique expression program that recapitulates neuronal growth and on the other hand, decreases the expression of adhesion genes, most likely due to the presence of a softer environment. The connection between growth in 3D spheres and the nervous system has been previously reported (and will be further explained in chapter 4. *Discussion*).

Further analysis of KEGG exclusive 3D pathways (Figure R15) showed expected terms related to the shape of the cell and the impact of cell-ECM interactions, such as down-regulation of genes associated to tight junctions (refer to Figure R8) and regulation of actin cytoskeleton. The cytoskeleton is the cellular component that is most clearly impacted, due to the rearrangement caused by the new environment and the physical forces acting on the cell membrane. On the other hand, Ras, MAPK (see chapter 4), and the Hippo signaling (Figure R7) pathways turned out to be enriched in 3D.






### 3.6. Possible molecular mechanism underlying the changes in gene expression



In order to provide the first insight into the mechanism leading to changes in gene expression depending on the cell growth conditions, we used Homer (Heinz et al., 2011) to search for enriched DNA binding motifs of transcription factors around the promoter/enhancer regions of the relevant genes (Figure R16). The most overrepresented binding motif found in genes changing expression in 3D, both as up- and down-regulated, was the sequence recognized by the transcription factor CDX2 (Caudal Type Homebox 2). CDX2 is critical in early intestinal extracellular matrix-mediated differentiation (Lorentz et al., 1997) and has been implicated as a master regulator of the intestinal homeostasis (Coskun et al., 2011), but has been very poorly studied in breast given its very low expression levels. However, it is known that CDX2 modulates a diverse set of processes including cell proliferation, differentiation, cell adhesion, migration, and tumorigenesis in colorectal cancer cells (Coskun et al., 2011). As several of these events are closely related to the extracellular matrix, it is not surprising that it showed up in our analysis.

In addition to CDX2, the binding motifs for the transcription factors YY1 and TFAP2A were also found enriched in the set of genes up-regulated in 3D (Fig R16).

3D upregulated genes (activated)

Motif	P-value	% of targets	Factor match
	1e-31	30.21%	CDX2
	1e-10	0.76%	YY1
	1e-9	0.88%	TFAP2A

3D downregulated genes (repressed)

Motif	P-value	% of targets	Factor match
	1e-36	43.39%	CDX2
	1e-16	11.83%	SP1

**Figure R 16 Homer motif analysis of 3D up- and down-regulated genes.**

A significant enrichment of the CDX2, YY1, AP2A and SP1 DNA binding motifs was found.

We therefore performed the knockdown of CDX2, YY1 and TFAP2A in T47D cells using specific shRNAs according to the protocol described in chapter 2.2. *Methods*. The extent of depletion reached for YY1 and TFAP2A proteins is shown in Figure R17A; but due to the unavailability of an optimal CDX2 commercial antibody and the very low abundance of this protein in T47D cells, the extent of CDX2 depletion was evaluated through RT-qPCR (Figure R17B).

All the analyzed knockdown cells presented a decrease in the proliferation rate in both 2D and 3D conditions compared to the control (shEmpty) cells (Figure R17C). However, when tested for sphere formation for a period of 10 days, CDX2-depleted cells were unable to form proper spheres in Matrigel (Figure R17D-E) and the impact was even more drastic compared to the effect observed in the other KD cells (Figure R17D-E).

Given that the majority of the gene expression changes in 3D is oriented towards repression; the YY1 KD became an exciting approach. This protein may be involved in the relocalization of specific loci to the nuclear periphery. It has been proposed (Harr, 2015) that a complex of YY1 with cKrox, HDAC3 and Lap2b is involved in the recruitment of genomic loci to repressed regions interacting with the lamina. Thus, we generated shcKrox cells. Unfortunately, cells depleted of shcKrox did not survive and further studies with this protein could not be carried out. As previously mentioned, the cells depleted of YY1 were viable but their proliferation in both 2D and 3D was reduced. Moreover, in shYY1 cells the 3D sphere formation

capacity was also affected compared to shEmpty cells (Figure R17D-E).

Lastly, the depletion of the transcription factor AP2A, which has been implicated in early morphogenesis and regulation of mammary gland growth and morphogenesis (Zhang et al., 2003), had a mild impact both in the formation of 3D spheres as well as in cell proliferation (Figure R17D-E).

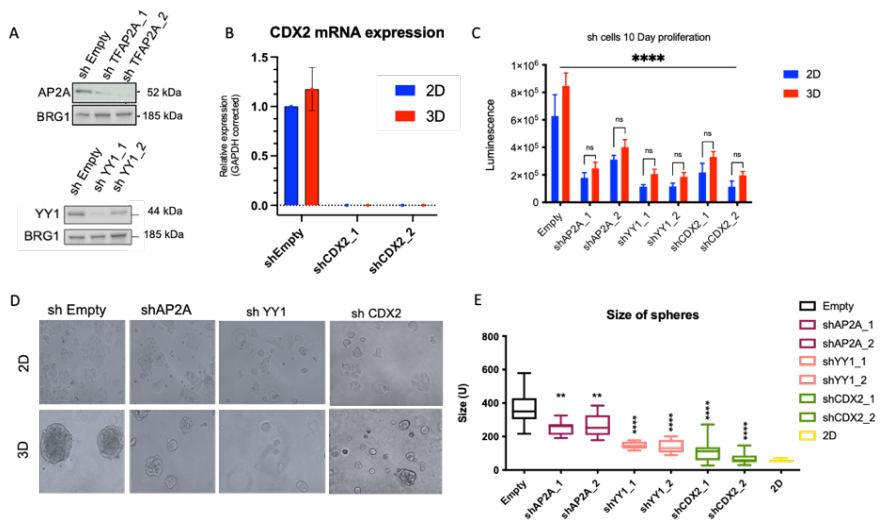


**Figure R17 Characterization of shAP2A, shYY1 and shCDX2 cells**

A) Western blots depicting the levels of AP2A and YY1 in shEmpty (Control), shAP2A and shYY1 cells. B) mRNA expression of CDX2 in shEmpty and shCDX2 cells. C) Cell proliferation assays performed in shEmpty and the different knockdown (KD) cells grown in 2D and 3D conditions (p value < 0.00005). D) Sphere formation assay performed in shEmpty and the different KD cells. E) Comparison of the average size (diameter) of spheres obtained from the different KD and the control (shEmpty) cells. The size of a 2D cell is included for comparison. p value \*\* < 0.005, \*\*\*\* < 0.00005.

In conclusion, the cell proliferation and the sphere formation capacities of T47D cells were mostly dependent on the transcription regulator YY1 and likely on CDX2, with a minor contribution of AP2A. Although these factors emerged from an analysis of genes exclusively regulated in 3D, their depletion also significantly affected their growth in 2D, which suggests that they are more general regulators.

## Chapter III. Impact of the ECM on genomic organization and signaling cascades

### 3.7. Genome architecture

Given the differences observed so far regarding the chromatin accessibility and organization, we hypothesized that a significant change would be expected in the overall 3D genome organization. To tackle this possibility, we performed Hi-C in T47D cells grown as 2D and 3D culture conditions.

First, we explored the chromosome compartments by analyzing the correlation between the eigen vectors obtained from the interaction of Hi-C matrices in 2D and 3D cultured cells at 1 MB resolution (Figure R18A). This analysis allowed the distinction of A (active) and B (inactive) chromatin compartments. It showed no substantial changes in the genome structure at this resolution ( $R=0.99$ ).

Next, we evaluated the genome compartmentalization at 100 kb resolution and found a limited number of changes between cells grown in 2D and in 3D cultures. The analysis identified fifty regions that changed from A (active) to B (inactive) in the 3D condition, while only nine regions changed from B to A. These findings are consistent with the changes in chromatin accessibility and gene expression reported above (Figures R11 and R13), confirming that the chromatin from cells cultured in 3D exhibits more compacted regions, leading to reduced gene expression.

Finally, we assessed the formation of topologically associating domains (TADs). As depicted in Figure R18C, in cells grown in 3D there is a decrease in total number of TADs (3,041 and 2,860 TADs in 2D and 3D, respectively) accompanied by a small increase in their size. This is due to the prevalence of TAD fusions (200) over splitting (60) or shifting (50) (Figure R18D upper panel). Figure R18D (lower panel) shows the Hi-C heatmap plot illustrating the preferential TAD fusions detected in 3D in chromosome X as an example.

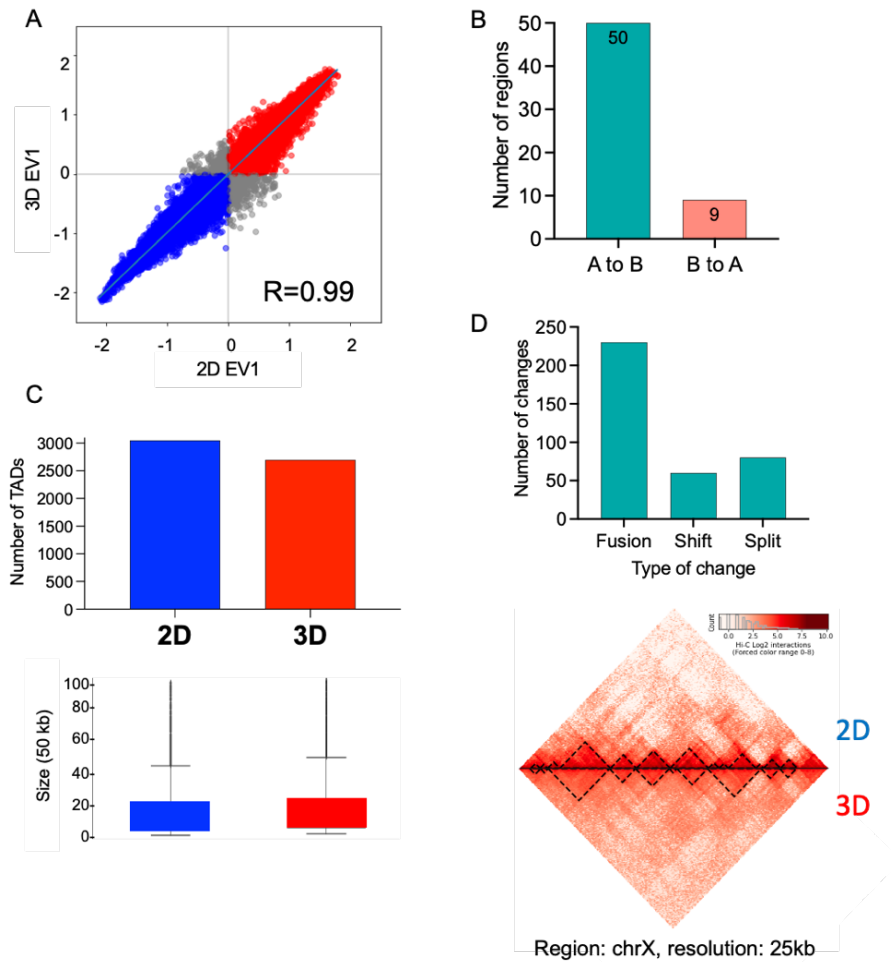


**Figure R18 Hi-C analyses of T47D cells grown in 2D vs 3D conditions**

A) Eigenvector correlation between Hi-C matrices obtained from 2D and 3D cells,  $R=0.99$ . B) Total number of compartment changes from 2D to 3D cells (bin= 50 kb) A to B: 50, B to A: 9. C) TAD changes from 2D to 3D cells, total number of TADs (top) and size of TADs (bottom). D) Type of TAD changes detected in 3D cells. Bottom, Hi-C heatmap of a region located in the X chromosome illustrating TADs fusion in 3D.

### 3.8. How the Hippo pathway impacts the genome architecture in 3D cells

Since the discovery of TADs, it became clear that TAD boundaries are universally enriched in CTCF and cohesin (Barutcu, 2015; Dixon et al., 2012; Nora et al., 2012). In fact, almost all TADs are bookmarked by CTCF ChIP-Seq peaks (Dixon et al., 2012). This suggests an important functional role of CTCF in TAD formation and maintenance.

CTCF is a highly conserved zinc finger protein and is best known as a **transcription factor**. It can function as a transcriptional activator, repressor or as an insulator protein, blocking the communication between enhancers and promoters (Kim et al., 2015). Thus, targeted degradation of CTCF can affect either enhancer-promoter looping or local insulation, promoting TAD fusions.

Therefore, to map the genome distribution of CTCF in both 2D and 3D conditions, we performed ChIP-seq experiments. Even though CTCF protein levels remain unchanged in 2D and 3D conditions (Figure R19A, left), we found that there is a 75 % loss of CTCF binding in 3D cells (Figure R19A, middle and right panels). This led us to hypothesize that the loss of CTCF binding could be responsible for the loss of TAD borders resulting in their fusion detected in 3D (Figure R18D).

Chromatin organization is crucial in gene transcription, and as previous reports have suggested, CTCF is an important insulator for accommodation of gene-enhancer looping. However, it remains poorly understood whether and how the 3D genome architecture is dynamically reorganized by external signals.

A recent study reports that LATS (Large Tumor Suppressor) kinases phosphorylate CTCF in the zinc finger linker and disables its DNA-binding activity (Luo et al., 2020). By applying cellular stress (glucose starvation), the authors were able to induce LATS nuclear translocation, and phosphorylation of CTCF at T347 and S402, that resulted in its dissociation from a small subset of its genomic binding sites. Loss of CTCF binding was able to disrupt local chromatin domains and down-regulate genes located in the neighborhood. This study suggests that external signals could

modulate the 3D genome by affecting CTCF genomic binding through phosphorylation (Luo et al., 2020).

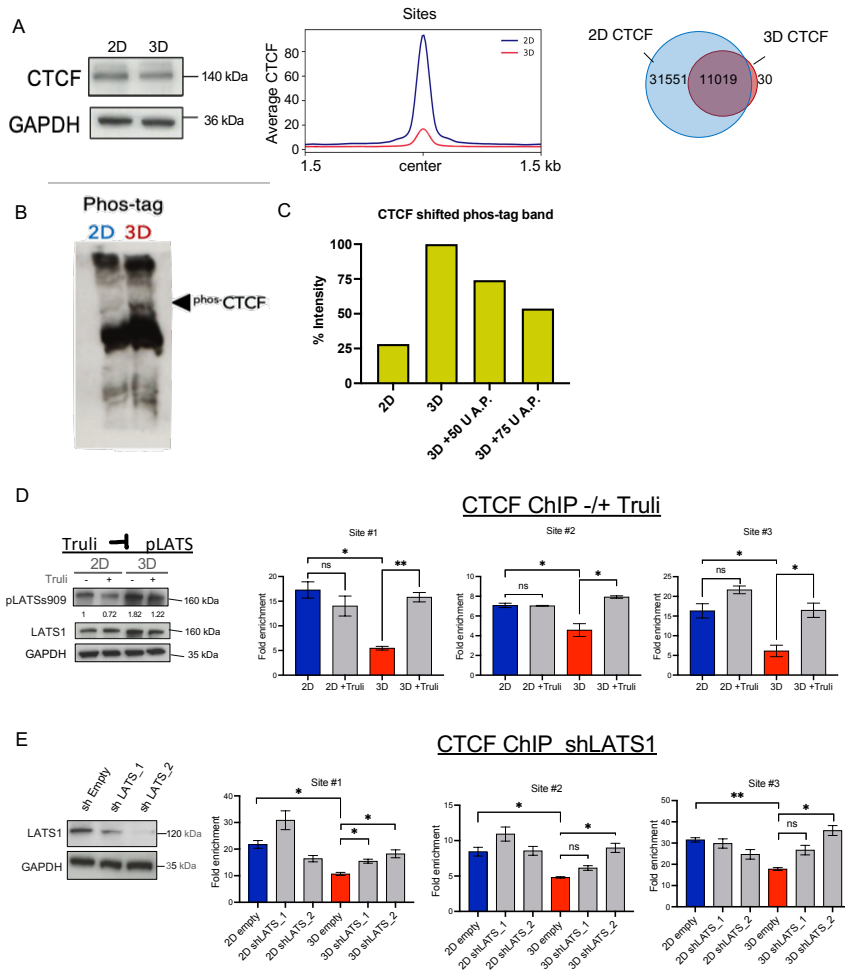


### Figure R19 shLATS control over CTCF

A) Western blot depicting comparable levels of CTCF protein between 2D and 3D T47D cells (left). Differential CTCF binding detected through ChIP-seq in 2D and 3D conditions (right). B) Phos-tag gel identifies phosphorylated band of CTCF protein exclusively in 3D cells. C) 2D and 3D protein extracts treated or not with 50 U or 75 U were analyzed in a phos-tag gel and the band corresponding to the candidate phospho-CTCF like in panel B were quantified using ImageJ. D) Western blot of T47D cells grown in 2D or 3D conditions and treated or not with the LATS inhibitor TRULI (left). ChIP-qPCR of CTCF in three sites where CTCF binding is lost in 3D, the association of CTCF is recovered after treatment with TRULI ( $n=2$ ,  $p$  value  $<0.05$ ). E) Western blot of LATS in

shLATS cell extract (left). ChIP-qPCR of three sites where CTCF binding is lost in 3D. The presence of CTCF is recovered in LATS KD cells (n=2, p value <0.05).

We focused on LATS not only because of its capacity to control CTCF binding, but also because it is a core kinase involved in the regulation of the extracellular-dependent Hippo pathway. In 3D condition, we have shown that the Hippo pathway is activated, resulting in the phosphorylation of YAP at serine 127 by the LATS kinase, its sequestration by 14-3-3 protein leading to cytoplasmic retention and further degradation (Figure R7).

Loss of CTCF binding found in 3D cells (Figure R19A) could be explained at least by two mechanisms: i) methylation of the CTCF DNA binding motif (Maurano et al., 2015; Wang et al., 2012) and ii) by a post-translational modification of the CTCF itself, such as phosphorylation.

The possibility that DNA methylation was involved was discarded after we performed digestion with a methylation-sensitive restriction enzyme of several regions which presented displacement of CTCF in 3D; no methylation in the CTCF motif was detected (data not shown).

Therefore, we evaluated the possibility that CTCF is preferentially found in a phosphorylated state in 3D cells. As no commercial phos-CTCF antibody is available, we performed a Phos-tag gel, that would allow detection of phos-CTCF as slow migrating bands depending on their state of phosphorylation.

When 2D and 3D extracts were analyzed in Phos-tag gels, we found a slow migrating band in 3D, which was not present in 2D (Figure R19B). To confirm that this band corresponded to a phosphorylated version of CTCF, we incubated 3D extracts in the presence of 50 U and 75 U of alkaline phosphatase (AP). The presence of the AP decreased proportionally the signal corresponding to the putative phospho-CTCF (Figure R19C), supporting the hypothesis that phosphorylated-CTCF is found in 3D cells.

Direct impact of LATS on CTCF phosphorylation was tested through a chemical inhibitor known as TRULI, a potent ATP-competitive inhibitor of LATS kinases (Kastan et al., 2021).










Incubation for 24 h with 10  $\mu$ M TRULI decreased the phosphorylated/activated version of LATS in 3D T47D cells (Figure R19D, left panel). Then, when we performed ChIP of CTCF in 2D and 3D cells in the presence and absence of TRULI and binding of CTCF was tested by RT-qPCR. As expected, a decrease in CTCF binding in 3D compared to 2D in three different regions was observed (R19D, right panel). Interestingly, CTCF binding was recovered upon LATS inhibition by TRULI.

To support these findings and to discard indirect effects of TRULI, we performed similar experiments in cells deficient of LATS (Figure R19E, left panel). As with TRULI, knockdown of LATS rescues CTCF binding in 3D cells (Figure R19E, right panel).

A feature of the CTCF sites that we found interesting was supported by HOMER motif analysis of the ATAC-seq peaks. The motif for CTCF tops the rank of enrichment in sites where accessibility is reduced in 3D (Figure R20). It is important to point out that even though BORIS (CTCF-L) is ranked as second, this protein is not present in breast cells, so it is likely that the motif is also referring to CTCF.

Although in 3D the Hippo pathway was ON and theoretically its nuclear effectors YAP/TAZ should not provide a very relevant function *per se*, the DNA binding motif of TEAD was also overrepresented among the ATAC sites that are less accessible in 3D (Figure R20). This could imply a Hippo-independent function of TEAD1/4.

Motif	P-value	% of targets sequences with motif	Factor match
	1e-438	12.1%	CTCF(Zf)
	1e-357	12.17%	BORIS(Zf)
	1e-146	22.02%	TEAD1
	1e-138	24%	TEAD3
	1e-135	19.73%	TEAD4
	1e-132	16.95%	TEAD
	1e-115	13.6%	TEAD2

#### Figure R20 HOMER motif analysis of the ATAC-seq peaks

HOMER motif analysis identifies significant enrichment of the CTCF, CTCFL and TEAD motifs in ATAC-seq peaks with decreased signal in 3D.

Several reports show that displacement of CTCF leads to a decrease in ATAC-seq signal and gene regulation (Franke et al., 2021.; Xu et al., 2021). This would suggest that in 3D, the impact of the Hippo pathway via LATS-dependent CTCF phosphorylation followed by its displacement results in a more compact chromatin at these sites. Therefore, whether these events are connected with the increased TAD fusion in 3D constitutes our next question.

We were able to detect regions where TAD fusions and CTCF displacement overlap in 3D (Figure R21A). However, the loss of CTCF binding was global and distributed throughout the entire genome, impacting on all TADs, irrespective of whether they change or not in 3D (Figure R21B). In Figure R21C-D, several examples are shown where the loss of CTCF was found at fused, shifted or split TADs. In some cases, these changes are associated with changes in the expression of neighboring genes, but this was not a rule, nor the direction of these changes. In fact, we identified several regions where the loss of CTCF did not have impact on the TAD structure at all (Figure R21C-E). Around 95 % of the TAD borders were conserved in 2D and 3D conditions.

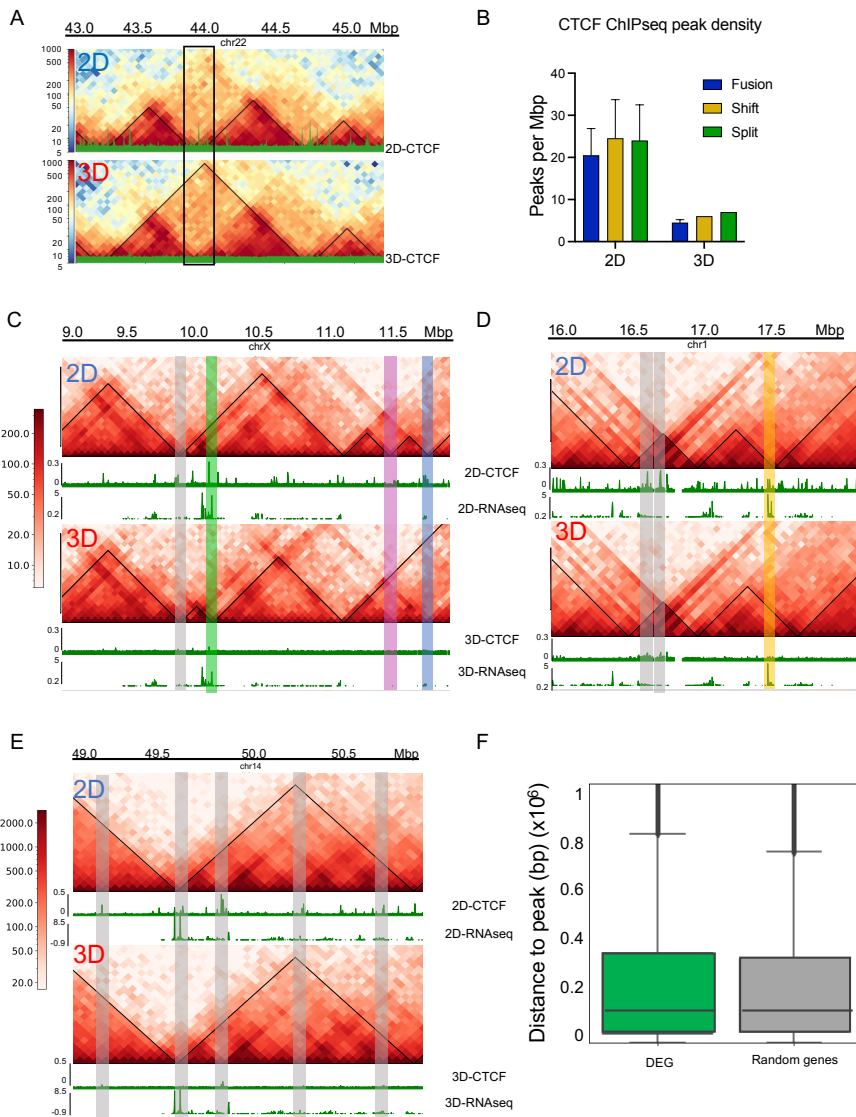


**Figure R 21 Loss of CTCF binding detected in 3D is not directly linked to TAD fusions**

A) Example of a 3D-exclusive TAD fusion event that overlaps with the loss of CTCF binding. B) Density of CTCF peaks in 3D-exclusive fused, split and shifted TADs. C) Loss of CTCF binding overlaps with: 3D-exclusive TAD split and DEG (green), TAD fusion (blue), unchanged TAD borders (gray), TAD fusions without any change in CTCF (purple). D) Loss of CTCF overlaps with TAD shift and DEG (yellow) as well as with unchanged TAD structure (gray). E) Loss of CTCF binding without any changes in TAD structure (gray). F) Distance between a CTCF peak to the most proximal differentially expressed gene in 3D. Plot

shows no differences in distance between DEG in 3D and random genes to CTCF binding regions.

By its original definition, the structure and function of a mammalian TAD require the binding of the CTCF protein and the cohesin complex at its borders (Dixon et al., 2012; Sofueva et al., 2013). Collectively, our findings suggest that besides CTCF binding, additional factors may play more relevant roles in establishing TAD boundary formation in breast cancer cells. In fact, CTCF would be dispensable on TAD formation in our system.

Lastly, the extent of CTCF binding begs the question of its role outside genome organization. Despite the presence of CTCF at nearly 90 % of TAD boundaries in mammalian cells (Dixon et al., 2012), the majority of its binding sites are within TADs near enhancers, promoters, or even gene bodies, pointing to a broad function of CTCF, including gene transcription activation, repression, elongation, and pre-mRNA splicing (Phillips & Corces, 2009).

Given that the largest impact we observed in 3D cells was on gene regulation and on CTCF displacement, we next asked whether these two events could be connected. For this, we interrogated whether genes affected in 3D present a CTCF site nearby. Our results suggest that both up- and down-regulated 3D genes are not significantly closer to a CTCF site and therefore may not be directly affected by its displacement (Figure R21F).

## Chapter IV. Comparison of the hormonal response of breast cancer cells grown as monolayer (2D) and spheroids (3D)

### 3.9. PR signaling upon hormonal stimulation

Our lab has extensively described the activation and transcriptional control by steroid hormones in breast cancer cells (Ballaré et al., 2013; Vicent et al., 2011; Beato et al., 2020; Vicent et al., 2009; Wright et al., 2016). These effects are dependent on the binding of a hormone receptor to promoter or enhancer regions to regulate the transcriptional activity of target genes. In our lab we have focused on studying the role of progestins and the progesterone receptor (PR).

In the presence of hormone, PR is bound to regions in the genome enriched in HREs where it triggers the recruitment of coregulators and chromatin remodeling complexes, and induces the formation of the transcription initiation complex. On the other hand, PR also exerts rapid *non-genomic* effects. As described, after 5 min of hormone a rapid transient activation of Src/p21<sup>ras</sup>/Erk kinase cascade is observed which is essential for progestin induced cell proliferation (Migliaccio et al., 1998).

This rapid effect of progestin is mediated by the interaction between the N terminal half of PR and the ligand binding domain of ER $\alpha$  in the cell membrane (Ballaré et al., 2003; Migliaccio et al., 1998). ER $\alpha$  interacts directly with c-Src and activates its tyrosine kinase activity to initiate the MAP kinase cell signaling cascade, leading to phosphorylation and activation of the PR at residue 294 (pPRs294). The activated ERK1/2, the kinase MSK1 and pPRs294 form a ternary complex that induces phosphorylation of H3 in S10 and chromatin remodeling (Vicent, 2006).

As all experiments and results obtained so far were carried out on cells grown in monolayer (2D), in this chapter, by comparing 2D vs 3D we pursue to address whether the hormonal response depends on the environment in which the cells are grown.

To perform experiments where the T47D spheroids are treated with hormone, first, cells need to be synchronized and arrested in G0/G1 by hormone deprivation treatment. For this, T47D cells were grown on a Matrigel lacking phenol red (compound with estrogenic activity) but retains all the components that allow 3D growth. After allowing these cells to grow for a period of 7 days, parallelly to 2D culture, the medium was changed to phenol red free-medium supplemented with charcoal dextran treated-FBS and incubated for 48 h followed by a final incubation with medium without FBS for 16 h prior to the treatment with 10 nM R5020.

First, we measured the level of expression of different transcription factors involved in the activation of PR in both growing conditions. As depicted in Figure R22A-B, the levels of PR, ER $\alpha$  and FOXA1 remained similar between both conditions. A slight increase in the levels of pPRs294 was detected in 3D compared to 2D in the absence and in the presence of R5020 (Figure R22A, top row). However, there were no differences either in the extent of pPRs294 signal induced by hormone (Figure R22C, left) or in the percentage of cells responding to the hormonal stimulus (Figure R22C, right). pPRs294 signal increased with hormone and its expression was detected throughout the spheroid, homogeneously distributed in all the cells conforming the sphere (Figure R22B), similar to the observed pattern for total PR in the immunostained z-projection of 3D cells (Figure R6).

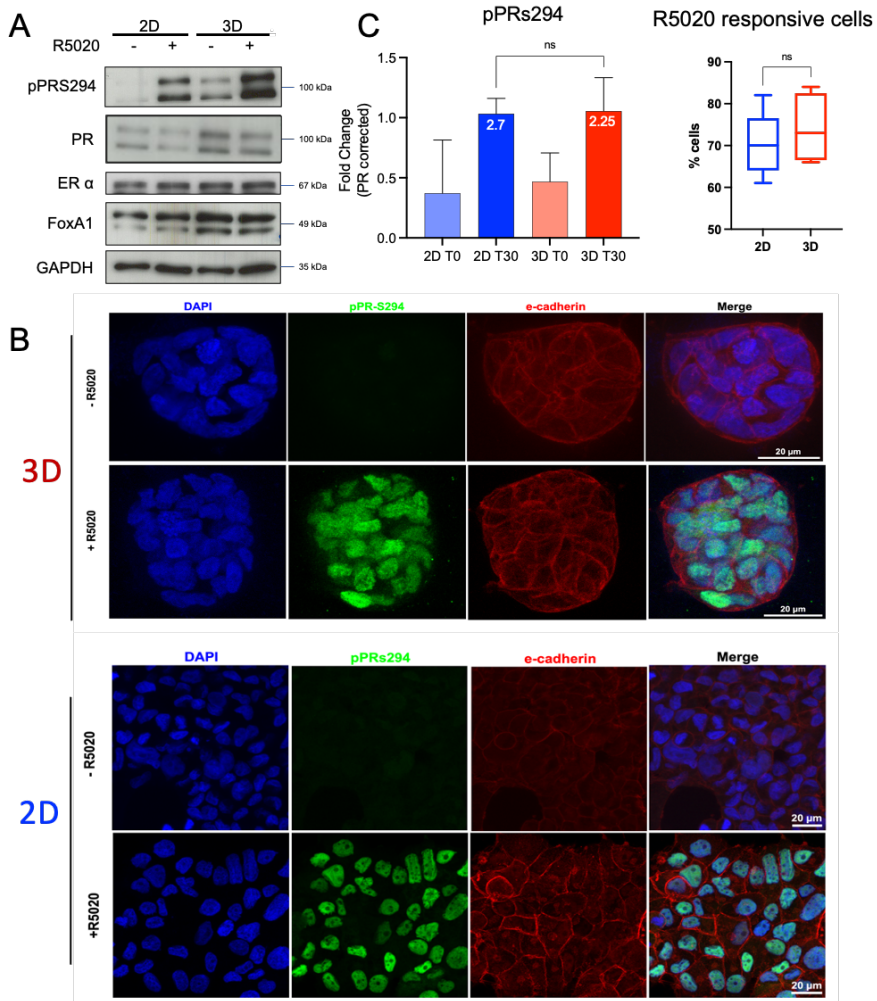


**Figure R22 Activation of Progesterone Receptor in T47D cells in response to 10 nM R5020 in 2D vs 3D cells**

A) Levels of PR, ER $\alpha$  and FOXA1 were assayed in 2D and 3D cells treated or not with 10 nM R5020 for 30 min. B) Immunostaining of 3D and 2D cells in the presence and in the absence of 10 nM of R5020 for 30 min, DAPI (blue), phosphoPR S294 (green), e-cadherin (red), and merge of all channels. C) Similar levels of PR activation between 2D and 3D conditions were observed (left). Similar percentage of T47D cells turned out to be responsive to hormone in both culture systems.

To globally evaluate the hormone-regulated genes in the spheroids and compare them to the classical 2D model, we performed RNA-seq experiments. Briefly, T47D cells grown in 2D or 3D were treated or not with R5020 for 6 hours, RNA was extracted, libraries were generated and submitted to massive sequencing. To our surprise, almost twice as many genes were modulated by hormone in 3D cells (3,503 vs 1,933,  $\log_2FC > 1$ , adj p value  $< 0.01$ ). Up-regulated genes were increased around 50 % and down-regulated genes increased by 140 % (Figure R23A). Most of the regulated genes in 3D are new responsive genes that were not regulated in 2D (1,029 and 1,254 genes for up and down-regulated genes, respectively) (Figure R23B).

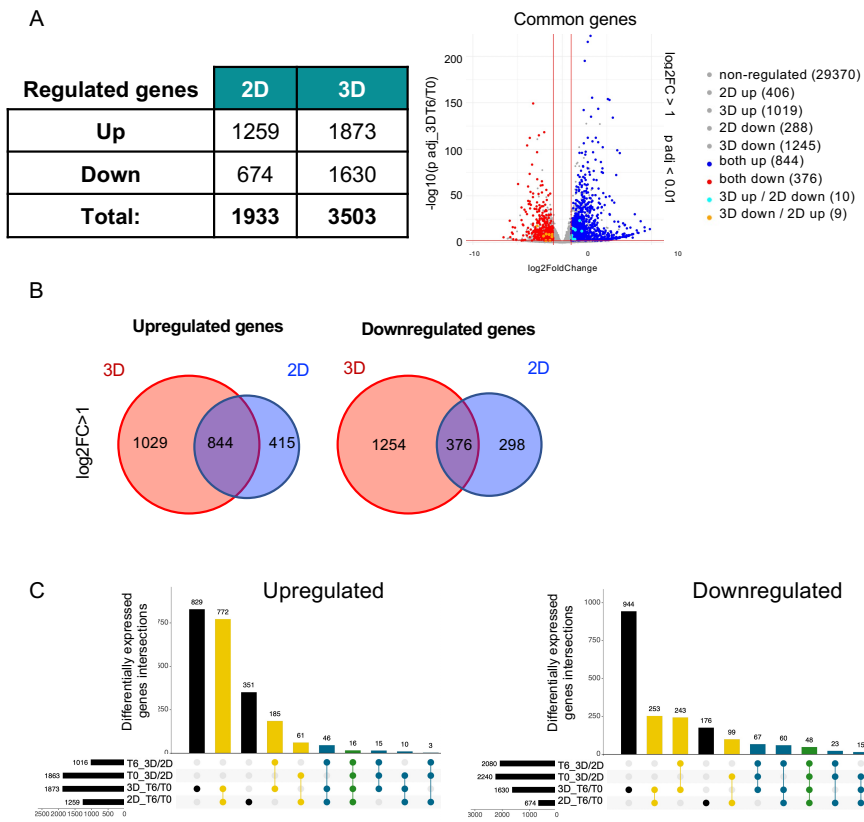


**Figure R23 Differential Expression Analysis performed in 2D and 3D T47D cells**



A) Left: Total number of up- and down-regulated genes detected in T47D cells grown in 2D and 3D conditions in the presence or absence of 10 nM R5020 during 6 h ( $\log_2FC > 1$ ,  $p \text{ adj} < 0.01$ ). Right: volcano plot of the distribution of genes regulated in both conditions. B) Venn diagrams of up- and down-regulated genes detected in 2D and 3D cells. C) Upset plots depicting the changes in expression and the number of genes when cells were treated with hormone and when changing cell culture. (Up-regulated) 829 genes are exclusively changing in 3D, 185 are exclusively activated in 3D and have the same basal level as in 2D but differ in the extent of activation; (down-regulated) 944 genes are exclusively regulated in 3D, 243 are exclusively repressed in 3D and have different extent of repression. One colored dot signifies a single change on expression regulation in the appointed condition. Two dots, refer to a shared change between expression regulation, etc.

In Figure R23A (right panel), the volcano plot helps to visualize the genes equally affected in both conditions (1,220 common genes). In fact, very few genes showed opposing regulation in 2D and 3D (19 genes).

We then tried to find whether there was a common trend in the changes observed in the differentially regulated genes. We observed that a new gene expression programme is engaged in 3D, with the majority of 3D exclusive regulated genes without significant changes at the basal levels (Figure R24C, first column) and despite being regulated, only a low number of genes differ in their basal or final expression. This finding points to an effect of the environment on the hormonal response.

A summary of the most significant terms from a Gene Set Enrichment Analysis (GSEA) performed on the specific groups of hormone-regulated genes is described below (Figure R23).

Interestingly, among the GO categories regulated by hormone in 3D we noticed that terms such as *cytoskeleton*, *actin filament organization*, *cell growth* and *cell-cell junction* appeared. These terms were also overrepresented when the extracellular matrix was the only variable incorporated into the analysis (previous Figure R14). Therefore, the hormone in 3D cells activated pathways aimed to reinforce biological processes associated with their own spherical nature.

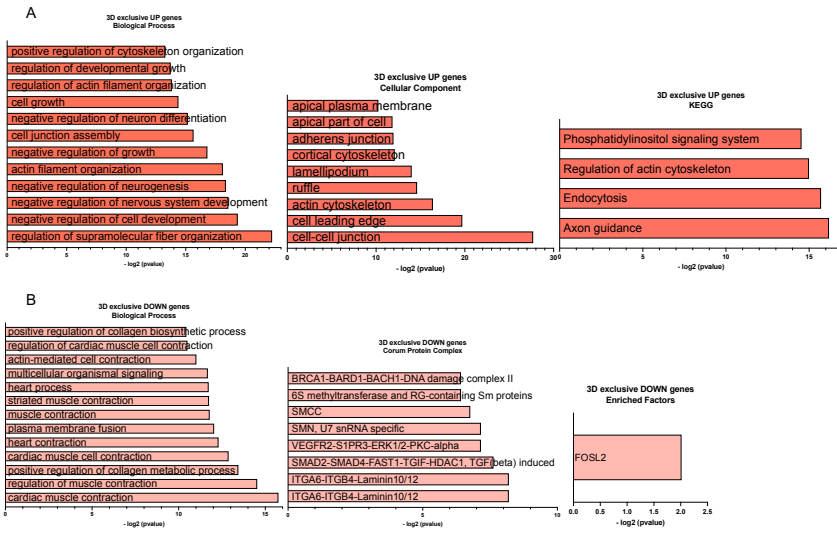


**Figure R 24 Significant GO terms in 3D T47D cells treated with R5020**

Using the DEA results, GO analysis was performed on 3D DEG. The top terms are shown. The main enriched terms for up-regulated genes are associated with cell structure, neurogenesis and neuron development, while the terms for down-regulated genes are related to cell membrane components and cell contraction.

Next, we focus on the new terms and our attention was drawn towards *neurogenesis*, *axon formation* and *neuronal organization* overall. The function of ECM in neurogenesis may be associated with particular patterns of proteolysis of the extracellular matrix. In this context, enzymes that modify the extracellular matrix and modulate both the axonal guidance and cell adhesion molecules are of particular relevance, for example, the matrix metalloproteinases (MMPs) are postulated to play important role in ECM remodeling required for many developmental processes (Wojcik-Stanaszek et al., 2011).

Regarding cellular components, the majority of the terms refer to cytoskeleton components. In migration the cell's front is a site of rapid actin polymerization promoted by the cytoskeleton dynamics. This promotes the formation of specialized membrane structures such as **ruffles**, **pseudopodia**, and **lamellipodia**, where interactions of the cell with other cells or with extracellular proteins are occurring (Guan et al., 2015). Not only by contact, but other authors have reported the effect of androgens on T47D cells

regulating the motility and invasion through actin cytoskeleton remodeling (Montt-Guevara et al., 2016).

Other terms associated to *heart contraction*, *cardiac muscle* and *heart process* emerged overrepresented in the 3D down-regulated genes (Figure R23B, bottom panel). ECM components have been found to be of considerable importance in the culture of 3D cardiac organoids. These structures rely heavily on the ECM integration of laminin, fibronectin and collagen (Jallerat & Feinberg, 2020). Moreover, ECM proteins and growth factors play crucial roles in myogenesis and muscle cells contraction, these substances are closely linked to the activation of integrin complexes on the cell membrane to regulate migration, proliferation and differentiation (Grzelkowska-Kowalczyk, 2016), changes in expression and/or secretion of proteoglycans, metalloproteinases, adhesion molecules, and growth factors in regenerating muscle tissue and differentiation. FOSL2 factor facilitates TGF- $\beta$ 1 induced migration (Wang et al., 2014), tightly linked to ECM-mediated regulation.

In light of our results, in the presence of hormone, breast cancer cells grown as spheroids responded in a differential manner to those grown as monolayers. The hormone in the spheroids regulated pathways that aim to reinforce and positively feedback the cell-ECM connection, such as cytoskeleton, neuronal and muscular development.

### **3.10. Progesterone receptor binding upon hormone stimulation**

As mentioned previously, changes caused by the exposure to R5020 is mediated by the activation of the Progesterone Receptor (PR). In the presence of hormone, the PR translocates to the nucleus where it actively regulates gene transcription.

In order to understand whether the observed environment-dependent changes in gene expression are associated with changes in PR binding to the genome, we carried out ChIP-seq experiments of PR in 2D and 3D cells treated or not with R5020. Moreover, it is worth studying PR binding in a differentially accessible chromatin presented in the two cell dimensions (Figure R11).

We prepared two replicates per condition and performed massive sequencing of the samples. At basal levels (T0), no binding of PR was detected. Only the peaks that appeared in both replicates per condition were used for further analysis (Figure R25A).

In line with the increased number of genes regulated in 3D, we also observed more PR binding sites (PRbs) in 3D. Almost all PRbs found in 2D were also present in 3D, but 8,196 new PRbs were exclusive for 3D (Figure R25A).

The genomic distribution of total PRbs in 3D is very similar to 2D (Figure R25B, upper panels). Compared to 2D exclusive, the distribution slightly changed in the 3D exclusive PRbs, with less PRbs in introns and more in Promoter, UTR and exons (Figure 25B, lower panels).

We measured the correlation between PR binding and the gene body/promoter of the DEG obtained from our RNA-seq. The number of genes being regulated by direct binding of PR is notoriously increased in 3D.

From the 8,196-3D exclusive PRbs, we took the 839 binding sites corresponding to promoter (8.54 % of total annotation) and overlapped it with 3D exclusive regulated genes to find if these new binding sites were directly responsible for this new 3D regulation.

In 2D, 104 of the regulated genes contained PRbs while this value increased to 311 in 3D (Figure R25C). Therefore, we identified 311 newly regulated genes directly bound by PR exclusively in 3D. This value was statistically significant as we tested the overlap of the same PRbs with 1,000 random genes (500 times) and resulted in an average of 10-40 genes with a p value =  $3.042e^{-06}$ . Regarding the direction of the hormonal effect, the majority corresponded to up-regulated genes (Figure R25C, right).

We can conclude that: i) the overlap between 3D PRBs and 3D regulated genes is significantly higher than would be expected by chance, ii) the number of genes being directly regulated by PR is higher in 3D compared to 2D and iii) a majority of these genes are up-regulated.

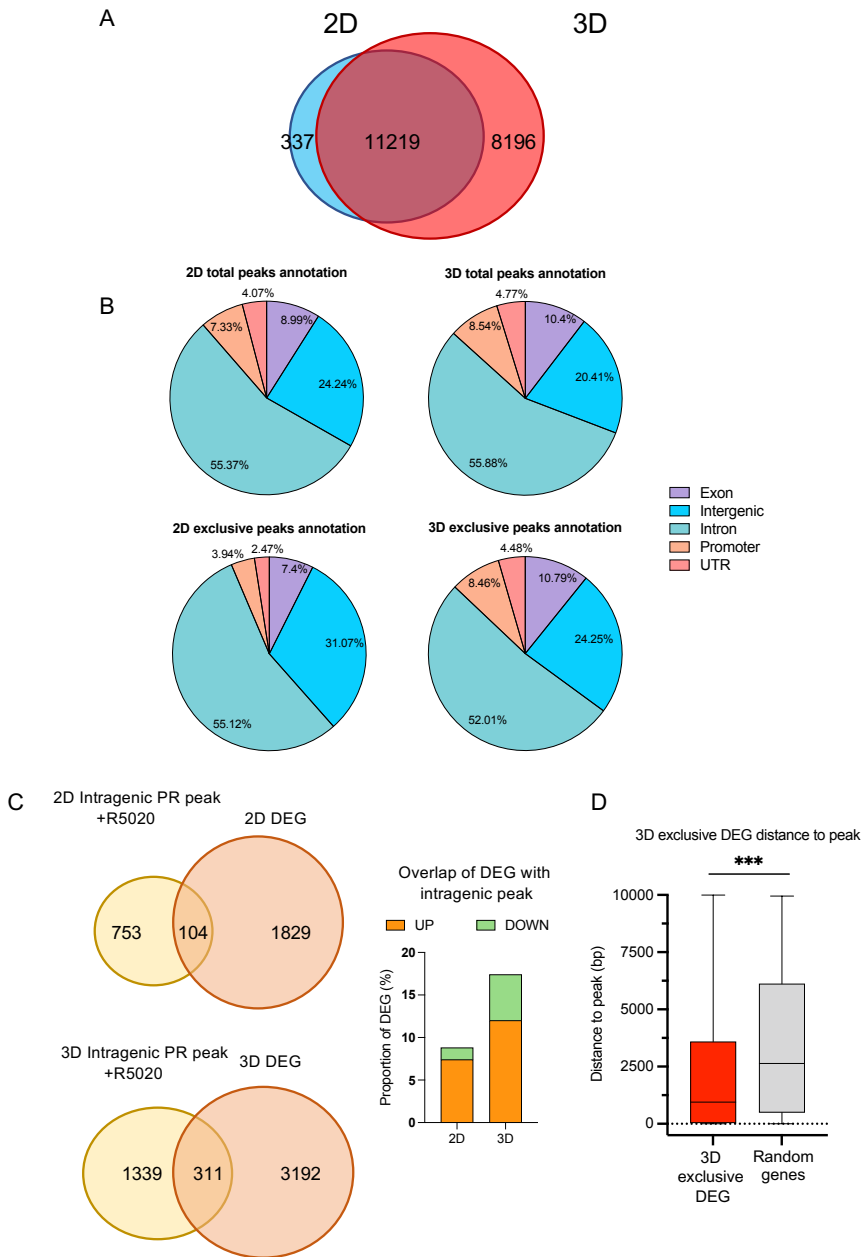


**Figure R 25** ChIP-seq of PR performed in 2D and 3D cells upon hormone exposure

A) Venn diagram of the total number of PR binding sites (PRBs) from two replicates of ChIP-seq performed in 2D and 3D T47D cells in the presence and in the absence of 10 nM R5020 for 30 min. B) Peak annotations of total and exclusive 2D or 3D PRBs. C) Venn diagrams showing the overlap of intragenic PRBs with differentially expressed genes after R5020 treatment (Left). Plot

depicting the percentage of DEG (up- or -regulated) that overlap with intragenic PRbs for both 2D and 3D cells (Right). D) Distance between enhancer-associated PRbs (those which overlapped with H3K27ac ChIP-seq signal) to the most proximal differentially expressed gene (3D exclusive).

However, as previously reported by our lab, the majority of the PRbs are localized far from the target genes, in enhancers (Ballaré et al., 2013). To map the hormone-dependent active enhancers we overlapped 3D exclusive PRbs (8,196 regions) with H3K27ac peaks obtained from a ChIP-seq. Then, we measured the distances between these peaks to the nearest significantly regulated gene in 3D (2,283 genes) or random genes. The 3D exclusive genes were significantly closer to 3D PRbs enriched in H3K27ac (enhancers), compared to random genes (Figure R25D). Thus, in 3D there is a defined programme aimed at the regulation of a distinct group of genes that involves the specific binding of the PR to the promoter/gene body of those genes as well as to their enhancers.

In order to carry out a more in-depth study of the PR binding exclusively detected in 2D or 3D, we performed a *de novo* Homer motif enrichment analysis. This analysis would allow us to find other transcription factors that might be cross-talking with the PR exclusively in 2D or 3D conditions. We present the most relevant and significant motifs obtained for each condition (Figure R26).

Several of the transcription factors that appeared overrepresented like Zbtb12, TEAD4/2, Znf768 and MAC1 have been previously reported to be associated to ECM, cell adhesion and mechanosensing. Briefly, Zbtb12 is involved in the regulation of extracellular matrix stiffness and control of RNA localization to promote cell migration (Wang et al., 2017).

Previously mentioned, TEAD is a well-known stream effector of the Hippo pathway, key regulator in development, tissue homeostasis and cancer progression (Dupont et al., 2011).

## 2D exclusive motif enrichment

Motif	P-value	% of targets	Factor match
	1e-250	65.41%	PR (NR)
	1e-136	70.56%	SPL11
	1e-84	59.76%	ZBTB12
	1e-43	71.66%	POL009.1
	1e-42	13.78%	TEAD4

## 3D exclusive motif enrichment

Motif	P-value	% of targets	Factor match
	1e-939	75.45%	PR (NR)
	1e-696	57.59%	ZNF768
	1e-520	61.60%	Bcl6
	1e-370	37.80%	MAC1
	1e-81	5.53%	TEAD2

**Figure R 26 HOMER *de novo* motif enrichment analysis for 2D and 3D PR exclusive peaks**

Moreover, Znf768 was shown to promote proliferation and repress senescence stream of growth factor signaling; while Mac1 is a described integrin that promotes cell adhesion and migration (Cao et al., 2006).

To demonstrate that a crosstalk between PR and these 3D-specific TFs is taking place, knockdown experiments followed by ChIPs of PR and gene transcription assays will be required.

### 3.11. Accessibility of the chromatin upon hormone exposure

When the PR binds to the target HRE, it becomes associated with coregulators: P300/CBP, SRC1-3, BAF, HDACs, NCOR, SMRT to remodel the chromatin making it more accessible to other TFs and RNApol II.

In cells grown as spheroids, we detected an increased number of hormone regulated genes as well as increased number of PRbs. We then asked if PR binding and chromatin remodeling is similar to the 2D condition.

We performed an ATAC-seq assay in 2D and 3D cells treated or not with hormone. We found that 'basal' accessibility is already decreased in 3D compared to 2D as previously observed when cells were grown in full medium (Figure R11). Upon hormone exposure both 2D and 3D reached the same level of accessibility (Figure R27A).

To evaluate if the gain of accessibility had any correlation with changes in gene expression, we selected all differentially expressed genes (up and non-regulated separately), for 3D and 2D (based on  $p \text{ adj} < 0.01$ ,  $|\log_2\text{FC}| > 1$ ) to check which genes had gained or lost accessibility (based on the differential ATAC-seq signal).

A significant proportion of up-regulated genes increased accessibility in 3D compared to 2D (Figure R27B, left panel). No differences were found for non-regulated genes (Figure R27B, middle and right panels).

We could also compare the accessibility of the 2D and 3D exclusive PR binding sites. First, observation points to the fact that both 2D and 3D exclusive PRbs are more open in the condition in which they have been identified. Thus, exclusive 2D PRbs are more open in 2D both at basal as well as with hormone compared to the same regions in 3D (Figure R27C). Similarly, in 3D cells the 3D exclusive PRbs gain accessibility by the presence of the progestin yet remain unaffected in 2D conditions (Figure R27C).

Recently in our lab, a classification of PR binding sites has been established according to their accessibility. The lowest progestin concentration that allows detection of ligand-dependent PRbs was



50 pM. At this low concentration 2,848 PRbs, termed 'Highly Accessible PR binding sites', (HAPRbs) were identified (Zaurin et al., in press).

Given that HAPRbs respond to physiologically low concentrations of hormone, we considered the importance of these regions in our 3D model. Results show that although similar levels of accessibility are reached with hormone in both 2D and 3D conditions, there is also a decreased basal accessibility in 3D cells (Figure R27C). It is important to note that HAPRbs are more accessible in 2D, probably because this is the model where they were originally defined.

Finally, we considered the possibility of the regulated genes localized in an ATAC-gained region to also overlap with the new binding of PR. For this we took the DEG from our RNA-seq overlapping with a newly accessible site from the result in Figure R27B and searched for PR peaks from our PR ChIP-seq data. A very small group of up-regulated and accessible genes owe their activation to PR binding in the gene body/promoter regions (61 genes). These would constitute a group of *bona fide* 3D hormone regulated genes (Figure R27D). However, a large majority of the accessible regulated genes in 3D are not close to a PR binding site. Pointing to the possibility of PR acting through long distance looping, bound to enhancers.

Our experiments suggest that a reorganized chromatin product of the extracellular environment allows a higher binding of PR in 3D cells, that will reflect in a higher number of genes regulated by hormone.

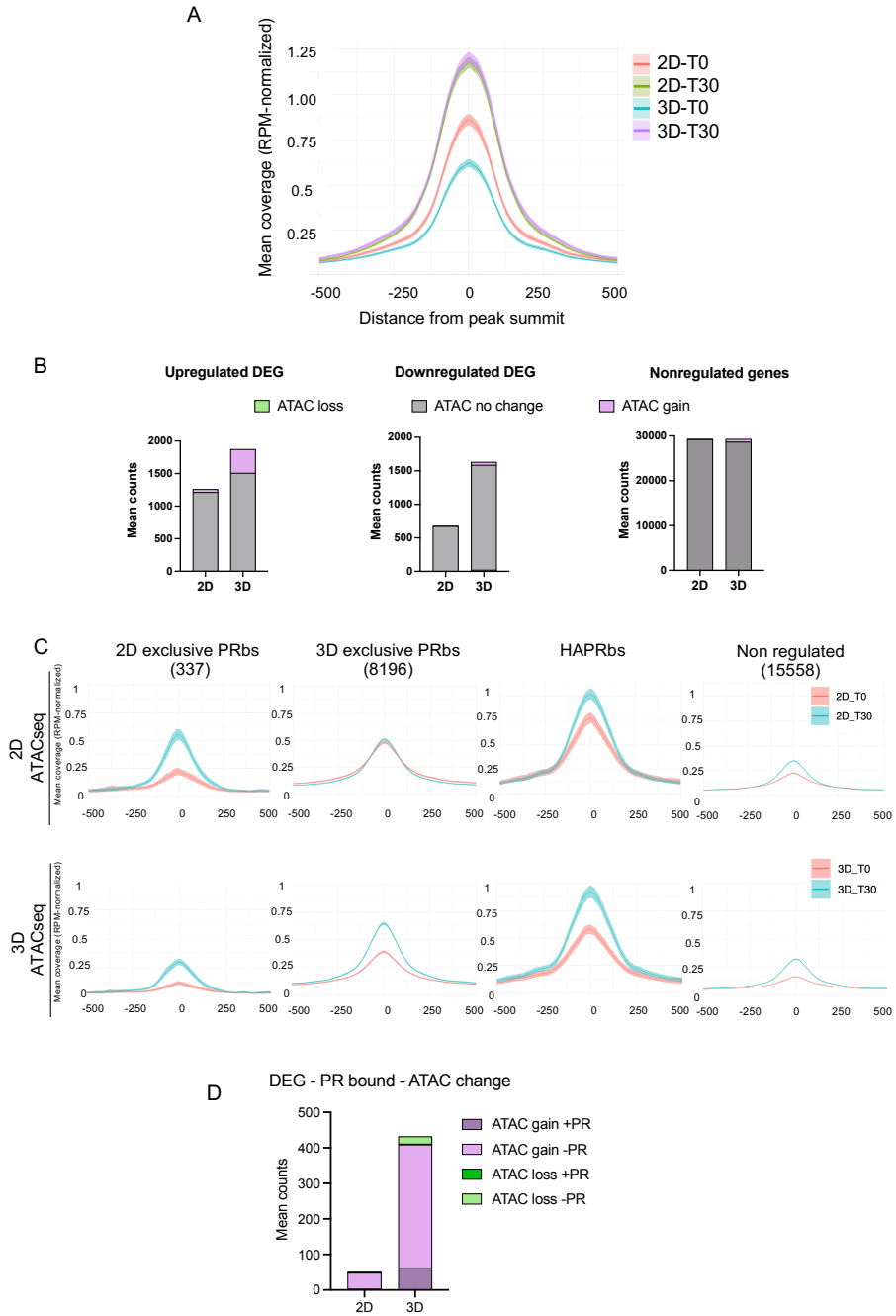


**Figure R 27 ATAC-seq analysis reveals a more pronounced chromatin remodeling in 3D cells treated with hormone**

A) Metaplot of normalized RPM obtained from ATAC-seq performed in T47D cells treated or not with hormone and grown in 2D or 3D conditions. B) Overlap of gain/loss ATAC-seq signal with DEG. C) Accessibility detected at 2D exclusive PRBs, 3D exclusive PRBs, High accessible PRBs and in random genes. D) Overlap of gain/loss ATAC-seq signal with DEG that also gain PR binding (combined analysis of ATAC-seq, RNA-seq and PR CHIP-seq).



## **4. Discussion**

This doctoral thesis attempts to answer how cell external factors, in our case particularly the extracellular matrix, influence the cell nucleus. In concrete, we want to understand how signaling pathways that are turned on in the 3D culture conditions affect the shape of the nucleus, the accessibility of the chromatin within, as well as the function and structure of the nuclear genome. Regarding the response to external signals, we have compared how progestins (R5020) act in breast cancer cells grown as monolayer or as spheres.

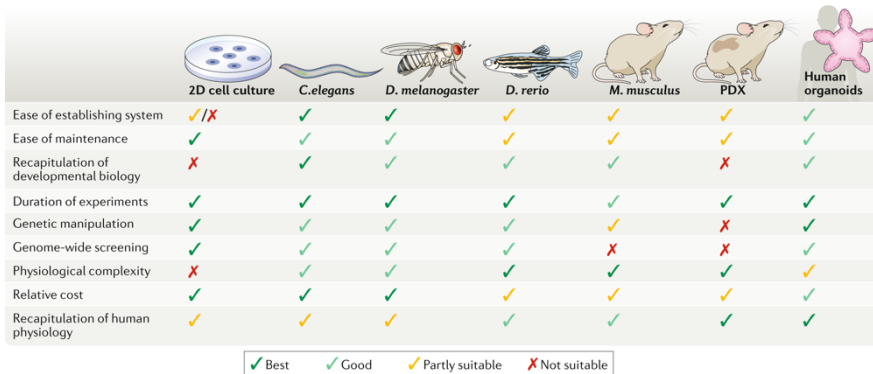
To approach these issues, we have chosen the T47D breast cancer cell line, from which the group has collected a large amount of data on transcription factor binding, gene expression, epigenetic changes, accessibility and genome structure in response to hormone, but always growing the cells as a monolayer.

We want to learn about cell signaling pathways, gene networks, the underlying mechanisms involved, transcription factors and chromatin remodelers that might have been overlooked in previous 2D experiments. The work reported here is a first step in the description and characterization of a more appropriate and physiological model for breast cancer.

In this section, I will discuss the results considering the current knowledge in the field. The topics will follow the same order as they were presented in the Results section.

### **4.1. General characterization of 3D breast cancer spheroid development**

3D cell culture approaches are becoming a useful tool in the field of biomedicine given that these techniques allow for a more suitable approach into the physiology of the human tissue. These techniques are now more commonly used in biomedical research due to their advantages over other 2D models (Kim et al., 2020).



	2D cell culture	<i>C. elegans</i>	<i>D. melanogaster</i>	<i>D. rerio</i>	<i>M. musculus</i>	PDX	Human organoids
Ease of establishing system	✓/✗	✓	✓	✓	✓	✓	✓
Ease of maintenance	✓	✓	✓	✓	✓	✓	✓
Recapitulation of developmental biology	✗	✓	✓	✓	✓	✗	✓
Duration of experiments	✓	✓	✓	✓	✓	✓	✓
Genetic manipulation	✓	✓	✓	✓	✓	✗	✓
Genome-wide screening	✓	✓	✓	✓	✗	✗	✓
Physiological complexity	✗	✓	✓	✓	✓	✓	✓
Relative cost	✓	✓	✓	✓	✓	✓	✓
Recapitulation of human physiology	✓	✓	✓	✓	✓	✓	✓

✓ Best    ✓ Good    ✓ Partly suitable    ✗ Not suitable

**Figure D 1 Comparison between the features of different models**

The most common model organisms used in biomedical research are *C. elegans*, *D. melanogaster*, *D. rerio* and *Mus musculus*, along with patient-derived xenografts (PDX) in mice. These models, as well as 2D cell cultures and human organoids, are assessed for their relative benefits and limitations. Relative scores are represented as being the best (dark green tick), good (light green tick), partly suitable (yellow tick) and not suitable (red cross). Adapted from (Kim et al., 2020).

However, finding an optimal scaffold matrix to mimic the physiological extracellular space is still challenging. After testing different hydrogels, we found that Matrigel gives the most optimal environment for T47D breast cancer cells, as it allows proper *in vivo* reconstitution of the breast acini as an organized sphere structure and not merely as an accumulation of cells (Figures R1, R2). The use of Matrigel in 3D culture represents a more affordable approach for biomedical studies. It allows reconstitution of physiological structures, presented a reproducible and moderate cell growth, and also showed hormone-dependent cell proliferation; thus, replicating the basic behaviour of tumor cells *in vivo*.

Morphologically, T47D cells grown as spheroids in soft Matrigel presented a more defined rounded nucleus with a smaller diameter, in comparison to the flattened stretched nucleus found in cells grown as monolayers on hard plastic. It has been widely reported that modifying the stiffness and composition of the used matrix can have an impact on cell growth, cell cycle, differentiation, and the activation of specific signaling pathways, such as the Hippo signaling pathway (Uroz et al., 2018; Garreta et al., 2019). Exposure of cells to a stiffer environment implies a force

transmission through focal adhesions leading to nuclear flattening and stretching of nuclear pores, reducing their mechanical resistance to molecular transport, increasing YAP nuclear import (Elosegui-Artola et al., 2017), and indirectly affecting gene expression. Conversely, on soft substrates, the nucleus is mechanically uncoupled from the matrix and not submitted to strong forces, inducing a balance between nuclear import and export of YAP through the nuclear pores (Elosegui-Artola et al., 2017).

Another process by which external forces impact on the cell nucleus is the unfolding of the INM (Inner Nuclear Membrane) produced upon stretching during adaptation of the cell to mechanical confinement. This mechanism comprises the activation of a calcium-dependent mechanotransduction pathway resulting in the nucleus adapting to their microenvironment (Venturini et al., 2020).

Considering that these external forces impinge on the nuclear membrane as well as the direct functional connection of the nuclear membrane, with lamins, nuclear matrix and chromatin (Van Steensel & Belmont, 2017), it is not surprising that these forces have a large impact on the genome architecture and on gene regulation.

## **4.2. Impact of the 3D growth on nuclear structure and function**

The differential distribution of DAPI nuclear staining in 2D and 3D indicating an increase in heterochromatin clumping in 3D led us to perform more accurate assays to study the chromatin state in both conditions. Therefore, we performed MNase and ATAC-seq experiments which confirmed that the chromatin in the 3D cultured cells is more compacted and thus, less accessible (Figure R10, R11). Interestingly, and in line with these results, we found an increased number of regulated genes in 3D cells (Figure R13). According to the GO, when cells are grown in Matrigel the cell appears to be losing tight adhesion to the plastic to become more motile. Terms as neurogenesis, extension of lamellipodia and

axon guidance, suggest that the cells in 3D present a higher degree of mobility to migrate in soft Matrigel.

The protrusions observed to be emerging from the cell membrane (pseudopodia) and the filopodia extending out from lamellipodia, are clear indicators of cell-matrix interactions. They are associated with cellular sensing mechanisms, involving **cell adhesion and cytoskeleton organization** strategies (Caswell & Zech, 2018), as supported by the GO terms of the regulated genes. These protrusions, connected in turn with the cytoskeleton, are essential for the cells to sense the environment and generate pulling forces when focal adhesions are established. These interactions are not present in 2D monolayer cell cultures, where the cell must adapt to the high stiffness of the plastic on which it grows.

When using traditional 2D cultures, essential extracellular signaling originally present in the tissue are lost. The use of 3D cultures bridges this gap between cell culture and tissue systems (Pampaloni et al., 2007). Important signaling pathways in breast cancer such as MAPK and ER $\alpha$  signaling pathways, which have been widely studied and described in 2D appear to be significantly different in 3D. For example, it was reported that the increase of MAPK activation in matrix embedded breast cancer cells attenuates the response to drug treatment (Gangadhara et al., 2016). On the other hand, studies on the role of ER $\alpha$  in breast cancer has widely relied on experiments comparing cancer cell lines with 'normal' non-tumoral HMT-3522 and MCF10A cell lines, because MECs are incapable of sustaining ER $\alpha$  expression under conventional culture conditions (Fridriksdottir et al., 2015). However, recent work has shown that by providing an ECM to the MECs and optimizing culture conditions, the expression of ER $\alpha$  can be sustained for a limited number of passages (Jin et al., 2018).

An underlying mechanism that might be involved in these effects, is the ECM-mediated activation of the integrin signaling. As multiple integrins are involved in the interaction of the cell with the components of the ECM, it would not be surprising if they were also regulating basic cellular processes such as the estrogen and stress response in 3D.



In 3D conditions, the Hippo pathway is activated and the nuclear effector YAP remains mainly in the cytoplasm (Figure R7) and is unable to regulate transcription through the TEAD1/4 DNA binding domain as it does in flattened 2D nuclei.

### 4.3. Caudal Type Homeobox 2 (CDX2)

Interestingly, CDX2, a protein mainly found in intestinal cells and not extensively studied in breast cancer, appeared to have a large effect on spheroid development. It is worth mentioning that CDX2, a transcription factor implicated in early intestinal extracellular matrix-mediated differentiation, is found overrepresented in the 3D cells.

Among the different proteins whose effect was tested in 3D through shRNA specific knockdowns, CDX2 depletion affects cell proliferation in 2D and 3D at comparable levels with other factors as TFAP2A, YY1 or LATS (Figure R17). However, the more striking result was the lack of ability of shCDX2 cells to form normal spheroids (Figure R17). Given that the CDX2 motif was associated to such a large fraction of deregulated transcripts in T47D cells grown in 3D (187 activated and 762 repressed), it will be important to elucidate the precise role of CDX2 in breast cancer cells. Lorentz et al. reported that laminin-1, an ECM component of the basement membrane, is a potent regulator of the expression of *CDX2* in colon adenocarcinoma Caco2-TC7 cells. Thus, CDX2 could play a key role in the cascade of events involved in ECM-mediated intestinal cell differentiation. However, the CDX2 protein is present at very low abundance in breast cancer cells (3.2 FPKM) compared to colorectal cancer (140 FPKM) or stomach cancer (90 FPKM) (source proteinatlas.org). Further analyses are required to understand the association between CDX2 and the ECM in the context of breast cancer.

### 4.4. Increased heterochromatin clusters near the nuclear lamina

Additional results show that T47D cells grown in 3D, exhibit a higher overlap of the nuclear lamina with heterochromatin marks, such as H3K9me2/3 compared to 2D

grown cells (Figure D2). A possible hypothesis that we have not tested yet, is that this more consistent heterochromatin might be responsible for the increase in regulated genes observed in 3D condition. The transcription factors CDX2, YY1, cKrox, CTCF or AP2A could be involved in the more robust heterochromatin near the nuclear lamina, as it has already been proposed for a YY1-cKrox (Harr et al., 2015). In 3D, these TFs would participate in gene repression by "driving" genes towards this heterochromatin fraction. ChIP-seq experiments of these TFs along with Lamin A/C and B1 would be the first step to address this question.

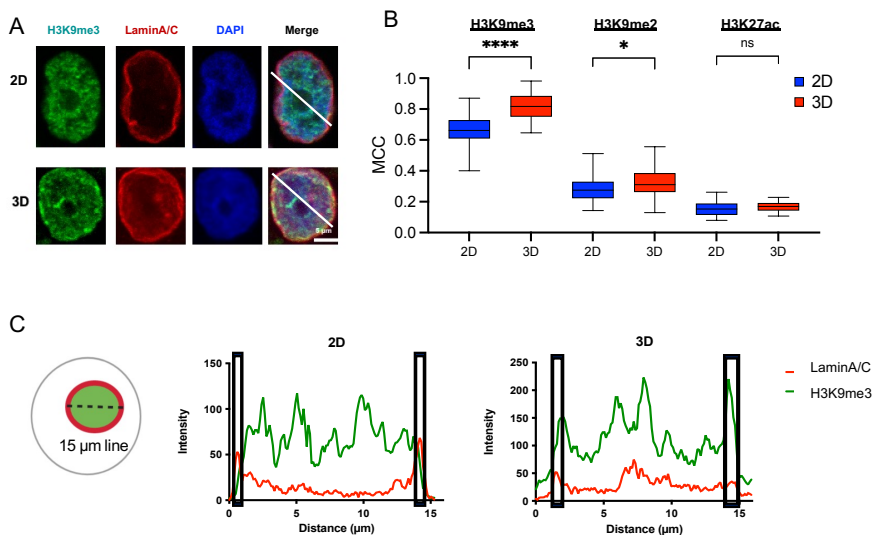


**Figure D 2 Overlap of heterochromatin H3K9me3 signal with Lamin A/C**

A) Immunostaining of H3K9me3 (green) and Lamin A/C (red) in a 2D and 3D cells. B) Measurement of the Mandel's colocalization coefficient for LaminA/C with H3K9me3 (2D: 0.66, 3D: 0.81) and with H3K9me2 (2D: 0.27, 3D: 0.31); overlap of H3K27ac is shown as control (2D: 0.15, 3D: 0.16). p value: \*\*\*\*<0.0001, \*<0.05, n=50. C) Measurement of the signal corresponding to H3K9me3 and LaminA/C obtained from IFs in a cross section of both 2D and 3D nuclei.

#### 4.5. Impact of the ECM on genomic organization and signaling cascades

Despite the changes in chromatin compaction detected by microscopy and nuclease accessibility, when the structure of the genome was assessed through Hi-C experiments, no significant

differences in the contact matrices were found at 1 Mb resolution (Figure R18). However, at deeper resolution we detected changes between cells grown in 2D and in 3D at the level of compartments, and at the level of TAD structure. It is important to mention that drastic changes in genome organization are only observed for events such as transdifferentiation or when different cell types are compared (Flyamer et al., 2017; Stadhouders et al., 2019; Vilarrasa-Blasi et al., 2021). For our analysis, we used T47D cells which differ only in the growth conditions but are not subjected to any sort of differentiation; hence we are not altering the identity of the cell. For this reason, we have focused our analysis on the moderate changes in genome structure that could explain the observed functional effects. Interestingly, we found that in 3D cells there is a higher number of TAD fusions over splits or shifts. Even though the levels of CTCF protein are similar, we detected less chromatin bound CTCF by ChIP-seq in 3D (Figure R19).

In an attempt to unravel the mechanism behind these findings, our current hypothesis points to an increased activity of the Hippo pathway in 3D which is translated into more phosphorylation of the hippo signaling kinase LATS in 3D (Figure R19). It has been reported that activated p-LATS can phosphorylate the architectural protein CTCF resulting in reduced binding to a small subset of genomic binding sites (Luo et al., 2020). In our system CTCF is more phosphorylated in 3D and inhibition or depletion of LATS in 3D cells restores the binding of CTCF in several CTCF binding regions. Therefore, it is possible that the Hippo pathway is turned ON in 3D impacting the cell nucleus through the reduction of CTCF binding, promoting TAD fusions and changes in gene regulation of the neighboring genes. As the dissociation we observed of CTCF in 3D is more extensive than previously reported (Luo et al., 2020), in 3D-grown breast cancer cells the role of p-LATS would be critical and CTCF would be more dependent on the Hippo pathway.

#### **4.6. Comparison of the hormonal response of breast cancer cells grown as monolayer (2D) and spheroids (3D)**

The ECM surrounding the cells is more than an acellular, insoluble proteinaceous mix; in fact, the ECM provides not only physical

scaffolds into which cells are embedded but also regulate many cellular processes including growth, migration, differentiation, survival, homeostasis, and morphogenesis due in part to the associated proteins (Theocharis et al., 2016).

The cells of origin for the T47D cells were tubular epithelial cells of the mammary gland that are in intimate contact with other cells and with the extracellular matrix (ECM), both of which provide not only biochemical signals, but a mechanical context as well. ECM composition and organization are tightly regulated throughout development of the mammary gland, resulting in corresponding regulation of the mechanical environment and proper tissue architecture. Mechanical regulation is also at play during breast carcinoma progression, as changes in ECM deposition, composition, and organization accompany breast carcinoma (Schedin & Keely, 2011).

One of the physiological processes to which the mammary epithelium is exposed, is the hormone, mainly estrogens and progestins, and this may be influenced by the presence of soluble factors and/or specific ECM molecules.

A connection between growth factors, integrins, steroid hormones, their receptors (SHRs) and the ECM in the mammary gland has been described. Briefly, the ECM composition can be remodeled by proteolytic enzymes, such as tissue serine proteases and matrix metalloproteinases (MMPs) (reviewed in Lochter & Bissell, 1995). In the normal mammary gland, MMPs cooperate with hormonal stimuli to induce morphological and functional changes. In breast cancer, MMPs have been associated with tumor growth, invasion, metastasis, and angiogenesis (Lochter et al., 1998). But reciprocally, MMP expression is regulated by progesterone, which inhibits the expression of MMP-1, -2, and -9 through regulation of AP-1 binding (Schroen & Brinckerhoff, 1996). Moreover, PR overexpression affects mammary gland organization by disrupting basement membrane organization (Simian & Bissell, 2017). The progestin R5020 regulates the expression of ECM proteins and their cellular receptors, integrins, during mammary gland development *in vivo*, suggesting that the coordinated regulation of hormone responsiveness and ECM/integrin expression may be

critical for normal mammary gland development as well as for breast cancer growth and progression (Santos et al., 2009).

Despite the fact that cells grown as spheroids are surrounded by other cells, they interact differentially with the ECM and receive nutrients and growth factors in a very heterogeneous manner. However, in response to hormone, we found that the expression of PR as well as its activation by R5020 were similar in 2D and 3D cells (Figure R22).

On the other hand, our RNA-seq data shows that the number of hormone-regulated genes is increased two-fold in 3D compared to 2D, particularly in regulated genes (1,630 vs. 674 down-regulated, and 1,873 vs 1,259 up-regulated, in 2D and 3D, respectively). These results are in line with those obtained from spheroids grown under uninduced conditions, where the prevailing mechanism in 3D was gene repression (Figure R13).

In cells grown in 3D, progestins regulate a group of breast cancer-associated genes that are also regulated in 2D including *CDH10*, *PGR*, *CHEK2*, *LSP1*, *TERT*, *SDPR*, but also a new set of genes associated to the ECM including members of the integrin family, Laminins, and *AKT3* which are not regulated in 2D cells.

Despite the fact that the 3D grown cells are included in a spherical structure and less exposed to the medium, that could hinder hormone access, their response to progestins is more efficient than cells grown in 2D. More genes are regulated at the same hormone concentration and induction time. Moreover, the increase in the number of hormone-regulated genes in 3D was accompanied by an increase in the number of PR binding sites detected by ChIP-seq and many of the 3D exclusive genes are closer to 3D exclusive PR peaks (Figure R25); of which only very few are found at the promoter regions (8 %) and most of them correspond to enhancers. All this happens despite the increase in chromatin condensation observed in cells grown as spheroids. In fact, ATAC-seq experiments have shown that in response to hormone the spheroids require a higher chromatin remodeling capacity that opens the chromatin at promoters and enhancers of regulated genes reaching the levels detected in 2D cells (Figure R27).

As a transcriptional coactivator, YAP needs to bind transcription factors to stimulate gene expression. Reported YAP target transcription factors include TEAD, p73, Runx2, and the ErbB4 cytoplasmic domain (discussed in Li et al., 2010). However, only TEAD has been demonstrated to be important for the growth-promoting function of YAP (Zhao et al., 2008).

Interestingly, the 3D exclusive PR binding peaks are enriched in the TEAD DNA binding motif. Since in 3D the Hippo pathway is activated and YAP is phosphorylated in S127 and tagged for degradation in the cytoplasm, we hypothesize that decreased levels of nuclear YAP allow an increase of free TEAD sites able to bind PR on chromatin. In this case the Hippo pathway would be releasing PR sites that regulate 3D unique genes. According to data from the lab, 20 % of PR binding sites that appeared only when YAP is depleted in 2D overlap with 3D exclusive PR binding sites ( $p \text{ value} < 2.2e^{-16}$ ) (Figure D3). These new sites would regulate new genes exclusive of a '3D spheroid' condition.

According to our model, YAP would compete with PR for binding of TEAD to 3D exclusive chromatin regions. As YAP does not bind to DNA directly, but rather *via* TEAD, the role of TEAD1, TEAD4 and TAZ in this proposed mechanism should be further elucidated.

Therefore, the impact of the Hippo pathway in 3D could be reflected at least in two ways: i) via p-LATS activation and phosphorylation of CTCF and ii) via YAP inactivation, releasing TEAD sites for PR binding. Moreover, it is possible to partially recapitulate the pattern of PR binding in '3D-like' conditions by silencing YAP in 2D T47D cells.

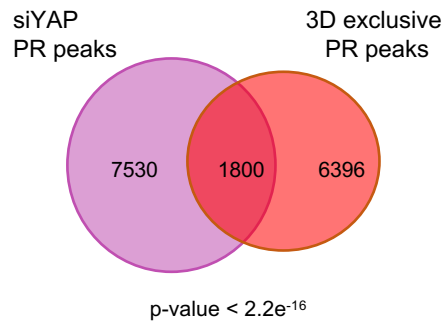


**Figure D 3 Venn diagram depicting the overlap between PR peaks detected in YAP KD cells grown in 2D and 3D-exclusive PR peaks**

Overlap of PR binding sites from ChIP-seq experiments performed in siYAP cells treated with hormone and the subset of 3D-exclusive PR peaks. Thus, a total of 1,800 PR binding sites of 3D exclusive PR peaks may be a result of YAP displacement detected in the 3D nucleus (p value <math>< 2.2 \times 10^{-16}</math>).

Overall, it appears that the genomic effects observed in our 3D model are not entirely correlated with changes in the genome structure, at least at the level of resolution we have used for our analyses. In our Hi-C experiments performed in 2D and 3D, the differences are subtle but definitely oriented towards gene repression (more transitions from A to B compartments) and increased fusion of TADs (Figure R18). Although Hippo-dependent CTCF depletion from TAD borders could explain the increase in TAD fusions detected in 3D, we observed that the CTCF displacement is broader and occurs equally in TAD fusions, splits or shifts.

Therefore, in 3D the massive displacement of CTCF is not accompanied by drastic changes in genome architecture, which would support an uncoupling between these two events. Previous work carried out in different systems has shown that CTCF may not be as essential in establishing genome structure/TADs (Barutcu et al., 2018), at least in the mammalian genome, but this is still a matter of debate. Collectively, our early findings suggest that apart from CTCF binding, additional mechanisms may play roles in establishing TAD boundary formation in breast cancer cells.

Chromatin looping interactions play an important role in constraining enhancer–promoter interactions and mediating transcriptional gene regulation. CTCF is thought to play a critical role in the formation of these loops (Xi et al., 2021). Thus, we can hypothesize that part of the changes we observe at the gene expression level both in the presence and absence of hormone in 3D, could be due to the depletion of CTCF, more associated with its role as a key factor involved in loop formation and enhancer-mediated activation.

This is only a first step into a more physiological model. We are aware that many additional steps are required to create the optimal ECM, before arriving at animal models. This is an insight into deciphering which pathways and factors are highlighted in 3D. Simple and more complex organoid systems have their pros and cons; but a higher level of complexity does not necessarily mean a better model. It is important to use the most appropriate level of complexity for a given study.

It will be important to develop a better understanding of how mechanosensing activates specific transcription factors and translocate them to the cell nucleus to establish whether there are any general principles for activation of transcription factors by mechanical cues.



## 5. Conclusions

1. Matrigel is the optimal hydrogel commercially available to perform 3D culture on breast cells. It promotes the mimicking of physiological acini, and the cells have a more physiological behavior and response.
2. T47D 3D breast cancer cells are able to proliferate better in the presence of the Matrigel and present a more rounded nucleus with a larger interacting surface.
3. We observe changes in several cell signaling pathways, among them Hippo, focal adhesion, ER $\alpha$  and MAPK pathways that confirm the modified mechanosensing of the 3D breast cancer cells.
4. DAPI staining, MNase digestion and ATAC-seq confirm that the genome is less accessible in 3D.
5. Lower accessibility reflects in increased gene repression in 3D. According to the GO of 3D exclusive down-regulated genes, cells are losing focal adhesion to the plastic to become more motile.
6. GSEA analysis of 3D exclusive genes highlights the TF CDX2. This protein is reported to be regulated by laminin, which is present in high levels in the Matrigel but CDX2 is poorly expressed in breast cells. CDX2 depletion severely compromised 3D sphere formation.
7. Changes in the way cells are grown have limited effects on genome architecture, nevertheless we have detected preferential displacement of the architectural protein CTCF in 3D.
8. The displacement of CTCF was at least partially due to its phosphorylation by the LATS kinase and could be responsible for at least part of the gene deregulation observed in 3D. Inhibition or depletion of LATS restores the binding of CTCF in several regions.
9. The presence of an ECM increased the impact of the hormone on the spheroids, resulting in a more efficient chromatin remodeling, increased number of PRbs and more genes being regulated by hormone.



## 6. Literature

- Ahlmann-Eltze, C., & Patil, I. (2021). ggsignif: Significance Brackets for “ggplot2”. R package version 0.6.1., (123). Retrieved from <https://cran.r-project.org/package=ggsignif>
- Alaskhar Alhamwe, B., Khalaila, R., Wolf, J., von Bülow, V., Harb, H., Alhamdan, F. H., Hill, C. S., Prescott, S. L., Ferrante, A., Renz, H., Garn, H., & Potaczek, D. P. (2018). Histone modifications and their role in epigenetics of atopy and allergic diseases. *Allergy, Asthma and Clinical Immunology*, 14(1). <https://doi.org/10.1186/s13223-018-0259-4>
- Asp, M., Giacomello, S., Larsson, L., Wu, C., Fürth, D., Qian, X., Wärdell, E., Custodio, J., Reimegård, J., Salmén, F., Österholm, C., Ståhl, P. L., Sundström, E., Åkesson, E., Bergmann, O., Bienko, M., Månsson-Broberg, A., Nilsson, M., Sylvén, C., & Lundberg, J. (2019). A Spatiotemporal Organ-Wide Gene Expression and Cell Atlas of the Developing Human Heart. *Cell*, 179(7), 1647–1660.e19. <https://doi.org/10.1016/j.cell.2019.11.025>
- Ballaré, C., Castellano, G., Gaveglia, L., Althammer, S., González-Vallinas, J., Eyra, E., Le Dily, F., Zaurin, R., Soronellas, D., Vicent, G. P., & Beato, M. (2013). Nucleosome-driven transcription factor binding and gene regulation. *Molecular cell*, 49(1), 67–79. <https://doi.org/10.1016/j.molcel.2012.10.019>
- Ballaré, C., Uhrig, M., Bechtold, T., Sancho, E., Di Domenico, M., Migliaccio, A., Auricchio, F., & Beato, M. (2003). Two domains of the progesterone receptor interact with the estrogen receptor and are required for progesterone activation of the c-Src/Erk pathway in mammalian cells. *Molecular and cellular biology*, 23(6), 1994–2008. <https://doi.org/10.1128/MCB.23.6.1994-2008.2003>
- Barcellos-Hoff, M. H., Aggeler, J., Ram, T. G., & Bissell, M. J. (1989). Functional differentiation and alveolar morphogenesis of primary mammary cultures on reconstituted basement membrane. *Development (Cambridge, England)*, 105(2), 223–235.
- Barutcu, A. R., Maass, P. G., Lewandowski, J. P., Weiner, C. L., & Rinn, J. L. (2018). A TAD boundary is preserved upon deletion of the CTCF-rich Firre locus. *Nature communications*, 9(1), 1444. <https://doi.org/10.1038/s41467-018-03614-0>
- Beato, M., Chalepakis, G., Schauer, M., & Slater, E. P. (1989). DNA regulatory elements for steroid hormones. *Journal of steroid biochemistry*, 32(5), 737–747. [https://doi.org/10.1016/0022-4731\(89\)90521-9](https://doi.org/10.1016/0022-4731(89)90521-9)

- Beato, M., & Vicent, G. P. (2012). Impact of chromatin structure and dynamics on PR signaling. The initial steps in hormonal gene regulation. *Molecular and cellular endocrinology*, 357(1-2), 37–42. <https://doi.org/10.1016/j.mce.2011.09.004>
- Beato, M., Wright, R., & Dily, F. L. (2020). 90 YEARS OF PROGESTERONE: Molecular mechanisms of progesterone receptor action on the breast cancer genome. *Journal of molecular endocrinology*, 65(1), T65–T79. <https://doi.org/10.1530/JME-19-0266>
- Bissell, M. J., Hall, H. G., & Parry, G. (1982). How does the extracellular matrix direct gene expression?. *Journal of theoretical biology*, 99(1), 31–68. [https://doi.org/10.1016/0022-5193\(82\)90388-5](https://doi.org/10.1016/0022-5193(82)90388-5)
- Blanchoin, L., Boujemaa-Paterski, R., Sykes, C., & Plastino, J. (2014). Actin dynamics, architecture, and mechanics in cell motility. *Physiological reviews*, 94(1), 235–263. <https://doi.org/10.1152/physrev.00018.2013>
- Boyle, S., Gilchrist, S., Bridger, J. M., Mahy, N. L., Ellis, J. A., & Bickmore, W. A. (2001). The spatial organization of human chromosomes within the nuclei of normal and emerin-mutant cells. *Human molecular genetics*, 10(3), 211–219. <https://doi.org/10.1093/hmg/10.3.211>
- Buenrostro, J. D., Wu, B., Chang, H. Y., & Greenleaf, W. J. (2015). ATAC-seq: A Method for Assaying Chromatin Accessibility Genome-Wide. *Current protocols in molecular biology*, 109, 21.29.1–21.29.9. <https://doi.org/10.1002/0471142727.mb2129s109>
- Buxboim, A., Swift, J., Irianto, J., Spinler, K. R., Dingal, P. C., Athirasala, A., Kao, Y. R., Cho, S., Harada, T., Shin, J. W., & Discher, D. E. (2014). Matrix elasticity regulates lamin-A,C phosphorylation and turnover with feedback to actomyosin. *Current biology : CB*, 24(16), 1909–1917. <https://doi.org/10.1016/j.cub.2014.07.001>
- Calalb, M. B., Polte, T. R., & Hanks, S. K. (1995). Tyrosine phosphorylation of focal adhesion kinase at sites in the catalytic domain regulates kinase activity: a role for Src family kinases. *Molecular and cellular biology*, 15(2), 954–963. <https://doi.org/10.1128/MCB.15.2.954>
- Carroll, J. S., Hickey, T. E., Tarulli, G. A., Williams, M., & Tilley, W. D. (2017). Deciphering the divergent roles of progestogens in breast cancer. *Nature reviews. Cancer*, 17(1), 54–64. <https://doi.org/10.1038/nrc.2016.116>

- Caswell, P. T., & Zech, T. (2018). Actin-Based Cell Protrusion in a 3D Matrix. *Trends in cell biology*, 28(10), 823–834. <https://doi.org/10.1016/j.tcb.2018.06.003>
- Chávez, S., & Beato, M. (1997). Nucleosome-mediated synergism between transcription factors on the mouse mammary tumor virus promoter. *Proceedings of the National Academy of Sciences of the United States of America*, 94(7), 2885–2890. <https://doi.org/10.1073/pnas.94.7.2885>
- Chlebowski, R. T., Anderson, G. L., Gass, M., Lane, D. S., Aragaki, A. K., Kuller, L. H., Manson, J. E., Stefanick, M. L., Ockene, J., Sarto, G. E., Johnson, K. C., Wactawski-Wende, J., Ravdin, P. M., Schenken, R., Hendrix, S. L., Rajkovic, A., Rohan, T. E., Yasmeen, S., Prentice, R. L., & WHI Investigators (2010). Estrogen plus progestin and breast cancer incidence and mortality in postmenopausal women. *JAMA*, 304(15), 1684–1692. <https://doi.org/10.1001/jama.2010.1500>
- Choquet, D., Felsenfeld, D. P., & Sheetz, M. P. (1997). Extracellular matrix rigidity causes strengthening of integrin-cytoskeleton linkages. *Cell*, 88(1), 39–48. [https://doi.org/10.1016/s0092-8674\(00\)81856-5](https://doi.org/10.1016/s0092-8674(00)81856-5)
- Clevers H. (2016). Modeling Development and Disease with Organoids. *Cell*, 165(7), 1586–1597. <https://doi.org/10.1016/j.cell.2016.05.082>
- Coskun, M., Troelsen, J. T., & Nielsen, O. H. (2011). The role of CDX2 in intestinal homeostasis and inflammation. *Biochimica et biophysica acta*, 1812(3), 283–289. <https://doi.org/10.1016/j.bbadis.2010.11.008>
- Coste, B., Xiao, B., Santos, J. S., Syeda, R., Grandl, J., Spencer, K. S., Kim, S. E., Schmidt, M., Mathur, J., Dubin, A. E., Montal, M., & Patapoutian, A. (2012). Piezo proteins are pore-forming subunits of mechanically activated channels. *Nature*, 483(7388), 176–181. <https://doi.org/10.1038/nature10812>
- Cremer, T., & Cremer, C. (2001). Chromosome territories, nuclear architecture and gene regulation in mammalian cells. *Nature reviews. Genetics*, 2(4), 292–301. <https://doi.org/10.1038/35066075>
- Cukierman, E., Pankov, R., & Yamada, K. M. (2002). Cell interactions with three-dimensional matrices. *Current opinion in cell biology*, 14(5), 633–639. [https://doi.org/10.1016/s0955-0674\(02\)00364-2](https://doi.org/10.1016/s0955-0674(02)00364-2)
- DANIEL, C. W., & DEOME, K. B. (1965). GROWTH OF MOUSE MAMMARY GLANDS IN VIVO AFTER MONOLAYER CULTURE. *Science (New York, N.Y.)*, 149(3684), 634–636. <https://doi.org/10.1126/science.149.3684.634>

- Dekker, J., Rippe, K., Dekker, M., & Kleckner, N. (2002). Capturing chromosome conformation. *Science (New York, N.Y.)*, *295*(5558), 1306–1311. <https://doi.org/10.1126/science.1067799>
- Di Croce, L., Koop, R., Venditti, P., Westphal, H. M., Nightingale, K. P., Corona, D. F., Becker, P. B., & Beato, M. (1999). Two-step synergism between the progesterone receptor and the DNA-binding domain of nuclear factor 1 on MMTV minichromosomes. *Molecular cell*, *4*(1), 45–54. [https://doi.org/10.1016/s1097-2765\(00\)80186-0](https://doi.org/10.1016/s1097-2765(00)80186-0)
- Discher, D. E., Janmey, P., & Wang, Y. L. (2005). Tissue cells feel and respond to the stiffness of their substrate. *Science (New York, N.Y.)*, *310*(5751), 1139–1143. <https://doi.org/10.1126/science.1116995>
- Dixon, J. R., Selvaraj, S., Yue, F., Kim, A., Li, Y., Shen, Y., Hu, M., Liu, J. S., & Ren, B. (2012). Topological domains in mammalian genomes identified by analysis of chromatin interactions. *Nature*, *485*(7398), 376–380. <https://doi.org/10.1038/nature11082>
- Dobin, A., Davis, C. A., Schlesinger, F., Drenkow, J., Zaleski, C., Jha, S., Batut, P., Chaisson, M., & Gingeras, T. R. (2013). STAR: ultrafast universal RNA-seq aligner. *Bioinformatics (Oxford, England)*, *29*(1), 15–21. <https://doi.org/10.1093/bioinformatics/bts635>
- Dokmanovic, M., Clarke, C., & Marks, P. A. (2007). Histone deacetylase inhibitors: overview and perspectives. *Molecular cancer research : MCR*, *5*(10), 981–989. <https://doi.org/10.1158/1541-7786.MCR-07-0324>
- Dostie, J., Richmond, T. A., Arnaout, R. A., Selzer, R. R., Lee, W. L., Honan, T. A., Rubio, E. D., Krumm, A., Lamb, J., Nusbaum, C., Green, R. D., & Dekker, J. (2006). Chromosome Conformation Capture Carbon Copy (5C): a massively parallel solution for mapping interactions between genomic elements. *Genome research*, *16*(10), 1299–1309. <https://doi.org/10.1101/gr.5571506>
- Dunnwald, L. K., Rossing, M. A., & Li, C. I. (2007). Hormone receptor status, tumor characteristics, and prognosis: a prospective cohort of breast cancer patients. *Breast cancer research : BCR*, *9*(1), R6. <https://doi.org/10.1186/bcr1639>
- Dupont, S., Morsut, L., Aragona, M., Enzo, E., Giulitti, S., Cordenonsi, M., Zanconato, F., Le Digabel, J., Forcato, M., Bicciato, S., Elvassore, N., & Piccolo, S. (2011). Role of YAP/TAZ in mechanotransduction. *Nature*, *474*(7350), 179–183. <https://doi.org/10.1038/nature10137>

- Dutta, D., Heo, I., & Clevers, H. (2017). Disease Modeling in Stem Cell-Derived 3D Organoid Systems. *Trends in molecular medicine*, 23(5), 393–410. <https://doi.org/10.1016/j.molmed.2017.02.007>
- Edlund, M., Lotano, M. A., & Otey, C. A. (2001). Dynamics of alpha-actinin in focal adhesions and stress fibers visualized with alpha-actinin-green fluorescent protein. *Cell motility and the cytoskeleton*, 48(3), 190–200. [https://doi.org/10.1002/1097-0169\(200103\)48:3<190::AID-CM1008>3.0.CO;2-C](https://doi.org/10.1002/1097-0169(200103)48:3<190::AID-CM1008>3.0.CO;2-C)
- Eisen, J. A., Sweder, K. S., & Hanawalt, P. C. (1995). Evolution of the SNF2 family of proteins: subfamilies with distinct sequences and functions. *Nucleic acids research*, 23(14), 2715–2723. <https://doi.org/10.1093/nar/23.14.2715>
- Elosegui-Artola, A., Andreu, I., Beedle, A., Lezamiz, A., Uroz, M., Kosmalska, A. J., Oria, R., Kechagia, J. Z., Rico-Lastres, P., Le Roux, A. L., Shanahan, C. M., Trepas, X., Navajas, D., Garcia-Manyes, S., & Roca-Cusachs, P. (2017). Force Triggers YAP Nuclear Entry by Regulating Transport across Nuclear Pores. *Cell*, 171(6), 1397–1410.e14. <https://doi.org/10.1016/j.cell.2017.10.008>
- Emerman, J. T., Enami, J., Pitelka, D. R., & Nandi, S. (1977). Hormonal effects on intracellular and secreted casein in cultures of mouse mammary epithelial cells on floating collagen membranes. *Proceedings of the National Academy of Sciences of the United States of America*, 74(10), 4466–4470. <https://doi.org/10.1073/pnas.74.10.4466>
- Engler, A. J., Sen, S., Sweeney, H. L., & Discher, D. E. (2006). Matrix elasticity directs stem cell lineage specification. *Cell*, 126(4), 677–689. <https://doi.org/10.1016/j.cell.2006.06.044>
- Falcon, S., & Gentleman, R. (2007). Using GOSTats to test gene lists for GO term association. *Bioinformatics (Oxford, England)*, 23(2), 257–258. <https://doi.org/10.1093/bioinformatics/btl567>
- Fatehullah, A., Tan, S. H., & Barker, N. (2016). Organoids as an in vitro model of human development and disease. *Nature cell biology*, 18(3), 246–254. <https://doi.org/10.1038/ncb3312>
- Felsenfeld, G., & Groudine, M. (2003). Controlling the double helix. *Nature*, 421(6921), 448–453. <https://doi.org/10.1038/nature01411>
- Filipescu, D., Müller, S., & Almouzni, G. (2014). Histone H3 variants and their chaperones during development and disease: contributing to epigenetic control. *Annual review of cell and*

*developmental biology*, 30, 615–646.

<https://doi.org/10.1146/annurev-cellbio-100913-013311>

- Fischle, W., Tseng, B. S., Dormann, H. L., Ueberheide, B. M., Garcia, B. A., Shabanowitz, J., Hunt, D. F., Funabiki, H., & Allis, C. D. (2005). Regulation of HP1-chromatin binding by histone H3 methylation and phosphorylation. *Nature*, 438(7071), 1116–1122. <https://doi.org/10.1038/nature04219>
- Flyamer, I. M., Gassler, J., Imakaev, M., Brandão, H. B., Ulianov, S. V., Abdennur, N., Razin, S. V., Mirny, L. A., & Tachibana-Konwalski, K. (2017). Single-nucleus Hi-C reveals unique chromatin reorganization at oocyte-to-zygote transition. *Nature*, 544(7648), 110–114. <https://doi.org/10.1038/nature21711>
- Franke, M., De la Calle-Mustienes, E., Neto, A., Almuedo-Castillo, M., Irastorza-Azcarate, I., Acemel, R. D., Tena, J. J., Santos-Pereira, J. M., & Gómez-Skarmeta, J. L. (2021). CTCF knockout in zebrafish induces alterations in regulatory landscapes and developmental gene expression. *Nature communications*, 12(1), 5415. <https://doi.org/10.1038/s41467-021-25604-5>
- Fraser, J., Ferrai, C., Chiariello, A. M., Schueler, M., Rito, T., Laudanno, G., Barbieri, M., Moore, B. L., Kraemer, D. C., Aitken, S., Xie, S. Q., Morris, K. J., Itoh, M., Kawaji, H., Jaeger, I., Hayashizaki, Y., Carninci, P., Forrest, A. R., C. A., Nicodemi, M. (2015). Hierarchical folding and reorganization of chromosomes are linked to transcriptional changes in cellular differentiation. *Molecular systems biology*, 11(12), 852. <https://doi.org/10.15252/msb.20156492>
- Freemont, A. J., & Hoyland, J. A. (1996). Cell adhesion molecules. *Clinical molecular pathology*, 49(6), M321–M330. <https://doi.org/10.1136/mp.49.6.m321>
- Fridriksdottir, A. J., Kim, J., Villadsen, R., Klitgaard, M. C., Hopkinson, B. M., Petersen, O. W., & Rønnov-Jessen, L. (2015). Propagation of oestrogen receptor-positive and oestrogen-responsive normal human breast cells in culture. *Nature communications*, 6, 8786. <https://doi.org/10.1038/ncomms9786>
- Friedl, P., & Alexander, S. (2011). Cancer invasion and the microenvironment: plasticity and reciprocity. *Cell*, 147(5), 992–1009. <https://doi.org/10.1016/j.cell.2011.11.016>
- Gangadhara, S., Smith, C., Barrett-Lee, P., & Hiscox, S. (2016). 3D culture of Her2+ breast cancer cells promotes AKT to MAPK switching and a loss of therapeutic response. *BMC cancer*, 16, 345. <https://doi.org/10.1186/s12885-016-2377-z>



- Garreta, E., Prado, P., Tarantino, C., Oria, R., Fanlo, L., Martí, E., Zalvidea, D., Trepát, X., Roca-Cusachs, P., Gavaldà-Navarro, A., Cozzuto, L., Campistol, J. M., Izpisúa Belmonte, J. C., Hurtado Del Pozo, C., & Montserrat, N. (2019). Fine tuning the extracellular environment accelerates the derivation of kidney organoids from human pluripotent stem cells. *Nature materials*, 18(4), 397–405. <https://doi.org/10.1038/s41563-019-0287-6>
- Ghiraldini, F. G., Filipescu, D., & Bernstein, E. (2021). Solid tumours hijack the histone variant network. *Nature reviews. Cancer*, 21(4), 257–275. <https://doi.org/10.1038/s41568-020-00330-0>
- Gil, R. S., & Vagnarelli, P. (2019). Protein phosphatases in chromatin structure and function. *Biochimica et biophysica acta. Molecular cell research*, 1866(1), 90–101. <https://doi.org/10.1016/j.bbamcr.2018.07.016>
- Grant P. A. (2001). A tale of histone modifications. *Genome biology*, 2(4), REVIEWS0003. <https://doi.org/10.1186/gb-2001-2-4-reviews0003>
- Greer, E. L., & Shi, Y. (2012). Histone methylation: a dynamic mark in health, disease and inheritance. *Nature reviews. Genetics*, 13(5), 343–357. <https://doi.org/10.1038/nrg3173>
- Grewal, S. I., & Elgin, S. C. (2002). Heterochromatin: new possibilities for the inheritance of structure. *Current opinion in genetics & development*, 12(2), 178–187. [https://doi.org/10.1016/s0959-437x\(02\)00284-8](https://doi.org/10.1016/s0959-437x(02)00284-8)
- Griffith, L. G., & Swartz, M. A. (2006). Capturing complex 3D tissue physiology in vitro. *Nature reviews. Molecular cell biology*, 7(3), 211–224. <https://doi.org/10.1038/nrm1858>
- Gronemeyer H. (1992). Control of transcription activation by steroid hormone receptors. *FASEB journal : official publication of the Federation of American Societies for Experimental Biology*, 6(8), 2524–2529. <https://doi.org/10.1096/fasebj.6.8.1592204>
- Gudjonsson, T., Rønnov-Jessen, L., Villadsen, R., Rank, F., Bissell, M. J., & Petersen, O. W. (2002). Normal and tumor-derived myoepithelial cells differ in their ability to interact with luminal breast epithelial cells for polarity and basement membrane deposition. *Journal of cell science*, 115(Pt 1), 39–50.
- Guilluy, C., Osborne, L. D., Van Landeghem, L., Sharek, L., Superfine, R., Garcia-Mata, R., & Burrridge, K. (2014). Isolated nuclei adapt to force and reveal a mechanotransduction pathway in the nucleus. *Nature cell biology*, 16(4), 376–381. <https://doi.org/10.1038/ncb2927>

- Gutierrez, R. M., & Hnilica, L. S. (1967). Tissue specificity of histone phosphorylation. *Science (New York, N.Y.)*, *157*(3794), 1324–1325. <https://doi.org/10.1126/science.157.3794.1324>
- Hanahan, D., & Weinberg, R. A. (2011). Hallmarks of cancer: the next generation. *Cell*, *144*(5), 646–674. <https://doi.org/10.1016/j.cell.2011.02.013>
- Harr, J. C., Luperchio, T. R., Wong, X., Cohen, E., Wheelan, S. J., & Reddy, K. L. (2015). Directed targeting of chromatin to the nuclear lamina is mediated by chromatin state and A-type lamins. *The Journal of cell biology*, *208*(1), 33–52. <https://doi.org/10.1083/jcb.201405110>
- Heinz, S., Benner, C., Spann, N., Bertolino, E., Lin, Y. C., Laslo, P., Cheng, J. X., Murre, C., Singh, H., & Glass, C. K. (2010). Simple combinations of lineage-determining transcription factors prime cis-regulatory elements required for macrophage and B cell identities. *Molecular cell*, *38*(4), 576–589. <https://doi.org/10.1016/j.molcel.2010.05.004>
- Humphrey, J. D., Dufresne, E. R., & Schwartz, M. A. (2014). Mechanotransduction and extracellular matrix homeostasis. *Nature reviews. Molecular cell biology*, *15*(12), 802–812. <https://doi.org/10.1038/nrm3896>
- Jain, N., Iyer, K. V., Kumar, A., & Shivashankar, G. V. (2013). Cell geometric constraints induce modular gene-expression patterns via redistribution of HDAC3 regulated by actomyosin contractility. *Proceedings of the National Academy of Sciences of the United States of America*, *110*(28), 11349–11354. <https://doi.org/10.1073/pnas.1300801110>
- Jiang, H., Lei, R., Ding, S. W., & Zhu, S. (2014). Skewer: a fast and accurate adapter trimmer for next-generation sequencing paired-end reads. *BMC bioinformatics*, *15*, 182. <https://doi.org/10.1186/1471-2105-15-182>
- Jin, L., Qu, Y., Gomez, L. J., Chung, S., Han, B., Gao, B., Yue, Y., Gong, Y., Liu, X., Amersi, F., Dang, C., Giuliano, A. E., & Cui, X. (2017). Characterization of primary human mammary epithelial cells isolated and propagated by conditional reprogrammed cell culture. *Oncotarget*, *9*(14), 11503–11514. <https://doi.org/10.18632/oncotarget.23817>
- Kastan, N., Gnedeva, K., Alisch, T., Petelski, A. A., Huggins, D. J., Chiaravalli, J., Aharanov, A., Shakked, A., Tzahor, E., Nagiel, A., Segil, N., & Hudspeth, A. J. (2021). Small-molecule inhibition of Lats kinases may promote Yap-dependent proliferation in postmitotic mammalian tissues. *Nature communications*, *12*(1), 3100. <https://doi.org/10.1038/s41467-021-23395-3>

- Kastner, P., Krust, A., Turcotte, B., Stropp, U., Tora, L., Gronemeyer, H., & Chambon, P. (1990). Two distinct estrogen-regulated promoters generate transcripts encoding the two functionally different human progesterone receptor forms A and B. *The EMBO journal*, 9(5), 1603–1614.
- Kechagia, J. Z., Ivaska, J., & Roca-Cusachs, P. (2019). Integrins as biomechanical sensors of the microenvironment. *Nature reviews. Molecular cell biology*, 20(8), 457–473. <https://doi.org/10.1038/s41580-019-0134-2>
- Kempfer, R., & Pombo, A. (2020). Methods for mapping 3D chromosome architecture. *Nature reviews. Genetics*, 21(4), 207–226. <https://doi.org/10.1038/s41576-019-0195-2>
- Kenny, P. A., Lee, G. Y., Myers, C. A., Neve, R. M., Semeiks, J. R., Spellman, P. T., Lorenz, K., Lee, E. H., Barcellos-Hoff, M. H., Petersen, O. W., Gray, J. W., & Bissell, M. J. (2007). The morphologies of breast cancer cell lines in three-dimensional assays correlate with their profiles of gene expression. *Molecular oncology*, 1(1), 84–96. <https://doi.org/10.1016/j.molonc.2007.02.004>
- Kim, D. H., & Wirtz, D. (2015). Cytoskeletal tension induces the polarized architecture of the nucleus. *Biomaterials*, 48, 161–172. <https://doi.org/10.1016/j.biomaterials.2015.01.023>
- Kim, J., Guermah, M., McGinty, R. K., Lee, J. S., Tang, Z., Milne, T. A., Shilatifard, A., Muir, T. W., & Roeder, R. G. (2009). RAD6-Mediated transcription-coupled H2B ubiquitylation directly stimulates H3K4 methylation in human cells. *Cell*, 137(3), 459–471. <https://doi.org/10.1016/j.cell.2009.02.027>
- Kim, J., Koo, B. K., & Knoblich, J. A. (2020). Human organoids: model systems for human biology and medicine. *Nature reviews. Molecular cell biology*, 21(10), 571–584. <https://doi.org/10.1038/s41580-020-0259-3>
- Kim, N. G., & Gumbiner, B. M. (2015). Adhesion to fibronectin regulates Hippo signaling via the FAK-Src-PI3K pathway. *The Journal of cell biology*, 210(3), 503–515. <https://doi.org/10.1083/jcb.201501025>
- Kim, S., Yu, N. K., & Kaang, B. K. (2015). CTCF as a multifunctional protein in genome regulation and gene expression. *Experimental & molecular medicine*, 47(6), e166. <https://doi.org/10.1038/emm.2015.33>
- Kim Y. Z. (2014). Altered histone modifications in gliomas. *Brain tumor research and treatment*, 2(1), 7–21. <https://doi.org/10.14791/btrt.2014.2.1.7>
- Kingston, R. E., & Narlikar, G. J. (1999). ATP-dependent remodeling and acetylation as regulators of chromatin

fluidity. *Genes & development*, 13(18), 2339–2352.  
<https://doi.org/10.1101/gad.13.18.2339>

- Kuo, M. H., & Allis, C. D. (1998). Roles of histone acetyltransferases and deacetylases in gene regulation. *BioEssays : news and reviews in molecular, cellular and developmental biology*, 20(8), 615–626.  
[https://doi.org/10.1002/\(SICI\)1521-1878\(199808\)20:8<615::AID-BIES4>3.0.CO;2-H](https://doi.org/10.1002/(SICI)1521-1878(199808)20:8<615::AID-BIES4>3.0.CO;2-H)
- Kutys, M. L., & Chen, C. S. (2016). Forces and mechanotransduction in 3D vascular biology. *Current opinion in cell biology*, 42, 73–79. <https://doi.org/10.1016/j.ceb.2016.04.011>
- Lagies, S., Schlimpert, M., Neumann, S., Wäldin, A., Kammerer, B., Borner, C., & Peintner, L. (2020). Cells grown in three-dimensional spheroids mirror in vivo metabolic response of epithelial cells. *Communications biology*, 3(1), 246.  
<https://doi.org/10.1038/s42003-020-0973-6>
- Le Dily, F., Baù, D., Pohl, A., Vicent, G. P., Serra, F., Soronellas, D., Castellano, G., Wright, R. H., Ballare, C., Filion, G., Marti-Renom, M. A., & Beato, M. (2014). Distinct structural transitions of chromatin topological domains correlate with coordinated hormone-induced gene regulation. *Genes & development*, 28(19), 2151–2162.  
<https://doi.org/10.1101/gad.241422.114>
- Le Dily, F., Vidal, E., Cuartero, Y., Quilez, J., Nacht, A. S., Vicent, G. P., Carbonell-Caballero, J., Sharma, P., Villanueva-Cañas, J. L., Ferrari, R., De Llobet, L. I., Verde, G., Wright, R., & Beato, M. (2019). Hormone-control regions mediate steroid receptor-dependent genome organization. *Genome research*, 29(1), 29–39. <https://doi.org/10.1101/gr.243824.118>
- Lee, E. Y., Parry, G., & Bissell, M. J. (1984). Modulation of secreted proteins of mouse mammary epithelial cells by the collagenous substrata. *The Journal of cell biology*, 98(1), 146–155. <https://doi.org/10.1083/jcb.98.1.146>
- Lee, G. Y., Kenny, P. A., Lee, E. H., & Bissell, M. J. (2007). Three-dimensional culture models of normal and malignant breast epithelial cells. *Nature methods*, 4(4), 359–365.  
<https://doi.org/10.1038/nmeth1015>
- Levental, K. R., Yu, H., Kass, L., Lakins, J. N., Egeblad, M., Erler, J. T., Fong, S. F., Csiszar, K., Giaccia, A., Wenginger, W., Yamauchi, M., Gasser, D. L., & Weaver, V. M. (2009). Matrix crosslinking forces tumor progression by enhancing integrin signaling. *Cell*, 139(5), 891–906.  
<https://doi.org/10.1016/j.cell.2009.10.027>

- Li, T., Guan, J., Huang, Z., Hu, X., & Zheng, X. (2014). RNF168-mediated H2A neddylation antagonizes ubiquitylation of H2A and regulates DNA damage repair. *Journal of cell science*, 127(Pt 10), 2238–2248. <https://doi.org/10.1242/jcs.138891>
- Li, Z., Zhao, B., Wang, P., Chen, F., Dong, Z., Yang, H., Guan, K. L., & Xu, Y. (2010). Structural insights into the YAP and TEAD complex. *Genes & development*, 24(3), 235–240. <https://doi.org/10.1101/gad.1865810>
- Lieberman-Aiden, E., van Berkum, N. L., Williams, L., Imakaev, M., Ragozcy, T., Telling, A., Amit, I., Lajoie, B. R., Sabo, P. J., Dorschner, M. O., Sandstrom, R., Bernstein, B., Bender, M. A., Groudine, M., Gnirke, A., Stamatoyannopoulos, J., Mirny, L. A., Lander, E. S., & Dekker, J. (2009). Comprehensive mapping of long-range interactions reveals folding principles of the human genome. *Science (New York, N.Y.)*, 326(5950), 289–293. <https://doi.org/10.1126/science.1181369>
- Lo, W. S., Trievel, R. C., Rojas, J. R., Duggan, L., Hsu, J. Y., Allis, C. D., Marmorstein, R., & Berger, S. L. (2000). Phosphorylation of serine 10 in histone H3 is functionally linked in vitro and in vivo to Gcn5-mediated acetylation at lysine 14. *Molecular cell*, 5(6), 917–926. [https://doi.org/10.1016/s1097-2765\(00\)80257-9](https://doi.org/10.1016/s1097-2765(00)80257-9)
- Lochter, A., & Bissell, M. J. (1995). Involvement of extracellular matrix constituents in breast cancer. *Seminars in cancer biology*, 6(3), 165–173. <https://doi.org/10.1006/scbi.1995.0017>
- Lochter, A., Sternlicht, M. D., Werb, Z., & Bissell, M. J. (1998). The significance of matrix metalloproteinases during early stages of tumor progression. *Annals of the New York Academy of Sciences*, 857, 180–193. <https://doi.org/10.1111/j.1749-6632.1998.tb10116.x>
- Lombardi, M. L., Jaalouk, D. E., Shanahan, C. M., Burke, B., Roux, K. J., & Lammerding, J. (2011). The interaction between nesprins and sun proteins at the nuclear envelope is critical for force transmission between the nucleus and cytoskeleton. *The Journal of biological chemistry*, 286(30), 26743–26753. <https://doi.org/10.1074/jbc.M111.233700>
- Lorentz, O., Duluc, I., Arcangelis, A. D., Simon-Assmann, P., Kedinger, M., & Freund, J. N. (1997). Key role of the Cdx2 homeobox gene in extracellular matrix-mediated intestinal cell differentiation. *The Journal of cell biology*, 139(6), 1553–1565. <https://doi.org/10.1083/jcb.139.6.1553>
- Luo, H., Yu, Q., Liu, Y., Tang, M., Liang, M., Zhang, D., Xiao, T. S., Wu, L., Tan, M., Ruan, Y., Bungert, J., & Lu, J. (2020). LATS kinase-mediated CTCF phosphorylation and selective loss of

genomic binding. *Science advances*, 6(8), eaaw4651.  
<https://doi.org/10.1126/sciadv.aaw4651>

- Makhija, E., Jokhun, D. S., & Shivashankar, G. V. (2016). Nuclear deformability and telomere dynamics are regulated by cell geometric constraints. *Proceedings of the National Academy of Sciences of the United States of America*, 113(1), E32–E40.  
<https://doi.org/10.1073/pnas.1513189113>
- Mammoto, A., Muyleart, M., Kadlec, A., Gutterman, D., & Mammoto, T. (2018). YAP1-TEAD1 signaling controls angiogenesis and mitochondrial biogenesis through PGC1 $\alpha$ . *Microvascular research*, 119, 73–83.  
<https://doi.org/10.1016/j.mvr.2018.04.003>
- Mangelsdorf, D. J., Thummel, C., Beato, M., Herrlich, P., Schütz, G., Umesono, K., Blumberg, B., Kastner, P., Mark, M., Chambon, P., & Evans, R. M. (1995). The nuclear receptor superfamily: the second decade. *Cell*, 83(6), 835–839.  
[https://doi.org/10.1016/0092-8674\(95\)90199-x](https://doi.org/10.1016/0092-8674(95)90199-x)
- Masood S. (1992). Estrogen and progesterone receptors in cytology: a comprehensive review. *Diagnostic cytopathology*, 8(5), 475–491.  
<https://doi.org/10.1002/dc.2840080508>
- Maurano, M. T., Wang, H., John, S., Shafer, A., Canfield, T., Lee, K., & Stamatoyannopoulos, J. A. (2015). Role of DNA Methylation in Modulating Transcription Factor Occupancy. *Cell reports*, 12(7), 1184–1195.  
<https://doi.org/10.1016/j.celrep.2015.07.024>
- McCauley, M. J., Huo, R., Becker, N., Holte, M. N., Muthurajan, U. M., Rouzina, I., Luger, K., Maher, L. J., 3rd, Israeloff, N. E., & Williams, M. C. (2019). Single and double box HMGB proteins differentially destabilize nucleosomes. *Nucleic acids research*, 47(2), 666–678. <https://doi.org/10.1093/nar/gky1119>
- Mehta, I. S., Kulashreshtha, M., Chakraborty, S., Kolthur-Seetharam, U., & Rao, B. J. (2013). Chromosome territories reposition during DNA damage-repair response. *Genome biology*, 14(12), R135. <https://doi.org/10.1186/gb-2013-14-12-r135>
- Migliaccio, A., Piccolo, D., Castoria, G., Di Domenico, M., Bilancio, A., Lombardi, M., Gong, W., Beato, M., & Auricchio, F. (1998). Activation of the Src/p21ras/Erk pathway by progesterone receptor via cross-talk with estrogen receptor. *The EMBO journal*, 17(7), 2008–2018.  
<https://doi.org/10.1093/emboj/17.7.2008>
- Musgrove, E. A., Swarbrick, A., Lee, C. S., Cornish, A. L., & Sutherland, R. L. (1998). Mechanisms of cyclin-dependent kinase



- inactivation by progestins. *Molecular and cellular biology*, 18(4), 1812–1825. <https://doi.org/10.1128/MCB.18.4.1812>
- Nacht, A. S., Pohl, A., Zaurin, R., Soronellas, D., Quilez, J., Sharma, P., Wright, R. H., Beato, M., & Vicent, G. P. (2016). Hormone-induced repression of genes requires BRG1-mediated H1.2 deposition at target promoters. *The EMBO journal*, 35(16), 1822–1843. <https://doi.org/10.15252/embj.201593260>
  - Nguyen, D. A., & Neville, M. C. (1998). Tight junction regulation in the mammary gland. *Journal of mammary gland biology and neoplasia*, 3(3), 233–246. <https://doi.org/10.1023/a:1018707309361>
  - Nora, E. P., Lajoie, B. R., Schulz, E. G., Giorgetti, L., Okamoto, I., Servant, N., Piolot, T., van Berkum, N. L., Meisig, J., Sedat, J., Gribnau, J., Barillot, E., Blüthgen, N., Dekker, J., & Heard, E. (2012). Spatial partitioning of the regulatory landscape of the X-inactivation centre. *Nature*, 485(7398), 381–385. <https://doi.org/10.1038/nature11049>
  - Oberdoerffer, P., & Sinclair, D. A. (2007). The role of nuclear architecture in genomic instability and ageing. *Nature reviews. Molecular cell biology*, 8(9), 692–702. <https://doi.org/10.1038/nrm2238>
  - Okonechnikov, K., Conesa, A., & García-Alcalde, F. (2016). Qualimap 2: advanced multi-sample quality control for high-throughput sequencing data. *Bioinformatics (Oxford, England)*, 32(2), 292–294. <https://doi.org/10.1093/bioinformatics/btv566>
  - Pampaloni, F., Reynaud, E. G., & Stelzer, E. H. (2007). The third dimension bridges the gap between cell culture and live tissue. *Nature reviews. Molecular cell biology*, 8(10), 839–845. <https://doi.org/10.1038/nrm2236>
  - Panciera, T., Azzolin, L., Cordenonsi, M., & Piccolo, S. (2017). Mechanobiology of YAP and TAZ in physiology and disease. *Nature reviews. Molecular cell biology*, 18(12), 758–770. <https://doi.org/10.1038/nrm.2017.87>
  - Paszek, M. J., Zahir, N., Johnson, K. R., Lakins, J. N., Rozenberg, G. I., Gefen, A., Reinhart-King, C. A., Margulies, S. S., Dembo, M., Boettiger, D., Hammer, D. A., & Weaver, V. M. (2005). Tensional homeostasis and the malignant phenotype. *Cancer cell*, 8(3), 241–254. <https://doi.org/10.1016/j.ccr.2005.08.010>
  - Patten, D. K., Corleone, G., Györfy, B., Perone, Y., Slaven, N., Barozzi, I., Erdős, E., Saiakhova, A., Goddard, K., Vingiani, A., Shousha, S., Pongor, L. S., Hadjiminias, D. J., Schiavon, G., Barry, P., Palmieri, C., Coombes, R. C., Scacheri, P., Pruneri, G.,

- & Magnani, L. (2018). Enhancer mapping uncovers phenotypic heterogeneity and evolution in patients with luminal breast cancer. *Nature medicine*, 24(9), 1469–1480. <https://doi.org/10.1038/s41591-018-0091-x>
- Pickup, M. W., Mouw, J. K., & Weaver, V. M. (2014). The extracellular matrix modulates the hallmarks of cancer. *EMBO reports*, 15(12), 1243–1253. <https://doi.org/10.15252/embr.201439246>
  - Pradhan, R., Ranade, D., & Sengupta, K. (2018). Emerin modulates spatial organization of chromosome territories in cells on softer matrices. *Nucleic acids research*, 46(11), 5561–5586. <https://doi.org/10.1093/nar/gky288>
  - Pratt, W. B., & Toft, D. O. (1997). Steroid receptor interactions with heat shock protein and immunophilin chaperones. *Endocrine reviews*, 18(3), 306–360. <https://doi.org/10.1210/edrv.18.3.0303>
  - Rajgor, D., & Shanahan, C. M. (2013). Nesprins: from the nuclear envelope and beyond. *Expert reviews in molecular medicine*, 15, e5. <https://doi.org/10.1017/erm.2013.6>
  - Richmond, T. J., Finch, J. T., Rushton, B., Rhodes, D., & Klug, A. (1984). Structure of the nucleosome core particle at 7 Å resolution. *Nature*, 311(5986), 532–537. <https://doi.org/10.1038/311532a0>
  - Rochefort, H., Bardon, S., Chalbos, D., & Vignon, F. (1984). Steroidal and nonsteroidal antiestrogens in breast cancer cells in culture. *Journal of steroid biochemistry*, 20(1), 105–110. [https://doi.org/10.1016/0022-4731\(84\)90196-1](https://doi.org/10.1016/0022-4731(84)90196-1)
  - Rossetto, D., Avvakumov, N., & Côté, J. (2012). Histone phosphorylation: a chromatin modification involved in diverse nuclear events. *Epigenetics*, 7(10), 1098–1108. <https://doi.org/10.4161/epi.21975>
  - Rowley, M. J., & Corces, V. G. (2018). Organizational principles of 3D genome architecture. *Nature reviews. Genetics*, 19(12), 789–800. <https://doi.org/10.1038/s41576-018-0060-8>
  - Rozwadowska, N., Kolanowski, T., Wiland, E., Siatkowski, M., Pawlak, P., Malcher, A., Mietkiewski, T., Olszewska, M., & Kurpisz, M. (2013). Characterisation of nuclear architectural alterations during in vitro differentiation of human stem cells of myogenic origin. *PLoS one*, 8(9), e73231. <https://doi.org/10.1371/journal.pone.0073231>
  - Santos, S. J., Aupperlee, M. D., Xie, J., Durairaj, S., Miksicek, R., Conrad, S. E., Leipprandt, J. R., Tan, Y. S., Schwartz, R. C., & Haslam, S. Z. (2009). Progesterone receptor A-regulated gene expression in mammary organoid cultures. *The Journal of steroid*



*biochemistry and molecular biology*, 115(3-5), 161–172.  
<https://doi.org/10.1016/j.jsbmb.2009.04.001>

- Schaller, M. D., Borgman, C. A., Cobb, B. S., Vines, R. R., Reynolds, A. B., & Parsons, J. T. (1992). pp125FAK a structurally distinctive protein-tyrosine kinase associated with focal adhesions. *Proceedings of the National Academy of Sciences of the United States of America*, 89(11), 5192–5196.  
<https://doi.org/10.1073/pnas.89.11.5192>
- Schaller, M. D., Hildebrand, J. D., Shannon, J. D., Fox, J. W., Vines, R. R., & Parsons, J. T. (1994). Autophosphorylation of the focal adhesion kinase, pp125FAK, directs SH2-dependent binding of pp60src. *Molecular and cellular biology*, 14(3), 1680–1688. <https://doi.org/10.1128/mcb.14.3.1680-1688.1994>
- Schedin, P., & Keely, P. J. (2011). Mammary gland ECM remodeling, stiffness, and mechanosignaling in normal development and tumor progression. *Cold Spring Harbor perspectives in biology*, 3(1), a003228.  
<https://doi.org/10.1101/cshperspect.a003228>
- Scheidereit, C., Geisse, S., Westphal, H. M., & Beato, M. (1983). The glucocorticoid receptor binds to defined nucleotide sequences near the promoter of mouse mammary tumour virus. *Nature*, 304(5928), 749–752.  
<https://doi.org/10.1038/304749a0>
- Schindelin, J., Arganda-Carreras, I., Frise, E., Kaynig, V., Longair, M., Pietzsch, T., Preibisch, S., Rueden, C., Saalfeld, S., Schmid, B., Tinevez, J. Y., White, D. J., Hartenstein, V., Eliceiri, K., Tomancak, P., & Cardona, A. (2012). Fiji: an open-source platform for biological-image analysis. *Nature methods*, 9(7), 676–682. <https://doi.org/10.1038/nmeth.2019>
- Schneider, R., & Grosschedl, R. (2007). Dynamics and interplay of nuclear architecture, genome organization, and gene expression. *Genes & development*, 21(23), 3027–3043.  
<https://doi.org/10.1101/gad.1604607>
- Serra, F., Baù, D., Goodstadt, M., Castillo, D., Filion, G. J., & Marti-Renom, M. A. (2017). Automatic analysis and 3D-modelling of Hi-C data using TADbit reveals structural features of the fly chromatin colors. *PLoS computational biology*, 13(7), e1005665.  
<https://doi.org/10.1371/journal.pcbi.1005665>
- Simian, M., & Bissell, M. J. (2017). Organoids: A historical perspective of thinking in three dimensions. *The Journal of cell biology*, 216(1), 31–40. <https://doi.org/10.1083/jcb.201610056>
- Sosa, B. A., Kutay, U., & Schwartz, T. U. (2013). Structural insights into LINC complexes. *Current opinion in structural biology*, 23(2), 285–291. <https://doi.org/10.1016/j.sbi.2013.03.005>

- Stadhouders, R., Filion, G. J., & Graf, T. (2019). Transcription factors and 3D genome conformation in cell-fate decisions. *Nature*, *569*(7756), 345–354. <https://doi.org/10.1038/s41586-019-1182-7>
- Stark R., Brown G. D. (2011). *DiffBind: Differential Binding Analysis of ChIP-Seq Peak Data*. *Bioconductor*. Available online at: <http://bioconductor.org/packages/release/bioc/html/DiffBind.html>.
- Starr, D. A., & Fridolfsson, H. N. (2010). Interactions between nuclei and the cytoskeleton are mediated by SUN-KASH nuclear-envelope bridges. *Annual review of cell and developmental biology*, *26*, 421–444. <https://doi.org/10.1146/annurev-cellbio-100109-104037>
- Stowers, R. S., Allen, S. C., Sanchez, K., Davis, C. L., Ebel, N. D., Van Den Berg, C., & Suggs, L. J. (2016). Extracellular Matrix Stiffening Induces a Malignant Phenotypic Transition in Breast Epithelial Cells. *Cellular and molecular bioengineering*, *10*(1), 114–123. <https://doi.org/10.1007/s12195-016-0468-1>
- Streuli, C. H., Bailey, N., & Bissell, M. J. (1991). Control of mammary epithelial differentiation: basement membrane induces tissue-specific gene expression in the absence of cell-cell interaction and morphological polarity. *The Journal of cell biology*, *115*(5), 1383–1395. <https://doi.org/10.1083/jcb.115.5.1383>
- Stutchbury, B., Atherton, P., Tsang, R., Wang, D. Y., & Ballestrem, C. (2017). Distinct focal adhesion protein modules control different aspects of mechanotransduction. *Journal of cell science*, *130*(9), 1612–1624. <https://doi.org/10.1242/jcs.195362>
- Swift, J., Ivanovska, I. L., Buxboim, A., Harada, T., Dingal, P. C., Pinter, J., Pajerowski, J. D., Spinler, K. R., Shin, J. W., Tewari, M., Rehfeldt, F., Speicher, D. W., & Discher, D. E. (2013). Nuclear lamin-A scales with tissue stiffness and enhances matrix-directed differentiation. *Science (New York, N.Y.)*, *341*(6149), 1240104. <https://doi.org/10.1126/science.1240104>
- Swift, J., & Discher, D. E. (2014). The nuclear lamina is mechano-responsive to ECM elasticity in mature tissue. *Journal of cell science*, *127*(Pt 14), 3005–3015. <https://doi.org/10.1242/jcs.149203>
- Tanabe, H., Müller, S., Neusser, M., von Hase, J., Calcagno, E., Cremer, M., Solovei, I., Cremer, C., & Cremer, T. (2002). Evolutionary conservation of chromosome territory arrangements in cell nuclei from higher primates. *Proceedings of the National Academy of Sciences of the United States of America*, *99*(7), 4424–4429. <https://doi.org/10.1073/pnas.072618599>

- Tang, D., Mehta, D., & Gunst, S. J. (1999). Mechanosensitive tyrosine phosphorylation of paxillin and focal adhesion kinase in tracheal smooth muscle. *The American journal of physiology*, 276(1), C250–C258. <https://doi.org/10.1152/ajpcell.1999.276.1.C250>
- Theocharis, A. D., Skandalis, S. S., Gialeli, C., & Karamanos, N. K. (2016). Extracellular matrix structure. *Advanced drug delivery reviews*, 97, 4–27. <https://doi.org/10.1016/j.addr.2015.11.001>
- Tomás-Bort, E., Kieler, M., Sharma, S., Candido, J. B., & Loessner, D. (2020). 3D approaches to model the tumor microenvironment of pancreatic cancer. *Theranostics*, 10(11), 5074–5089. <https://doi.org/10.7150/thno.42441>
- Uhler, C., & Shivashankar, G. V. (2017). Regulation of genome organization and gene expression by nuclear mechanotransduction. *Nature reviews. Molecular cell biology*, 18(12), 717–727. <https://doi.org/10.1038/nrm.2017.101>
- van Steensel, B., & Belmont, A. S. (2017). Lamina-Associated Domains: Links with Chromosome Architecture, Heterochromatin, and Gene Repression. *Cell*, 169(5), 780–791. <https://doi.org/10.1016/j.cell.2017.04.022>
- Uroz, M., Wistorf, S., Serra-Picamal, X., Conte, V., Sales-Pardo, M., Roca-Cusachs, P., Guimerà, R., & Trepap, X. (2018). Regulation of cell cycle progression by cell-cell and cell-matrix forces. *Nature cell biology*, 20(6), 646–654. <https://doi.org/10.1038/s41556-018-0107-2>
- Venturini, V., Pezzano, F., Català Castro, F., Häkkinen, H. M., Jiménez-Delgado, S., Colomer-Rosell, M., Marro, M., Tolosa-Ramon, Q., Paz-López, S., Valverde, M. A., Weghuber, J., Loza-Alvarez, P., Krieg, M., Wieser, S., & Ruprecht, V. (2020). The nucleus measures shape changes for cellular proprioception to control dynamic cell behavior. *Science (New York, N.Y.)*, 370(6514), eaba2644. <https://doi.org/10.1126/science.aba2644>
- Vicent, G. P., Ballaré, C., Nacht, A. S., Clausell, J., Subtil-Rodríguez, A., Quiles, I., Jordan, A., & Beato, M. (2006). Induction of progesterone target genes requires activation of Erk and Msk kinases and phosphorylation of histone H3. *Molecular cell*, 24(3), 367–381. <https://doi.org/10.1016/j.molcel.2006.10.011>
- Vicent, G. P., Ballaré, C., Zaurin, R., Saragüeta, P., & Beato, M. (2006). Chromatin remodeling and control of cell proliferation by progestins via cross talk of progesterone receptor with the estrogen receptors and kinase signaling pathways. *Annals of the New York Academy of Sciences*, 1089, 59–72. <https://doi.org/10.1196/annals.1386.025>

- Vicent, G. P., Zaurin, R., Ballaré, C., Nacht, A. S., & Beato, M. (2009). Erk signaling and chromatin remodeling in MMTV promoter activation by progestins. *Nuclear receptor signaling*, 7, e008. <https://doi.org/10.1621/nrs.07008>
- Vicent, G. P., Nacht, A. S., Zaurin, R., Font-Mateu, J., Soronellas, D., Le Dily, F., Reyes, D., & Beato, M. (2013). Unliganded progesterone receptor-mediated targeting of an RNA-containing repressive complex silences a subset of hormone-inducible genes. *Genes & development*, 27(10), 1179–1197. <https://doi.org/10.1101/gad.215293.113>
- Vicent, G. P., Zaurin, R., Nacht, A. S., Li, A., Font-Mateu, J., Le Dily, F., Vermeulen, M., Mann, M., & Beato, M. (2009). Two chromatin remodeling activities cooperate during activation of hormone responsive promoters. *PLoS genetics*, 5(7), e1000567. <https://doi.org/10.1371/journal.pgen.1000567>
- Vidal, E., le Dily, F., Quilez, J., Stadhouders, R., Cuartero, Y., Graf, T., Marti-Renom, M. A., Beato, M., & Filion, G. J. (2018). OneD: increasing reproducibility of Hi-C samples with abnormal karyotypes. *Nucleic acids research*, 46(8), e49. <https://doi.org/10.1093/nar/gky064>
- Vignali, M., Hassan, A. H., Neely, K. E., & Workman, J. L. (2000). ATP-dependent chromatin-remodeling complexes. *Molecular and cellular biology*, 20(6), 1899–1910. <https://doi.org/10.1128/MCB.20.6.1899-1910.2000>
- Vilarrasa-Blasi, R., Soler-Vila, P., Verdaguer-Dot, N., Russiñol, N., Di Stefano, M., Chapaprieta, V., Clot, G., Farabella, I., Cuscó, P., Kulis, M., Agirre, X., Prosper, F., Beekman, R., Beà, S., Colomer, D., Stunnenberg, H. G., Gut, I., Campo, E., Marti-Renom, M. A., & Martin-Subero, J. I. (2021). Dynamics of genome architecture and chromatin function during human B cell differentiation and neoplastic transformation. *Nature communications*, 12(1), 651. <https://doi.org/10.1038/s41467-020-20849-y>
- Vogel, V., & Sheetz, M. (2006). Local force and geometry sensing regulate cell functions. *Nature reviews. Molecular cell biology*, 7(4), 265–275. <https://doi.org/10.1038/nrm1890>
- von der Ahe, D., Janich, S., Scheidereit, C., Renkawitz, R., Schütz, G., & Beato, M. (1985). Glucocorticoid and progesterone receptors bind to the same sites in two hormonally regulated promoters. *Nature*, 313(6004), 706–709. <https://doi.org/10.1038/313706a0>
- Wagh, K., Ishikawa, M., Garcia, D. A., Stavreva, D. A., Upadhyaya, A., & Hager, G. L. (2021). Mechanical Regulation of

Transcription: Recent Advances. *Trends in cell biology*, 31(6), 457–472. <https://doi.org/10.1016/j.tcb.2021.02.008>

- Walker R. A. (2008). Immunohistochemical markers as predictive tools for breast cancer. *Journal of clinical pathology*, 61(6), 689–696. <https://doi.org/10.1136/jcp.2006.041830>
- Wang, H. B., Dembo, M., Hanks, S. K., & Wang, Y. (2001). Focal adhesion kinase is involved in mechanosensing during fibroblast migration. *Proceedings of the National Academy of Sciences of the United States of America*, 98(20), 11295–11300. <https://doi.org/10.1073/pnas.201201198>
- Wang, H., Maurano, M. T., Qu, H., Varley, K. E., Gertz, J., Pauli, F., Lee, K., Canfield, T., Weaver, M., Sandstrom, R., Thurman, R. E., Kaul, R., Myers, R. M., & Stamatoyannopoulos, J. A. (2012). Widespread plasticity in CTCF occupancy linked to DNA methylation. *Genome research*, 22(9), 1680–1688. <https://doi.org/10.1101/gr.136101.111>
- Wang, H., Wang, L., Erdjument-Bromage, H., Vidal, M., Tempst, P., Jones, R. S., & Zhang, Y. (2004). Role of histone H2A ubiquitination in Polycomb silencing. *Nature*, 431(7010), 873–878. <https://doi.org/10.1038/nature02985>
- Wang, Y., Li, M., Stadler, S., Correll, S., Li, P., Wang, D., Hayama, R., Leonelli, L., Han, H., Grigoryev, S. A., Allis, C. D., & Coonrod, S. A. (2009). Histone hypercitrullination mediates chromatin decondensation and neutrophil extracellular trap formation. *The Journal of cell biology*, 184(2), 205–213. <https://doi.org/10.1083/jcb.200806072>
- Wood, A., & Shilatifard, A. (2004). Posttranslational modifications of histones by methylation. *Advances in protein chemistry*, 67, 201–222. [https://doi.org/10.1016/S0065-3233\(04\)67008-2](https://doi.org/10.1016/S0065-3233(04)67008-2)
- Wozniak, M. A., Modzelewska, K., Kwong, L., & Keely, P. J. (2004). Focal adhesion regulation of cell behavior. *Biochimica et biophysica acta*, 1692(2-3), 103–119. <https://doi.org/10.1016/j.bbamcr.2004.04.007>
- Wright, R. H., Castellano, G., Bonet, J., Le Dily, F., Font-Mateu, J., Ballaré, C., Nacht, A. S., Soronellas, D., Oliva, B., & Beato, M. (2012). CDK2-dependent activation of PARP-1 is required for hormonal gene regulation in breast cancer cells. *Genes & development*, 26(17), 1972–1983. <https://doi.org/10.1101/gad.193193.112>
- Wright, R. H., Lioutas, A., Le Dily, F., Soronellas, D., Pohl, A., Bonet, J., Nacht, A. S., Samino, S., Font-Mateu, J., Vicent, G. P., Wierer, M., Trabado, M. A., Schelhorn, C., Carolis, C., Macias, M. J., Yanes, O., Oliva, B., & Beato, M. (2016). ADP-ribose-derived nuclear ATP synthesis by NUDIX5 is required for chromatin

- remodeling. *Science (New York, N.Y.)*, 352(6290), 1221–1225. <https://doi.org/10.1126/science.aad9335>
- Xi, W., & Beer, M. A. (2021). Loop competition and extrusion model predicts CTCF interaction specificity. *Nature communications*, 12(1), 1046. <https://doi.org/10.1038/s41467-021-21368-0>
  - Xu, B., Wang, H., Wright, S., Hyle, J., Zhang, Y., Shao, Y., Niu, M., Fan, Y., Rosikiewicz, W., Djekidel, M. N., Peng, J., Lu, R., & Li, C. (2021). Acute depletion of CTCF rewires genome-wide chromatin accessibility. *Genome biology*, 22(1), 244. <https://doi.org/10.1186/s13059-021-02466-0>
  - Xu, R., Nelson, C. M., Muschler, J. L., Veiseh, M., Vonderhaar, B. K., & Bissell, M. J. (2009). Sustained activation of STAT5 is essential for chromatin remodeling and maintenance of mammary-specific function. *The Journal of cell biology*, 184(1), 57–66. <https://doi.org/10.1083/jcb.200807021>
  - Yang, T., Zhang, F., Yardimci, G. G., Song, F., Hardison, R. C., Noble, W. S., Yue, F., & Li, Q. (2017). HiCRep: assessing the reproducibility of Hi-C data using a stratum-adjusted correlation coefficient. *Genome research*, 27(11), 1939–1949. <https://doi.org/10.1101/gr.220640.117>
  - Zaidel-Bar, R., Ballestrem, C., Kam, Z., & Geiger, B. (2003). Early molecular events in the assembly of matrix adhesions at the leading edge of migrating cells. *Journal of cell science*, 116(Pt 22), 4605–4613. <https://doi.org/10.1242/jcs.00792>
  - Zanconato, F., Cordenonsi, M., & Piccolo, S. (2019). YAP and TAZ: a signalling hub of the tumour microenvironment. *Nature reviews. Cancer*, 19(8), 454–464. <https://doi.org/10.1038/s41568-019-0168-y>
  - Zhang Y. (2003). Transcriptional regulation by histone ubiquitination and deubiquitination. *Genes & development*, 17(22), 2733–2740. <https://doi.org/10.1101/gad.1156403>
  - Zhang, Y., Liu, T., Meyer, C. A., Eeckhoute, J., Johnson, D. S., Bernstein, B. E., Nusbaum, C., Myers, R. M., Brown, M., Li, W., & Liu, X. S. (2008). Model-based analysis of ChIP-Seq (MACS). *Genome biology*, 9(9), R137. <https://doi.org/10.1186/gb-2008-9-9-r137>
  - Zhao, B., Ye, X., Yu, J., Li, L., Li, W., Li, S., Yu, J., Lin, J. D., Wang, C. Y., Chinnaiyan, A. M., Lai, Z. C., & Guan, K. L. (2008). TEAD mediates YAP-dependent gene induction and growth control. *Genes & development*, 22(14), 1962–1971. <https://doi.org/10.1101/gad.1664408>

- Zhao, Z., & Shilatifard, A. (2019). Epigenetic modifications of histones in cancer. *Genome biology*, 20(1), 245. <https://doi.org/10.1186/s13059-019-1870-5>
- Zhu, L. J., Gazin, C., Lawson, N. D., Pagès, H., Lin, S. M., Lapointe, D. S., & Green, M. R. (2010). ChIPpeakAnno: a Bioconductor package to annotate ChIP-seq and ChIP-chip data. *BMC bioinformatics*, 11, 237. <https://doi.org/10.1186/1471-2105-11-237>

## Abbreviations

°C	Celsius
μL	microliters
2D	Two dimension
3D	Three dimension
AJ	Adherens Junctions
ATAC-seq	Assay for Transposase-Accessible Chromatin Sequencing
ATP	Adenosine Triphosphate
BC	Breast cancer
BCC	Breast cancer cells
BSA	Bovine serum albumin
Bp	base pair
cDNA	complementary DNA
CSC	Cancer stem cells
ChIP-seq	Chromatin Immunoprecipitation sequencing
CT	Chromosome territories
DAPI	4',6-diamidino-2-phenylindole
DBD	DNA binding domain
DEA	Differential expression analysis
DEG	Differentially expressed gene
DMSO	Dimethyl sulfoxide
DNA	Deoxyribonucleic acid
ECM	Extracellular matrix
EDTA	Ethylenediaminetetraacetic acid
EMT	Epithelial-mesenchymal transition
ER	Estrogen receptor
FA	Focal adhesion
FBS	Fetal bovine serum
GO	Gene ontology
h	hours
HAPRbs	High accessibility progesterone receptor binding sites
HAT	Histone acetyltransferases
HCR	Hormone control region
HDAC	Histone deacetyltransferases
HMT	Histone methyltransferases



IF	Immunofluorescence
INM	Inner nuclear membrane
IP	Immunoprecipitation
Kb	kilobases
LBD	Ligand binding domain
IrECM	laminin rich extracellular matrix
Mb	Megabases
MEC	Mammary epithelial cells
Min	minutes
mL	milliliters
MMTV	Mouse mammary tumour virus
MMP	Matrix metalloproteinases
MNase	Micrococcal nuclease
ONM	Outer nuclear membrane
PBS	Phosphate-buffered saline
PCA	Principal component analysis
PCR	Polymerase chain reaction
PFA	Paraformaldehyde
PIC	Protease inhibitor cocktail
PR	Progesterone receptor
PTM	Postranslational modification
RNA	Ribonucleic acid
RNA-seq	Ribonucleic acid sequencing
RT	Room temperature
SH	Steroid hormone
SHR	Steroid hormone receptor
TAD	Topologically associating domain
TF	Transcription factor
TJ	Tight junctions
TSS	Transcription start site
V	Voltage